Aus der Abteilung Neurogenetik
(Direktor Prof. Dr. rer. nat. K.-A. Nave)
des Max-Planck-Instituts für Experimentelle Medizin
in Göttingen

# Neuron-Glia Crosstalk: Investigating Immune-Cell Modulation in the CNP1 Null Mutant Mouse

INAUGURAL-DISSERTATION

Zur Erlangung des Doktorgrades
der Medizinischen Fakultät der
Georg-August-Universität zu Göttingen

vorgelegt von

Marie Louise Aicher

aus

Tübingen, Deutschland

Göttingen 2022

| | |
|---|---|
| Dekan: | Prof. Dr. med. W. Brück |

## Betreuungsausschuss

| | |
|---|---|
| Betreuer/in: | Prof. Dr. rer. nat. K.-A. Nave |
| Ko-Betreuer/in: | Prof. Dr. med. C. Stadelmann-Nessler |

## Prüfungskommission

| | |
|---|---|
| Referent: | Prof. Dr. rer. nat. K.-A. Nave |
| Ko-Referent/in: | Prof. Dr. med. C. Stadelmann-Nessler |
| Drittreferent/in: | Prof. Dr. hum. biol. M. Schön |

Datum der mündlichen Prüfung: 1. März 2023

Hiermit erkläre ich, die Dissertation mit dem Titel "Neuron-Glia Crosstalk: Investigating Immune-Cell Modulation in the CNP1 Null Mutant Mouse" eigenständig angefertigt und keine anderen als die von mir angegebenen Quellen und Hilfsmittel verwendet zu haben.

Bern, 20.03.2022

Marie Louise Aicher

Die Daten, auf denen die vorliegende Arbeit basiert, wurden teilweise publiziert:

Mukherjee C, Kling T, Russo B, Miebach K, Kess E, Schifferer M, Pedro LD, Weikert U, Fard MK, Kannaiyan N, Rossner M, Aicher ML, Goebbels S, Nave K-A, Krämer-Albers E-M, Schneider A, Simons M (2020): Oligodendrocytes Provide Antioxidant Defense Function for Neurons by Secreting Ferritin Heavy Chain. Cell Metabolism 32, 259-272.e10

# Contents

**List of figures** ..... **IV**

**List of tables** ..... **V**

**Abbreviations** ..... **VI**

**Abstract** ..... **IX**

**1 Introduction** ..... **1**

1.1 The central nervous system ..... 1

1.2 Development, composition and function of myelin ..... 2

1.3 2´, 3´-cyclic nucleotide 3´-phosphodiesterase (CNP1) ..... 4

1.4 CNP1 null mutant mice and associated diseases in humans ..... 5

1.5 Neuroinflammation and the role of glial cells and immunomodulatory molecules ..... 7

1.6 Aim of the study ..... 10

**2 Material and methods** ..... **13**

2.1 Materials ..... 13

2.1.1 Chemicals and consumables ..... 13

2.1.2 Machines ..... 15

2.1.3 Solutions and buffers ..... 15

2.1.4 Antibodies ..... 19

2.1.5 Oligonucleotides and primers ..... 20

2.1.6 Enzymes ..... 21

2.1.7 Microscopes, software and statistical analysis ..... 21

2.2 Methods ..... 22

2.2.1 Animals ..... 22

2.2.2 Genotyping ..... 23

2.2.3 Histology and immunohistochemistry ..... 25

2.2.4 Myelin preparation ..... 26

2.2.5 RNA isolation, cDNA synthesis and qRT-PCRs ..... 28

2.2.6 Western Blot ..... 29
2.2.7 RNA-Sequencing ..... 31
2.2.8 Statistical analysis ..... 32

**3 Results ..... 35**

3.1 CNP1 null mutant mice depict a normal postnatal development in addition to an inflammatory reaction according to the RNA-Sequencing of purified myelin. ..... 35
3.1.1 At P18 myelination is in progress, therefore two different ages (P18 and P75) were examined. ..... 35
3.1.2 CNP1 null mutant mice exhibit a progressive phenotype and the myelin is contaminated with many immunomodulatory molecules at P75. ..... 36
3.2 Attempt to define a prodromal phase without inflammation in the myelin that allows the detection of oligodendrocyte-derived molecules mediating the early disease pathology of CNP1 null mutants at P20. ..... 40
3.3 Sensitive qRT-PCR analysis casted doubt on the existence of a prodromal phase in CNP1 null mutants at P20. ..... 44
3.4 Characteristics of astrocytes and microglia in CNP1 null mutant mice at P75 ..... 47
3.4.1 Loss of CNP1 induces cytotoxic (A1) and neuroprotective (A2) astrocytes at P75. ..... 47
3.4.2 Loss of CNP1 induces proinflammatory and phagocytic microglia with a DAM-like phenotype at P75 ..... 47
3.4.3 Deletion of the adaptor molecule MyD88 of the NF-κB pathway leads to an amelioration of neurodegeneration, but this pathway is not (exclusively) responsible for the recruitment and activation of immune cells in CNP1 null mutant mice. ..... 50
3.5 Altered RNA composition and MCT1 protein abundance in myelin of CNP1 null mutant mice ..... 52
3.5.1 qRT-PCR analysis as a readout for the integrity of cytoplasmic channels in myelin of CNP1 null mutant mice. ..... 52
3.5.2 The decreased abundance of MCT1 protein in myelin of CNP1 null mutants might result from an altered transport along cytoplasmic channels and might contribute to the observed dysfunction and degeneration of axons ..... 54

**4 Discussion ..... 55**

4.1 Characterization of neuroinflammation in CNP1 null mutant mice, a disease model of neurologic and psychiatric condition in humans ..... 55

4.2 Oligodendrocytes as potentially early immunomodulatory cells in CNP1 null mutant mice. ..... 59

4.3 RNA expression analysis provides evidence for a perturbed function of cytosolic channels in CNP1 mutant mice. ..... 65

**5 Supplement ..... 68**

**6 References ..... 69**

# List of figures

Figure 1: Integrated hypothetical model of primary and secondary pathology of CNP1 null mutants based on literature and own findings. 12

Figure 2: Myelin preparation 27

Figure 3: RNA-Seq. of purified myelin from CNP1 null mutant mice: normal postnatal development at P18 and inflammatory phenotype at P75. 39

Figure 4: A prodromal phase in CNP1 null mutant mice as defined by RNA-Seq. and qRT-PCR of purified myelin P18/P20. 41

Figure 5: A prodromal phase in CNP1 null mutant mice as defined by immunohistochemistry at P18. 42

Figure 6: Early upregulation of immunomodulatory markers potentially derived from oligodendrocytes by qRT-PCR at P20. 44

Figure 7: Unexpected early upregulation of some astroglial and microglial markers in qRT-PCR at P20. 46

Figure 8: Loss of CNP1 induces cytotoxic and neuroprotective astrocytes and proinflammatory and phagocytic microglia with a DAM-phenotype. 49

Figure 9: Deletion of MyD88 leads to an amelioration of neurodegeneration, but this pathway is not (exclusively) responsible for the recruitment and activation of immune cells in CNP1 null mutant mice. 51

Figure 10: Altered RNA composition and MCT1 protein abundance in myelin of CNP1 null mutant mice. 53

Figure S1: Gene ontology pathway analysis 68

# List of tables

Table 1: General chemicals ..... 13
Table 2: Chemicals of protein biochemistry ..... 13
Table 3: Chemicals of molecular biology ..... 14
Table 4: Chemicals of immunohistochemistry ..... 14
Table 5: Consumables ..... 14
Table 6: Machines ..... 15
Table 7: Primary antibodies ..... 19
Table 8: Secondary antibodies ..... 20
Table 9: Primers for genotyping ..... 20
Table 10: Primers for qRT-PCRs ..... 20
Table 11: Procedure of CNP1-PCR ..... 24
Table 12: Procedure of MyD88-PCR ..... 24
Table 13: Procedure of cDNA synthesis ..... 29
Table 14: Procedure of qRT-PCR ..... 29

# Abbreviations

General abbreviations

| | |
|---|---|
| AIF1 | Allograft inflammatory factor 1; synonym IBA1 |
| Aldh1l1 | Aldehyde Dehydrogenase 1 Family Member L1 |
| ANOVA | Analysis of variance |
| APP | Amyloid precursor protein |
| *Aqua dest.* | *Aqua destillata* |
| ATP1A1 | ATPase Na+/K+ Transporting Subunit Alpha 1 |
| BSA | Bovine serum albumin |
| CD3 | Cluster of differentiation 3 |
| CNP1 | 2, 3-Cyclic Nucleotide 3-Phosphodiesterase |
| CNS | Central nervous system |
| DAB | Diaminobenzidine |
| DAM | Disease/ damage-associated microglia |
| DAMPs | Damage-associated molecular patterns |
| DEG | Differentially expressed gene |
| DEPC | Diethylpyrocarbonate treated water |
| DNA | Deoxyribonucleotide acid |
| EAE | Experimental autoimmune encephalomyelitis |
| EDTA | Ethylenediaminetetraacetic acid |
| FPKM | Fragments per kilo base per million mapped reads |
| FTH1 | Ferritin heavy chain |
| FTL | Ferritin light chain |
| GFAP | Glial fibrillary acidic protein |
| GSEA | Gene Set Enrichment Analysis |
| IBA1 | Ionized calcium-binding adaptor molecule 1; synonym AIF1 |
| IHC | Immunohistochemistry |
| IL-1β | Interleukin 1β |
| IL1RL1 | IL-1 receptor growth stimulation expressed gene 2; synonym ST2 |
| IL-33 | Interleukin-33 |
| imOLG | Immune oligodendroglia |
| iNOS | Inducible nitric oxide synthetase; synonym NOS2 |
| ITGAM | Integrin Subunit Alpha M |
| KO | Knockout |
| Log2FC | log2 fold change |
| MAC3 | Macrophage-3 antigen; synonyms Cd107b and Lamp2 |
| MACS | Magnetic Activated Cell Sorting |
| MAPK | Mitogen-activated protein kinase |
| MBP | Myelin basic protein |
| MCT1 | Monocarboxylic acid transporter 1; synonym SLC16A1 |
| MHC | Major histocompatibility complex |
| MOBP | Myelin Associated Oligodendrocyte Basic Protein |
| MOG | Myelin oligodendrocyte glycoprotein |
| mRNA | Messenger RNA |
| MS | Multiple sclerosis |
| MyD88 | Myeloid differentiation primary response 88 |
| NES | Normalized enrichment score |
| NF-κB | Nuclear factor κ light chain enhancer of activated B-cells |
| NOS2 | Nitric oxide synthetase 2; synonym iNOS |
| OPC | Oligodendrocyte progenitor/ precursor cell |
| P | Postnatal day |
| PAGE | Polyacrylamide gel electrophoresis |
| PAMPs | Pathogen-associated molecular patterns |
| PBS | Phosphate-Buffered Saline |

| | |
|---|---|
| PCR | Polymerase chain reaction |
| PFA | Paraformaldehyde |
| PLP | Myelin proteolipid protein |
| qRT-PCR | Quantitative real time PCR |
| RIN | RNA integrity number |
| RNA | Ribonucleic acid |
| RNA-Seq. | RNA-Sequencing |
| Rpm | Revolutions per minute |
| SDS | Sodium dodecyl sulfate |
| Slc16A1 | Solute Carrier Family 16 Member 1; synonym MCT1 |
| ST2 | IL-1 receptor growth stimulation expressed gene 2; synonym IL1RL1 |
| TBS | Tris-buffered saline |
| TBST | Tris-buffered saline with Tween20 |
| TLR | Toll like receptor |
| TNFAIP6 | Tumor Necrosis Factor α (TNFα) induced protein 6; synonym TSG-6 |
| TNFα | Tumor necrosis factor α |
| TSG-6 | TNF stimulated gene 6 protein; synonym TFNAIP6 |
| UCMS | Unpredictable chronic mild stress |
| WT | Wildtype |

## Abbreviations of further genes/ RNAs

| | |
|---|---|
| Abca8a | ATP Binding Cassette Subfamily A Member 8 |
| Apoe | Apolipoprotein E |
| Aqp4 | Aquaporin 4 |
| Arg1 | Arginase 1 |
| Aspg | Asparaginase |
| B2m | Beta-2-Microglobulin |
| Bmp4 | Bone Morphogenetic Protein 4 |
| C1q | Complement C1q |
| C1qa | Complement C1q A Chain |
| C1qc | Complement C1q C Chain |
| C3 | Complement C3 |
| Ccl2 | C-C Motif Chemokine Ligand 2 |
| Ccl4 | C-C Motif Chemokine Ligand 4 |
| Ccl5 | C-C Motif Chemokine Ligand 5 |
| Ccl6 | C-C Motif Chemokine Ligand 6 |
| Cd107b | Cd107 Antigen-like Family Member b; synonym Lamp2 |
| Cd109 | Cluster of differentiation 109 |
| Cd14 | Cluster of differentiation 14 |
| Cd16 | Cluster of differentiation16; synonym Fcgr3 |
| CD163 | Cluster of differentiation 163 |
| CD206 | Cluster of differentiation 206; synonym Mannose receptor C type-1 |
| Cd44 | Cluster of differentiation 44 |
| Cd68 | Cluster of differentiation 68 |
| Cd74 | Cluster of differentiation 74 |
| Cd86 | Cluster of differentiation 86 |
| Cdk5r2 | Cyclin Dependent Kinase 5 Regulatory Subunit 2 |
| Cfb | Complement Factor B |
| Cldn5 | Claudin 5 |
| Clec7a | C-Type Lectin Domain Containing 7A; synonym Dectin-1 |
| Cst7 | Cystatin F |
| Ctsb | Cathepsin B |
| Ctsd | Cathepsin D |
| Cx3cr1 | C-X3-C Motif Chemokine Receptor 1 |

| | |
|---|---|
| Cxcl10 | C-X-C Motif Chemokine Ligand 10 |
| Emp1 | Epithelial Membrane Protein 1 |
| Eno2 | Enolase 2 |
| Fcgr2b | Fc Fragment of IgG Receptor IIb |
| Fn1 | Fibronectin 1 |
| Gbp2 | Guanylate Binding Protein 2 |
| Ggta1 | Glycoprotein Alpha-Galactosyltransferase 1 (Inactive) |
| Gpnmb | Glycoprotein Nonmetastatic Melanoma Protein B |
| Gsx1 | Genomic Screened Homeo Box 1 |
| H2-D1 | H-2 class I histocompatibility antigen, D-B alpha chain |
| H2-K1 | H-2 class I histocompatibility antigen, K-D alpha chain |
| Hexβ | Hexosaminidase Subunit Beta |
| Hprt | Hypoxanthine Phosphoribosyltransferase |
| Il-13 | Interleukin 13 |
| Il-4 | Interleukin 4 |
| Il-10 | Interleukin 10 |
| Il18R | Interleukin 18 Receptor 1 |
| Il1R | Interleukin 1 Receptor Type 1 |
| Itgax | Integrin Subunit Alpha X |
| Krt12 | Keratin 12 |
| Krt20 | Keratin 20 |
| Lilrb4a | Leukocyte Immunoglobulin Like Receptor B4 |
| Lpl | Lipoprotein Lipase |
| Lyz2 | Lysozyme C-2 |
| Mal | Myelin And Lymphocyte Protein |
| Marcksl1 | Macrophage myristoylated alanine-rich C kinase substrate |
| Ms4a7 | Membrane Spanning 4-Domains A7 |
| Mx1 | MX Dynamin Like GTPase 1 |
| Ndrg2 | N-myc downstream-regulated gene 2 protein |
| Nr4a3 | Nuclear Receptor Subfamily 4 Group A Member 3 |
| Ocln | Occludin |
| Osmr | Oncostatin M Receptor |
| P2ry12 | Purinergic Receptor P2Y12 |
| Rbfox3 | RNA Binding Fox-1 Homolog 3 |
| RetnlB | Resistin Like Beta |
| Rplp0 | Ribosomal Protein Lateral Stalk Subunit P0 |
| S100a10 | S100 Calcium Binding Protein A10 |
| S100β | S-100 Protein Subunit Beta |
| Scd3 | Acyl-CoA desaturase 3 |
| Serpina3n | Serpin Family A Member 3 |
| Sirt2 | Sirtuin 2 |
| Slamf8 | SLAM Family Member 8 |
| Slc1a3 | Solute Carrier Family 1 Member 3 |
| Spp1 | Secreted Phosphoprotein 1 |
| Srd5a1 | Steroid 5 Alpha-Reductase 1 |
| Tgfβ | Transforming Growth Factor Beta |
| Timp1 | TIMP Metallopeptidase Inhibitor 1 |
| Tlr1 | Toll like receptor 1 |
| Tlr2 | Toll like receptor 2 |
| Tmem119 | Transmembrane Protein 119 |
| Trem2 | Triggering Receptor Expressed On Myeloid Cells 2 |
| Tubb3 | Tubulin Beta 3 Class III |
| Tyrobp | TYRO protein tyrosine kinase-binding protein |
| Vim | Vimentin |

Genes/ RNAs are written in small letters, proteins are written in capital letters.

# Abstract

Myelin sheaths built by oligodendrocytes in the central nervous system (CNS) are not only important insulators that enable the fast saltatory propagation of action potentials but also fulfill metabolic support functions to their underlying axons. 2',3'-cyclic nucleotide 3' phosphodiesterase (CNP1) constitutes 4% of total CNS myelin proteins and is disease-relevant in humans and mice. First, a homozygous missense mutation in CNP1 was recently associated with a hypomyelinating dystrophy in humans and second, a reduced CNP1 gene expression causes an age-dependent catatonia-depression syndrome in mouse and man.

By immunohistochemistry and RNA-Seq. on purified myelin-enriched fractions, we aimed at investigating which changes occur at early ages in CNP1 null mutants and may thus be initial mediators of disease pathology. We found that signs of neuroinflammation and neurodegeneration were largely absent at the age of P18 but obvious at P75, suggesting that the earlier age represents a prodromal phase of pathology. Nevertheless, by sensitive qRT-PCR, we identified the anti-inflammatory Tnfaip6 and the alarmin Il-33 upregulated in mutant myelin as early as P20 consistent with the idea that these molecules are secreted by CNP1 deprived oligodendrocytes. Although these candidates are thus possible initial disease modifiers, it remains to be analyzed in future experiments, whether they are indeed oligodendrocyte-derived, since subsequent analyses by qRT-PCR questioned, that P20 can be fully regarded as prodromal stage of CNP1-related pathology.

When analyzing astroglial and microglial RNAs in purified myelin at P75, we noted that astrocytes exhibit features of A1 (C3, Ggta1, Gbp2) and A2 (Cd109, Cd14, Emp1) cells, and that microglia express pro-inflammatory M1 markers (Ccl6, Fcgr3, Cd86) as well as M2 markers (Clec7a, Trem2) typical for phagocytosing cells. Additionally, Toll-like-receptors (Tlr) 1 and 2 were found upregulated. A subsequent immunohistochemical analysis of CNP1-MyD88-double mutants identified the TLR-associated MyD88-pathway in microglia as instrumental in inducing axonal pathology in CNP1-deficient mice.

Finally, we hypothesized that the previously reported pathology of cytosolic channels in CNP1 null mutant myelin results in a quantitative alteration of transported mRNAs and proteins. By qRT-PCR we found Mbp-mRNA higher in abundance in myelin of mutants at P20, compatible with the idea that an increased local translation of this mRNA is causatively linked to the reported earlier closure of cytosolic myelin channels due to an increased presence of MPB-protein, the only myelin protein absolutely necessary for myelin compaction. At P75 we found Fth1-mRNA, which is reported to be extremely abundant in myelin, reduced by 70% in CNP1 null mutants. This may be of relevance for the pathology since the secretion of Fth1 by oligodendrocytes is suggested to serve as a protective mechanism against iron-induced axonopathy. At P75 we also found the abundance of MCT1 protein, an oligodendroglial axon supporting monocarboxylate transporter, reduced. Hence, the pathology of cytosolic myelin channels may indeed disrupt the transport of proteins essential for axonal support.

# 1 Introduction

## 1.1 The central nervous system

The central nervous system (CNS) is composed of the brain and the spinal cord and mainly consists of grey and white matter and cerebral spinal fluid. Grey matter contains neuronal cell bodies and some glial cells, whereas white matter harbors myelinated and unmyelinated axons, which are the connections between neurons, as well as most glial cells. Amongst glial cells are oligodendrocytes and astrocytes, both derived from the neuroectoderm and microglia, which are derived from primitive myeloid progenitors (Ginhoux et al. 2010). There is an extensive crosstalk between glial cells amongst each other as well as between glial cells and neurons in health and disease, which is exhibited by secreted molecules such as neurotransmitters, cytokines and exosomes as well as direct coupling of the cells. The energy demand of the CNS is very high and neurons completely depend on glucose or monocarboxylates such as lactate, whereas astrocytes and oligodendrocytes are predominately glycolytic (Magistretti and Allaman 2018) and capable of storing glucose and supporting neurons (Pellerin and Magistretti 1994; Pellerin et al. 1998; Simpson et al. 2007; Fünfschilling et al. 2012; Lee et al. 2012; Saab et al. 2013).

Oligodendrocytes are the myelin producing cells in the CNS and build up to 50 processes that wrap up many different axonal segments with myelin. This enables a fast saltatory action potential propagation because the exchange of ions is facilitated only in unmyelinated parts of axons, the so-called nodes of Ranvier. Oligodendrocytes have high metabolic rates especially during myelination and the high energy demand upon development is partly supplied by lactate from astrocytes via Monocarboxylic acid transporter 1 (MCT1, SLC16A1) (Rinholm et al. 2011; Simons and Nave 2015).

Astrocytes build the blood brain barrier and are important for the exchange of metabolic substrates from the blood as well as metabolic support of neurons and oligodendrocytes (Pellerin and Magistretti 1994; Pellerin et al. 1998; Tekkök et al. 2005; Simpson et al. 2007; Suzuki et al. 2011). Moreover, astrocytes are involved in the formation and function of synapses and brain homeostasis by maintaining a balanced concentration of ions and neurotransmitters and preventing neurons from glutamate excitotoxicity for instance (Sofroniew and Vinters 2010). Upon inflammation and CNS damage, astrocytes are involved in a reactive gliosis reaction and build glial scars to shield the healthy brain from the side of injury (Sofroniew and Vinters 2010).

Microglia, the resident macrophages of the CNS, constantly survey the CNS and are involved in a plethora of functions including chemotaxis, recognition of foreign particles, phagocytosis and tissue reparation. Microglia also play an important role in brain development (Kaur et al. 2017) and myelination (Bennett and Barres 2017; Hagemeyer et al. 2017; Wlodarczyk et al. 2017). Upon inflammation, microglia exert various pro- and anti-inflammatory functions and they are supported by an immigration of peripheral immune cells through the blood brain barrier.

## 1.2 Development, composition and function of myelin

Myelination occurred late in evolution parallel to hinge jaws. The first species that contains myelin in the CNS is cartilaginous fish (Zalc et al. 2008). The emergence of the myelin basic protein (MBP), the most important protein for myelin compaction in the CNS (Aggarwal et al. 2013), was an important step for myelination (Nave and Werner 2021). After the migration of oligodendrocyte progenitor cells (OPCs) to their final destination, they start to mature to newly formed and myelinating oligodendrocytes and produce the myelin sheath (Stadelmann et al. 2019). Myelination can be subdivided into intrinsic myelination, that occurs around birth and in early childhood, and adaptive myelination, that is not finished until postnatal day (P) 45 – 60 (Baumann and Pham-Dinh 2001) and even later in the cortex in mice. In humans, myelination continues until old age (Stadelmann et al. 2019) and is presumably a requirement for higher cognitive functions such as learning (Fields 2008; Filley and Fields 2016). The regulation of myelination in the CNS is highly complex and not yet fully understood (Mitew et al. 2014) and is also modified by axonal activity (Fields 2008; Gibson et al. 2014; Fields 2015; Hughes and Appel 2016). In case of diseases such as multiple sclerosis (MS), newly formed oligodendrocytes from OPCs can rebuild myelin, although remyelination is often incomplete and associated with a lifelong accumulation of neurological deficits (Franklin et al. 2012).

Axons in the CNS are wrapped up spirally with myelin from the innermost tongue (Snaidero et al. 2014; Snaidero and Simons 2017). The composition of myelin differs from that of other plasma membranes as myelin contains more lipids (cholesterol and sphingolipids, including galactocerebroside and sulphatide), making up for approx. 70% of the dry mass (Jahn et al. 2009). Proteomic analyses of purified myelin gave evidence, that myelin proteolipid protein (PLP) makes up for most of the proteins (38%), 30% of all proteins are MBP, 2´, 3´-cyclic nucleotide 3´-phosphodiesterase (CNP1) makes up 5% and myelin oligodendrocyte glycoprotein (MOG) 1% (Jahn et al. 2020) in addition to many more proteins known to be located in the myelin sheath. Myelin can be divided into a compact and a non-compact compartment

(Arroyo and Scherer 2000) and the different compartments contain specific proteins. MPB for example is mainly found in compact myelin, whereas non-compact myelin, for example, contains CNP1 and is also rich in cytoplasm, microtubules and vesicular structures. Non-compact myelin constitutes a system of cytosolic channels (also named cytoplasmic or myelinic channels) that comprises paranodal loops, outer tongues, inner tongues and additional cytoplasm-filled pockets within the compact myelin sheaths. Cytosolic channels are most prominent during myelination and have been recently better described by high-pressure freezing electron microscopy (Snaidero et al. 2014; Möbius et al. 2016; Snaidero et al. 2017). Beside its role as an insulator for fast saltatory propagation of action potentials, myelin serves as a protective isolator of axons from the extracellular milieu and thus mostly prevents electrical coupling between axons, so-called ephaptic events (Nave and Werner 2021). Moreover, myelin fulfills functions independent from isolation such as metabolic support with substrates such as lactate and pyruvate from glycolytic metabolism in oligodendrocytes (Edgar and Nave 2009; Fünfschilling et al. 2012; Lee et al. 2012; Saab et al. 2013; Philips and Rothstein 2017; Philips et al. 2021). Taken together, these functions are an important prerequisite for the well-being and long-term maintenance of axons. MCT1, a transporter for monocarboxylates such as lactate and pyruvate, is expressed in myelin (Rinholm et al. 2011) and has been shown to be localized at the adaxonal myelin membrane enabling a shuffle of metabolic substrates from myelin to the underlying axons (Lee et al. 2012; Saab et al. 2013). Mice with oligodendrocytes lacking MCT1 develop a dysfunction and loss of axons and neurons as well as hypomyelination (Philips et al. 2021). Moreover, oligodendrocytes and myelin function as an important storage of iron within ferritin (Francois et al. 1981; LeVine and Macklin 1990). Ferritin is an iron regulatory protein, that is composed of two types isotypes, ferritin heavy chain (Fth1) and ferritin light chain (Ftl), and can store up to 5000 iron molecules (Jian et al. 2016). FTH1 protein is secreted in vesicles by oligodendrocytes and a lack of Fth1 in oligodendrocytes has been recently shown to cause neurodegeneration and neuroinflammation (Mukherjee et al. 2020) as well as hypomyelination (Wan et al. 2020).

Myelin enriched fractions can be biochemically isolated (Smith 1969; Norton and Poduslo 1973; Jahn et al. 2009) and comprise lipid membranes as well as non-compact myelin including cytoplasm and ribonucleic acids (RNAs). The myelin transcriptome at the age of 6 months correlates well with the myelin proteome in wildtype mice (Thakurela et al. 2016) and contains a number of many different RNA molecules (approx. 21939) that is surprisingly comparable with the number of identified RNAs in myelinating oligodendrocytes (approx. 22462) (Zhang et al. 2014). Moreover, the myelin transcriptome is enriched for oligodendroglially expressed RNAs (Thakurela et al. 2016) since myelin is in continuum with the

oligodendroglial soma. Thus, as an oligodendroglial compartment, myelin can be analyzed for oligodendroglial reactions. This approach however has limitations, since the transcriptome of myelin has previously been described to represent a distinct entity (Thakurela et al. 2016). Most RNAs isolated from myelin likely diffuse from the oligodendrocyte´s cell soma within non-compact myelin such as cytosolic channels into the myelin sheath. However, the transcriptome of myelin is also highly enriched for specific RNAs actively transported into the myelin sheath and located in specific myelin sheath assembly sides (MSAS) such as Mbp-messenger RNA(mRNA) (Trapp et al. 1987; Ainger et al. 1993; Müller et al. 2013), Myelin Associated Oligodendrocyte Basic Protein(Mobp)-mRNA and Fth1-mRNA (Gould et al. 2000). Local translation of those RNAs is thought to allow for a rapid and selective incorporation of proteins depending on the local demands during myelination. MBP-mRNA has been even shown to being transported with proteins and RNAs necessary for its local translation (Colman et al. 1982; Barbarese et al. 1995) in RNA granules (Ainger et al. 1993) and the transport occurs most likely along microtubules with kinesin as a motor protein (Ainger et al. 1993; Carson et al. 1998). It is likely but not known so far, that this mechanism is similar for other suggested transported mRNAs such as Mobp and Fth1. Myelin proteins are especially needed during the process of myelination in young animals but also for a constant slow turnover due to loss of myelin and as an adaptive mechanism upon learning (Bergles and Richardson 2015; Buscham et al. 2019).

## 1.3 2´, 3´-cyclic nucleotide 3´-phosphodiesterase (CNP1)

CNP1 is a membrane-bound protein that is preferentially expressed by oligodendrocytes in the CNS and that is predominantly found in the non-compact myelin compartment (Trapp et al. 1988; Braun et al. 1988). *In-vitro* CNP1 has catalytic activity (Lee et al. 2001), however, this is not proven for its *in-vivo* function, which is not yet fully understood. CNP1 has been also suggested to be important for process outgrowth and arborization in oligodendrocytes and an overexpression of CNP1 leads to process outgrowth *in-vitro* (Lee et al. 2005) and *in-vivo* to aberrant myelin sheaths, a decrease of MBP in some myelin lamellae (Yin et al. 1997) and more non-compact myelin (Gravel et al. 1996). Interestingly, CNP1 binds RNA *in-vivo* and has been also shown to suppress mRNA translation *in-vitro* (Gravel et al. 2009). CNP1 has an important structural role for non-compact myelin and has been suggested to antagonize the function of MBP (Gravel et al. 1996; Yin et al. 1997) by preventing a complete compaction of myelin and enabling the development and maintenance of cytosolic channels (Snaidero et al. 2017). Those cytosolic channels are supposed to connect the oligodendroglial soma with the adaxonal myelin sheath and seem to be a prerequisite for myelination,

transport and diffusion of molecules (Snaidero et al. 2014; Snaidero et al. 2017). Cytoplasm-rich regions also contain microtubules (Snaidero et al. 2017) and since CNP1 copolymerizes with tubulin and interacts with actin (Gravel et al. 1996; Lee et al. 2005), it may regulate microtubule assembly (Bifulco et al. 2002) and influence transport into the myelin sheath. Not only mRNAs are transported along microtubules, but also other molecules such as proteins, organelles, vesicles and peroxisomes (Islinger et al. 2018). Extracellular vesicles, that are increasingly known to be crucial for intercellular communication and have been shown to be released from oligodendrocyte lineage cells (Krämer-Albers 2020), support axons during deprivation of nutrients, a mechanism that is disrupted in both CNP1- and PLP-deficient mice (Frühbeis et al. 2020). Thus, CNP1 might be a prerequisite for the transport of molecules from the oligodendroglial soma to the adaxonal myelin compartment and hence for the support of neurons and the long-term integrity of axons (Nave 2010; Simons and Nave 2015). Interestingly, after developmental myelination has ceased the number of cytosolic channels decreases (Snaidero et al. 2014; Snaidero et al. 2017) and the abundance of CNP1 protein has been also shown to decrease upon aging (Hagemeyer et al. 2012).

## 1.4 CNP1 null mutant mice and associated diseases in humans

The loss of CNP1 primary affects oligodendrocytes. Nevertheless, the myelin sheath of CNP1 null mutant animals appears rather normal on a structural level and is composed of compact and non-compact myelin and also the number of oligodendrocytes seems unaltered at the age of 3.5 months (Lappe-Siefke et al. 2003). CNP1 null mutant mice develop no symptoms until the age of 4 months, when they start to demonstrate neurological symptoms such as tremors, ataxia, convulsions and hindlimb impairments (Lappe-Siefke et al. 2003) as well as behavioral abnormalities such as anxiety (Edgar et al. 2011). At the age of 9 to 15 months the mice also develop anatomical abnormalities such as a kyphosis as well as weakness, weight loss and gait abnormalities (Lappe-Siefke et al. 2003). The progressive disease course leads to a reduction of total brain size and widely enlarged ventricles at 1 year of age (Lappe-Siefke et al. 2003). Finally, the mutation leads to a premature death at around 1 year on average (Lappe-Siefke et al. 2003). The mutants develop a transport dysfunction in axons as indicated by amyloid-beta precursor protein (APP) positive swellings and a resulting degeneration of neurons as well as an increase of activated microglia (Lappe-Siefke et al. 2003), which are both already present at P28 (Wieser et al. 2013). Previous experiments have demonstrated the important role of microglia in the pathology in CNP1 null mutant mice (Wieser et al. 2013; Janova et al. 2018). Additionally, there is an activation of astrocytes and also the adaptive immune system represented by an immigration of CD3+ T-cells especially

into white matter tracts (Wieser et al. 2013). The lack of CNP1 induces ultrastructural alterations in non-compact myelin for example in the structure of paranodes (Lappe-Siefke et al. 2003; Rasband et al. 2005) and inner tongues in myelin (Edgar et al. 2009), as well as a recently reported diminution of cytosolic channels, a system of cytoplasmic-rich channels within myelin sheaths, compared to wildtype animals (Snaidero et al. 2017). Oligodendrocytes lacking CNP1 are incapable of protecting axons in stress settings such as injury, which has been demonstrated in a model of brain trauma induced by cryolesions acting as a second hit in young CNP1 null mutant mice and accelerating behavioral abnormalities as well as axonal degeneration and inflammation, primary induced by the innate immune system, compared to CNP1-heterozygous and wildtype animals (Wieser et al. 2013).

Recently, a novel homozygous missense variant of CNP1 (S82L) has been discovered to cause a severe hypomyelinating leukodystrophy inducing, after a suggested normal development during the first year of life, symptoms such as neuroregression and irritability as well as poor growth, convulsions, progressive microencephaly and reduced white matter volume. This disease leads to a premature death in humans (Al-Abdi et al. 2020). The affected individual expressed a decreased abundance and lower stability of CNP1 as well as defects in cytoskeletal organization in fibroblasts (Al-Abdi et al. 2020).

Moreover, reduced expression of CNP1 is linked to an age dependent catatonia-depression syndrome that is similar in heterozygous CNP1 mice and humans with reduced CNP1 expression (Hagemeyer et al. 2012). Heterozygous CNP1 mice show behavioral abnormalities and a low-grade neuroinflammation and neurodegeneration, but only after around 19 months of age (Hagemeyer et al. 2012) or upon chronic social stress (Cathomas et al. 2019). CNP1 is reported to be reduced in neurological and psychiatric patients in several studies (Aston et al. 2005; Peirce et al. 2006; Mitkus et al. 2008; Natalia Silva et al. 2013), although the results are inconsistent by now (Che et al. 2009). Partial loss of function of CNP1 in patients due to the single nucleotide polymorphism rs2070106 (A/A instead of G/G) causing a reduced CNP1 expression by approx. 30% on RNA-level is associated with catatonia (Hagemeyer et al. 2012), which is a psychomotor symptom that can be diagnosed in a variety of psychiatric diseases. In humans there is a positive correlation between age and enhanced catatonia-depression score with the prevalence of rs2070106, as revealed by exploiting the Göttingen Research Association for Schizophrenia database that comprises over 1000 schizophrenic patients (Ribbe et al. 2010; Hagemeyer et al. 2012).

## 1.5 Neuroinflammation and the role of glial cells and immunomodulatory molecules

Inflammation is a common feature of several neurodegenerative and autoimmune CNS diseases (Amor et al. 2010; Amor et al. 2014) and mostly triggered by the activation and recruitment of cells of the adaptive and innate immune system including microglia and astrocytes as well as immigrating T-cells, B-cells and natural killer cells (Amor et al. 2010). Neuroinflammation and neuronal degeneration trigger each other and can lead to a vicious cycle of destruction with detrimental consequences to the environment due to the low regenerative capacities of CNS tissue.

Microglial phenotypes differ morphologically and can be divided into resting cells, exhibiting many thin processes, and activated, amoeboid like cells with fewer, shorter and thicker processes. Since microglia carry out various functions, they have been suggested to be categorized into M1 and M2 microglia similar to a concept of M1 and M2 macrophages. M1 microglia, induced by LPS and IFNγ stimulation, exhibit an upregulation of inducible nitric oxide synthetase (iNOS) and express proinflammatory cytokines such as interleukin (IL) 1β, tumor necrosis factor α (TNFα), CD86, IL-6, IL-12 via the transcription factor nuclear factor kappa-light-chain-enhancer (NF-ϰB) (Cherry et al. 2014; Tang and Le 2016; Afridi et al. 2020). M2 microglia, induced after treatment with IL-4, IL-13, IL-10 or TGFβ, are reparative, promote phagocytosis of debris and express proteins associated with cellular stability and repair. M2 microglia express molecules such as arginase 1 (Arg1), chitinase-3-like protein, RetnlB, mannose receptor C type-1 (CD206), IL-4, IL-10, CD163, Trem2 and Dectin-1 (Clec7a) (Cherry et al. 2014; Tang and Le 2016). This simplified classification does not fully resemble the complex and dynamic biology of microglia *in-vivo* especially under disease (Martinez and Gordon 2014; Ransohoff 2016; Bachiller et al. 2018). Thus, another subpopulation of microglia has been recently identified in a murine model of Alzheimer's disease and patients with Alzheimer's disease, so called disease-associated microglia (DAM) (Keren-Shaul et al. 2017). DAM can be induced by pathogen-associated molecular patterns (PAMPs) and damage-associated molecular patterns (DAMPs) (Seol et al. 2020). DAM have phagocytotic, certain pro-inflammatory and also anti-inflammatory capacity (Keren-Shaul et al. 2017). Moreover, they express genes involved in lysosomal function and lipid metabolism (Deczkowska et al. 2018). There is a Trem2 independent and Trem2 dependent induction causing the switch from homeostatic microglia to DAM. DAM express marker antigens are such as Aif1/Iba1, Trem2, Clec7a, Lpl, Spp1, Lyz2, Ms4a7, Gpnmb, Itgax, Ctsd, Cst7, B2m, Fth1, Ctsb, Tyrobp, Ccl6, Lilrb4a, H2-D1, Cd74 and Hexβ.

Next to the state of activation and molecular pattern of expressed molecules of microglia, it is necessary to unravel pathways of microglia activation because these shed further light on the underlying pathology and enable the investigation of possible rescuing procedures. Microglia and other cells of the brain express a variety of toll like receptors (TLR) (Olson and Miller 2004), which are important receptors of the innate immune system (Lehnardt 2009). TLRs are responsible for neurotoxic processes in the course of various CNS diseases (Lehnardt 2009). Antagonizing TLR1/2 for instance has led to a reduced secretion of TNFα *in-vitro* (Daniele et al. 2015). Most TLRs interact with Myeloid differentiation primary response gene 88 (MyD88) except for TLR3 (Yamamoto et al. 2003). The adaptor molecule MyD88 is part of a frequently found pathway of immune cell activation and TLRs and MyD88 have been found to play a role in various autoimmune diseases such as MS and neurodegenerative diseases such as Alzheimer's disease, Parkinson's disease and Amyotrophic lateral sclerosis (Xiang et al. 2015). MyD88 is an adaptor protein that also links Interleukin-33 (IL-33), IL1R, IL18R and most of the TLRs to downstream signaling molecules like TRAF6 and an activation of this pathway results in the synthesis of pro-inflammatory cytokines via NF-κB or mitogen-activated protein kinase (MAPK) (Lehnardt 2009). It has been demonstrated, that TLRs and MyD88 play an important role in neuronal death, oligodendrocyte injury (Okun et al. 2009) and demyelination in the CNS. Moreover, MyD88 has been demonstrated to play a crucial role in the recruitment of inflammatory cells such as leukocytes after a mechanical injury of the brain (Rosenberger et al. 2015).

Activated astrocytes also undergo a plethora of changes upon neuroinflammation including changes in morphology, proliferation and gene expression profiles (Zamanian et al. 2012). Recently, a similar concept of polarization has been suggested for activated astrocytes, dividing these cells into cytotoxic A1 astrocytes (Clarke et al. 2018) and neuroprotective, anti-inflammatory A2 astrocytes (Liddelow et al. 2017). Whether the differentiation of A1 astrocytes is facilitated by proinflammatory microglia (Liddelow et al. 2017) is under current debate (Hartmann et al. 2019). A1 astrocytes express markers such as C3, Cfb and Mx1 and promote neuronal and oligodendroglial death since they have no protective capacities anymore (Liddelow et al. 2017). A1 astrocytes increase upon aging as well as various neurodegenerative diseases such as Alzheimer's disease, Amyotrophic lateral sclerosis or MS (Liddelow et al. 2017; Clarke et al. 2018). In contrast, A2 astrocytes, which express S100a10 (Fujita et al. 2018), are induced by ischemia (Liddelow et al. 2017) and they are important for the maintenance of brain homeostasis and protection of neurons (Liddelow et al. 2017; Fujita et al. 2018). There are also typical astroglial markers that are expressed by both A1 and A2 cells

such as glial fibrillary acidic protein (Gfap), Slc1a3, Aldehyde Dehydrogenase 1 Family Member L1 (Aldh1l1) (Liddelow et al. 2017), Ndrg2 and S100β (Zhang et al. 2019). However, the biology of astrocytes is more complex upon inflammatory stimulation and also highly diverse in a time and brain region dependent manner (Hasel et al. 2021).

Oligodendrocytes are complex cells with a high demand of energy substrates making them vulnerable to stress upon oxygen deprivation, lack of energy or inflammation for instance (Zeis and Schaeren-Wiemers 2008; Bradl and Lassmann 2010). However, there is growing evidence, that oligodendrocytes can protect themselves from inflammation and also play an active role during the initiation and maintenance of neuroinflammation (Peferoen et al. 2014; Zeis et al. 2016; Jäkel et al. 2019). Oligodendrocytes are suggested to communicate with microglia via the expression of immune receptors and the production of cytokines, chemokines and other molecules, especially under stress conditions to recruit and activate microglia (Cannella and Raine 2004; Balabanov et al. 2007; Tzartos et al. 2008; Peferoen et al. 2014; Zeis et al. 2016). In MS lesions it was shown that oligodendroglial abnormalities such as apoptosis (Barnett and Prineas 2004; Trapp 2004) or a lack of oligodendrocytes (Traka et al. 2016) lead to a subsequent inflammatory response. Thus, oligodendrocytes are suggested to induce or strengthen inflammation by recruiting and activating microglia.

Secreted immunomodulatory molecules play an important role in neuroinflammation and neurodegeneration. TNFα induced protein 6 (TNFAIP6), also called TNFα stimulated gene 6 (TSG-6) is a secreted, hyaluronan-binding molecule. Its secretion is induced by TNFα and IL-1 (Wisniewski et al. 1993). TNFAIP6 has been shown previously to have anti-inflammatory effects (Wisniewski and Vilček 1997; Bárdos et al. 2001) and might serve as a potential biomarker of inflammatory disease activity. It has been detected to be associated with glial scar formation after a spinal cord injury (Coulson-Thomas et al. 2016). Interestingly, TNFAIP6 has been shown to express neuroprotective features and a therapeutic potential after brain injury has been observed in the brain of mice (Watanabe et al. 2013) and rats (Bertling et al. 2016). IL-33 is a cytokine secreted upon pro-inflammatory stimuli. It is known to be secreted by a variety of different cells and its RNA is highly abundant in the CNS (Hudson et al. 2008). Binding of IL-33 to the IL-1 receptor growth stimulation expressed gene 2 (ST2) (also known as Il1rl1) leads to an activation of NF-κB resulting in the translation of pro-inflammatory molecules (Miller 2011). In the CNS, IL-33 acts as a DAMP and alarmin and has been shown to alert the immune systems upon inflammatory processes by activating microglia and enhancing the production of pro- and anti-inflammatory molecules (Yasuoka et al. 2011). Interestingly, IL-33 has been shown to be also secreted by oligodendrocytes in

MS, which also express the receptor ST2 (Allan et al. 2016) and IL-33 is described to be involved in Alzheimer's disease (Chapuis et al. 2009; Yu et al. 2012; Saresella et al. 2020).

## 1.6 Aim of the study

Dysfunction of myelin is increasingly regarded to be crucial for a variety of neurological and psychiatric diseases, which are of high relevance in terms of demographic transition of our society, enhanced diagnoses and increasing costs for medical care and therapies. Therefore, a better understanding of I) functional consequences of CNP1 loss of function mutations as well as II) the roles of oligodendrocytes and myelin in neuroinflammation and neurodegeneration and III) the crosstalk between neurons and glial cells have important implications for CNP1 associated human diseases and conditions of neuroinflammation and neurodegeneration in general.

The chronological order and causal link between the loss of CNP1 on the one hand and neurodegeneration and neuroinflammation on the other hand are not yet fully resolved. Consequently, as a main question of interest, we want to firstly examine the early inflammatory process in myelin and whole brain lysate of CNP1 null mutant mice. In order to investigate, whether the observed inflammation is solely a reaction to axonal damage or whether it is also directly caused by the lack of CNP1, we aim to shed light on early oligodendroglial reactions to the loss of CNP1 that might influence the pathology of CNP1 deficient mice. A secretion of immunomodulatory molecules and toxic myelin products could modulate pathology in early and more advanced stages of the disease. Since the disease is clearly linked to a loss of a myelin protein and the inflammation is localized to the white matter, we investigate biochemically purified myelin, presenting the first data of a myelin transcriptome of CNP1 null mutant mice, as a suitable marker to analyze local reactions of oligodendrocytes and other glial cells to a disturbance of the myelin sheath.

Secondly, after identifying TLRs upregulated in our first analysis, we decided to further characterize astrocytes and microglia in CNP1 null mutants and investigate a common downstream signaling pathway activating NF-κB via the adaptor molecule MyD88 in activated microglial cells *in-vivo*. Hypothetically, if the MyD88-pathway was detrimental for the activation of microglia in this mouse model, a lack of MyD88 would lead to a decreased activation of microglia causing less inflammatory reaction and an amelioration of neurodegeneration in CNP1-MyD88 double mutant mice compared to CNP1 null mutants.

Since CNP1 is involved in the generation and maintenance of cytosolic channels (Snaidero et al. 2017), we furthermore want to utilize quantitative mRNA- and Western blot analyses

of purified myelin to offer insight into the functional consequences of a lack of CNP1 for mRNA and protein transport in cytosolic channels.

Thus, the aim of the study is to increase knowledge about the role of CNP1 in myelin and oligodendroglial dysfunction regarding transport into the myelin sheath and axonal support as well as the inflammatory reaction and glial crosstalk in CNP1 depleted mice.

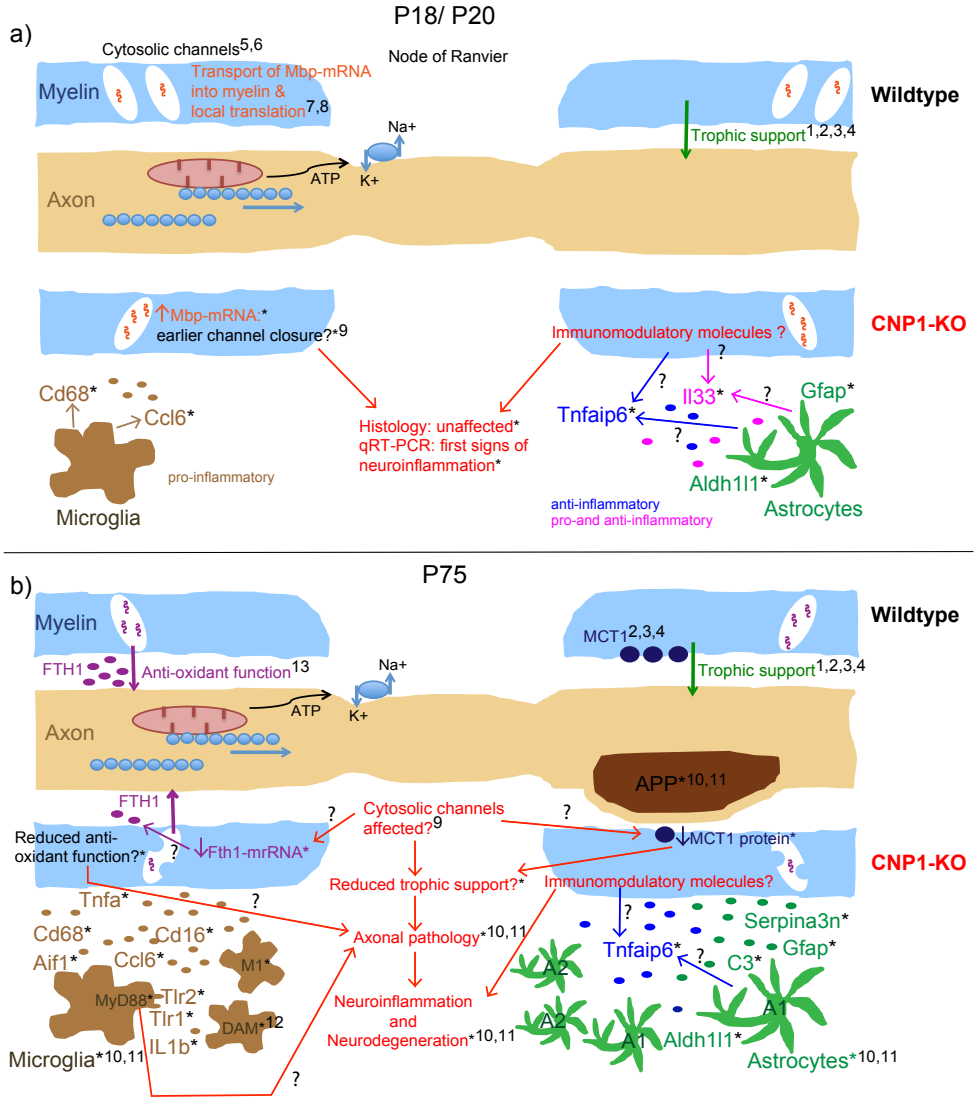


**Figure 1: Integrated hypothetical model of primary and secondary pathology of CNP1 null mutants based on literature and own findings.**

a) Myelin and oligodendrocytes are important for the long-term maintenance of axons as they shield the largest parts of the axon from the environment and support axons with energy metabolites (1, Fünfschilling et al. 2012; 2, Saab et al. 2016; 3, Lee et al. 2012; 4, Philips et al. 2021). Even though histopathology and RNA-Seq. are unaffected, CNP1 null mutant mice at P20 already show signs of an early pro-inflammatory reaction with an increased expression of microglial (Cd68, Ccl6) and astroglial (Gfap, Aldh1l1) mRNAs by sensitive qRT-PCR. Two immunomodulatory molecules (Tnfaip6, Il-33) are possibly secreted from oligodendrocytes and may influence the disease pathology early. The myelin contains cytosolic channels (5, Snaidero et al. 2014) filled with RNAs (6, Thakurela et al. 2016), that are partly actively transported into the myelin sheath and translated locally as shown for Mbp (7, Trapp et al. 1987; 8, Ainger et al. 1993). The null mutant mice depict higher concentrations of Mbp-mRNA in myelin, which may cause an earlier/ stronger closure of cytosolic channels (9, Snaidero et al. 2017). Neurodegeneration is absent at that age. b) CNP1 null mutant animals at P75 depict a microgliosis, astrogliosis and neurodegeneration including APP positive swellings in axons (10, Lappe-Siefke et al. 2003; 11, Wieser et al. 2013). Microglia are pro-inflammatory and express a DAM-like pattern (12, Depp et al. 2021), astrocytes express typical A1 and A2 genes. The myelin of older mice depicts fewer/ tighter closed cytosolic channels (13, Snaidero et al. 2014). A pathology of cytosolic channels in CNP1 null mutant mice may cause reduced Fth1-mRNA concentration with a possible resulting reduced anti-oxidant function as shown in mice with oligodendrocytes deficient for Fth1 (14, Mukherjee [...] Aicher et al. 2020). Moreover, a channel perturbation may result in reduced amounts of MCT1-protein in myelin of null mutants with a reduction of the metabolic glial support (2, Saab et al. 2016; 3, Lee et al. 2012; 4, Philips et al. 2021). Both pathologies probably cause neurodegeneration and further neuroinflammation in CNP1 null mutants. Findings from the literature are labelled with numbers (1 – 14), own findings are labelled with an asterisk.

# 2 Material and methods

## 2.1 Materials

### 2.1.1 Chemicals and consumables

**Table 1: General chemicals**

| Product | Company |
|---|---|
| Bovine Serum Albumine (BSA) | BioMol |
| Low fat milk powder | Frema |
| Sodium chloride | Merck |
| RNAse Away (Molecular BioProducts) | Carl Roth |
| Nuclease-free water | Promega |
| Ethanol 99% denatured 1% MEK | Chemie-Vertrieb Hannover |
| Ethanol | Merck |
| Methanol | J.T.Baker |
| Chloroform | Merck |

**Table 2: Chemicals of protein biochemistry**

| Product | Company |
|---|---|
| Acrylamide | Serva |
| Ammonium persulfate | BioRad |
| Bromophenol blue | Sigma |
| Complete Mini (Protease inhibitors) | Roche |
| Formaldehyde 37% | Merck |
| Glycine | Sigma |
| 2-Mercaptoethanol | Fluka |
| PhosStop (Phosphatase inhibitors) | Roche |
| Prestained Page Ruler Plus | Thermo Fisher |
| Nu-PAGE SDS (Sodium dodecyl sulfate) running buffer | Thermo Fisher |
| TEMED | Serva |
| Trizma Base | Sigma |
| Tween20 (Polysorbate) | Merck |
| Sucrose, RNase/ DNase free | Carl Roth |
| DC Protein Assay Kit | BioRad |
| Western Lightning Plus ECL | Perkin Elmer Life Sciences |
| DC Protein Assay | Bio-Rad (5000112) |

**Table 3: Chemicals of molecular biology**

| Product | Company |
|---|---|
| Agarose | AppliChem |
| GelRed | Biotrend |
| GenRuler 1 kb DNA ladder | Thermo Fisher |
| GenRuler 100 bp DNA ladder | Thermo Fisher |
| GoTaq II polymerase | Promega |
| Power SybrGreen | Applied Biosystems |
| Trizol Reagent | Invitrogen |
| Superscript III-reverse Transcriptase | Invitrogen |
| Co-Precipitant Pink | Bioline |
| Fast Green | Sigma F7252 |
| EDTA | Merck |
| DNase I | Roche |
| Agilent RNA 6000 Nano Kit | Agilent |
| Genomic DNA-Isolation Kit | Nexttec |
| RNeasy Mini Kit | Quiagen |

**Table 4: Chemicals of immunohistochemistry**

| Product | Company |
|---|---|
| Goat serum | Gibco |
| Haematoxylin (hemalaum solution) | Merck |
| Horse serum | Gibco |
| Paraformaldehyde, pure | Serva |
| Hydrogen Peroxide 3% H2O2 | Merck |
| Eukitt | ORSAtec |
| DAB Substrate Kit (Substrate Buffer and Chromogen) | Zytomed |
| Vectastain Elite ABC Kit | Vector/ Linaris |
| LSAB2 | DAKO |

**Table 5: Consumables**

| Product | Company |
|---|---|
| Coverslips 24x36 mm, 24x50 mm | Thermo Fisher |
| Histobond slides | Marienfeld |
| PVDF Western Blotting membranes Hybond P Aversham (pore size 0.45 µm) | Bioscience |
| Light Cycler 480 multiwell Plate 384 white | Roche |
| Light Cycler 480 multiwell Plate 384 sealing foil | Roche |
| 96-well PCR plate | Thermo Fisher |
| Barrier tips sterile 10 µl, 20 µl, 100 µl, 200 µl, 1000 µl | Thermo Fisher |
| Diamond tips 10 µl, 200 µl, 1000 µl | Gilson |
| SurPhob tips sterile 10 µl, 200 µl | Biozym |
| Parafilm | Bemis |
| Eppendorf safe-lock tubes 0.5 ml, 2 ml, 5 ml | Eppendorf |
| Biopsy cassettes | Formafix |
| Immersol 518 N | Zeiss |
| NuPAGE precast gel | Thermo Fisher |
| Whatman filter papers 3mm | GE Healthcare Life Sciences |

### 2.1.2 Machines

**Table 6: Machines**

| Product | Company |
|---|---|
| Agilent 2100 Bioanalyzer | Agilent |
| Axiophot Imager Z.1 | Zeiss |
| Centrifuge 5424R | Eppendorf |
| Embedding center AP280-1, 2, 3 | Microm |
| Intas ECL ChemoStar | Intas |
| Light Cycler 480 | Roche |
| NanoDrop2000 Spectraphotometer | Thermo Fisher |
| PCR-machine Thermocycler | Biometra |
| Sled microtome | Microm |
| Tissue Processor HMP110 | Microm |
| UV illuminator | Intas |
| Wet Chamber Blotting System | Thermo Fisher |
| Sorval wX+ Ultra Series Centrifuge | Thermo Fisher |
| Biofuge fresco | Heraeus |
| Biofuge Pico | Heraeus |
| Heat Sealer | 4titude |
| Axioskop microscope | Zeiss |
| Power Source | STARLAB |
| Chamber gel electrophoresis for PCR | MPIEM Feinmechanik |
| Waterbath 1000 | Pfm medical |
| XCell SureLockTM Mini-Cell Elecrophoresis | Thermo Fisher |
| Pipetman multistep multichannel | Gilson |
| Multipette pipette | Eppendorff |
| Multichannel pipette 10 µl, 200 µl | Eppendorff |
| Pipetman P2-P1000 | Gilson |
| T10 basic Ultraturrax | IKA |
| Platereader Eon spectralphotometer | BioTek |

### 2.1.3 Solutions and buffers

#### 2.1.3.1 General solutions and buffers

Phosphate-Buffered Saline (PBS) (10x)

1.7 M Sodium chloride (NaCl)

34 mM Potassium chloride (KCl)

40 mM ($Na_2HPO_4$) x $H_2O$ 18.4 mM ($KH_2PO_4$) x 2 $H_2O$

Adjusted to pH 7.2 with 1 M NaOH

*ad* 1000 ml *aqua destillata (dest.)*

Citrat buffer (0.1 M, pH 6)

9 ml stock solution A

0.1 M citric acid solution

41 ml stock solution B

0.1 M Sodium citrate solution

*ad* 500 ml *aqua bidest*

PBS/BSA

20 ml phosphate buffer stock solution A

80 ml phosphate buffer stock solution B

1.8g NaCl

1 g BSA

*ad* 100 ml *aqua dest.*

Tris-buffered saline (TBS)

1.36 M NaCl

26 mL KCl

250 mM Tris-Base

Adjust to pH 7.5 with 6 M HCl

*ad* 1000 ml *aqua dest.*

2.1.3.2 Solutions and buffers for animal perfusions

Avertin

1 g Tribromethanol

0.81 ml Amylalcohol

71.49 ml *aqua bidest*

Prewarmed *aqua dest.* (40°C) was added to Tribromethanol and amyl alcohol. The solution was stirred for 10 min and sterile-filtered. Afterwards the solution thawed and prewarmed in the dark before the injection into the animals.

Paraformaldehyde (PFA) (4%)

100 ml 37% formaldehyde (filtrated through two filter papers)

400 ml $H_20$

100 ml stock solution A

27.6 g $NaH_2PO_4$ in 1 l *aqua dest.*

400 ml stock solution B

35.6 g $Na_2HPO_4$ in 1 l *aqua dest.*

Approx. 100 ml per mouse were used.

### 2.1.3.3 Solutions and buffers for molecular biology

dNTPs

25 mM of dATP, dGTP, dCTP, dTTP (Merck)

20x Tris borate EDTA (TBE) buffer (gel electrophoresis)

108 g TrisBase

55 g Boric acid

3.6 g Ethylenediaminetetraacetic acid (EDTA)

### 2.1.3.4 Protein biochemical solutions

Transfer buffer

100 ml 20% methanol (MeOH)

25 ml 20x Nu Polyacrylamide gel electrophoresis (PAGE) transfer buffer

375 ml $H_20$

Tris buffered Saline with Tween20 (TBST)

1x TBS

200 mM Tris/HCl

1370 mM NaCl

adjusted to pH 7.4

0.05% Tween 20

Sodium dodecyl sulfate (SDS) sample buffer (4x)

40% [w/v] Glycerol

240 mM Tris/Cl pH 6.8

8% [w/v] SDS

0.04% [w/v] Bromophenol blue

Fast Green (1x)

10 ml 10x stock solution

5 mg fast green

60 ml *aqua dest.*

6.7 ml glacial acetic acid

*ad* 70 ml *aqua dest.*

30 ml MeOH

90 ml wash solution

6.7% acetic acid in 30% MeOH

2.1.3.5 Solutions for histology

Citrate Buffer (0.01 M, pH 6.0, freshly prepared)

9 ml of stock solution A (stored at 4°C)

0.1 M citric acid ($C_6H_8O_7$ x $H_2O$)

21.01 g citric acid (citric acid monohydrate)

*ad* 1000 ml *aqua bidest*

41 ml of stock solution B (stored at 4°C)

0.1 M sodium citrate ($C_6H_5Na_3O_7$ x $2H_2O$

29.41 m sodium citrate (Tri-sodium citrate dihydrate)

ad 1000 ml *aqua bidest*

450 ml *aqua bidest*

Tris Buffer

100 ml of stock solution A (0.5 M)

60.57 g TRIS(hydroxymethyl)-aminomethan

500 ml *aqua bidest*

30 ml HCl

Adjusted to pH 7.6 with 1 M HCl

*ad* 1000 ml *aqua bidest*

9 g NaCl

*ad* 1000 ml *aqua bidest*

Tris buffered milk (2%)

20 g low fat milk powder

1000 ml Tris buffer

The solution was stirred for approx. 20 min at room temperature and filtrated through a paper filter. It was stored at 4°C for max. two days.

TE buffer

20 mM Tris

1 mM EDTA

0.37 g EDTA

Adjusted to pH 9.0 with HCl

*ad* 1000 ml *aqua bidest*

HCl-Alcohol

0.09% [v/v] Hydrogen chloride fuming 70% [v/v] Ethanol

Scott's solution

0.2% [w/v] Potassium hydrogen carbonate 2% [w/v] Magnesium sulphate

#### 2.1.3.6 Solutions for myelin preparation

Diethylpyrocarbonate(DEPC)-treated water (0.1%)

1 ml DEP was applied to 1 l $H_20$. The solution was kept for at least 12 hours at 37°C and autoclaved twice for 30 min.

Sucrose solution

0.32 M sucrose: 27.38 g sucrose *ad* 250 ml DEPC water. Sterile filtered.

0.85 M sucrose: 72.75 g of sucrose *ad* 250 ml DEPC water. Sterile filtered.

Tris-buffered saline (TBS)

1370 mM NaCl

200 mM Tris/HCl pH 7.4

*ad* 200 ml *aqua dest.*

### 2.1.4 Antibodies

**Table 7: Primary antibodies**

| Antibody | Species | Description | Dilution | Supplier/ Company | Application |
|---|---|---|---|---|---|
| APP | Mouse | monoclonal | 1:1000 | Millipore | Immunohistochemistry |
| Atp1a1 | Mouse | monoclonal | 1:2000 | Abcam | Western blot |
| CD3 | Rat | monoclonal | 1:150 | Abcam | Immunohistochemistry |
| CD3 | Rat | monoclonal | 1:250 | Abcam | Immunohistochemistry |
| Fth1 | Rabbit | polyclonal | 1:800 | Abcam | Western blot |
| GFAP | Mouse | monoclonal | 1:200 | Dako | Immunohistochemistry |
| Iba1 | Goat | polyclonal | 1:1000 | Abcam | Immunohistochemistry |
| Mac3 | Rat | monoclonal | 1:400 | BD Biosci-ences | Immunohistochemistry |
| Mct1 | Rabbit | polyclonal | 1:1000 | Kathrin Kusch | Western blot |
| TSG-6 | Rat | monoclonal | Western blot: 1:1000, 1:500; IHC: 1:100 | Santa Cruz | Immunohistochemistry (IHC), Western blot |
| TSG-6 | Rabbit | polyclonal | 1:200, 1:100 | Abcam | Immunohistochemistry |

**Table 8: Secondary antibodies**

| Antibody | Species | Dilution | Supplier/ Company | Application |
|---|---|---|---|---|
| HRP-conjugated anti-mouse | goat | 1:10000 | Dianova | Western blot |
| HRP-conjugated anti-rabbit | goat | 1:10000 | Dianova | Western blot |

### 2.1.5 Oligonucleotides and primers

The primers were all designed by the AGCT-lab of the Max-Planck-Institute of Experimental medicine. Some primers were already available. I designed the others using the ensemble genome browser 95 and the Roche database. All primers were controlled for their specificity with a melting curve analysis before performing the experiments. The results were normalized with housekeeper genes and compared to general cell markers for microglial and astrocytic cells.

**Table 9: Primers for genotyping**

| Gene | Primer | Sequence 5´-3´ |
|---|---|---|
| CNP1 | puro3 - 1955 | CATAGCCTGAAGAACGAGA |
| | CNP1-E3sense - 2016 | GCCTTCAAACTGTCCATCTC |
| | CNP1-E3santiense - 7315 | CCCAGCCCTTTTATTACCAC |
| MyD88 | 19809 | TGGCATGCCTCCATCATAGTTAACC |
| | 19810 | GTCAGAAACAACCACCACCATGC |
| | 19811 | ATCGCCTTCTATCGCCTTCTTGACG |

**Table 10: Primers for qRT-PCRs**

| RNA | Direction | Sequence 5´-3´ |
|---|---|---|
| Aif1 = Iba1 | Forward | CCGAGGAGACGTTCAGCTAC |
| | Reverse | TGTTTTTCTCCTCATACATCAGAATC |
| Aldh1l1 | Forward | CGAGTTGAAAAACGTCAGCTT |
| | Reverse | AATGACAAGGTGCCAGGTG |
| Arg1 | Forward | GAATCTGCATGGGCAACC |
| | Reverse | GAATCCTGGTACATCTGGGAAC |
| Atp1a1 (housekeeper) | Forward | GGCCTTGGAGAACGTGTG |
| | Reverse | TCGGGAAACTGTTCGTCAG |
| Ccl6 | Forward | TCTTTATCCTTGTGGCTGTCC |
| | Reverse | TGGAGGGTTATAGCGACGAT |
| Cd163 | Forward | CCTGGATCATCTGTGACAACA |
| | Reverse | TCCACACGTCCAGAACAGTC |
| Cd206 | Forward | CCACAGCATTGAGGAGTTTG |
| | Reverse | ACAGCTCATCATTTGGCTCA |
| Cd68 | Forward | GGACTACATGGCGGTGGA |
| | Reverse | GATGAATTCTGCGCCATGAA |
| Cxcl10 | Forward | GCTGCCGTCATTTTCTGC |
| | Reverse | TCTCACTGGCCCGTCATC |

| RNA | Direction | Sequence 5´-3´ |
|---|---|---|
| Fth1 | Forward | CAGACCGTGATGACTGGGAG |
| | Reverse | CTCAATGAAGTCACATAAGTGGGG |
| Gfap | Forward | TGCTCCTGCTTCGAGTCCTT |
| | Reverse | TCAAGAGGAACATCGTGGTAAAGA |
| Hprt (housekeeper) | Forward | CCTGGTTCATCATCGCTAATC |
| | Reverse | TCCTCCTCAGACCGCTTTT |
| IL-1β | Forward | AGTTGACGGACCCCAAAAG |
| | Reverse | TTTGAAGCTGGATGCTCTCAT |
| Il-33 | Forward | GGTGAACATGAGTCCCATCA |
| | Reverse | CGTCACCCCTTTGAAGCTC |
| iNOS = Nos2 | Forward | TGAACTTGAGCGAGGAGCA |
| | Reverse | TTCATGATAACGTTTCTGGCTCT |
| Mbp | Forward | AACATTGTGACACCTCGAACA |
| | Reverse | AGAGCGGCTGTCTCTTCCT |

### 2.1.6 Enzymes

GoTaq DNA Polymerase

Superscript

Proteinase K

### 2.1.7 Microscopes, software and statistical analysis

Zen Blue for imaging of the histology

Image J version 1.47 and Fiji version 1.0 for analyses of histology and Western blots

Lightcycler 480 software version 1.5 for analysis of qRT-PCRs

Microsoft Excel for Mac 2011 for statistical analyses

Microsoft Power Point for Mac 2011 for the creation of figures

GraphPad Prism 8.0 (GraphPad Software, San Diego, CA) for statistical analysis

Adobe Illustrator CC2017 for the creation of figures

Adobe Photoshop CC2017 for the creation of figures

GSEA version 4.1.0, 2003 – 2019 (Broad Institute, Inc., Massachusetts Institute of Technology, and Regents of the University of California) for gene ontology pathway analysis

R (version 3.0.5) for differential gene expression analysis of RNA-Seq. data

## 2.2 Methods

### 2.2.1 Animals

#### 2.2.1.1 Genotype, background and housing of mouse mutants

For investigating the crosstalk of different cells in the CNS, animal experiments with mice were conducted. Wildtype, CNP1 heterozygous, CNP1 null mutant, MyD88 null mutant and MyD88-CNP1-double knockout animals were used. All animals had a C57Bl6 background. Both female and male animals were included. The experiments were performed with littermates whenever possible.

The CNP1 animals and their wildtype controls were bred at the animal facility of the MPIEM (Göttingen). The MyD88 cohort (MyD88 null mutants, MyD88-CNP1 double knockout, some of the CNP1 null mutants and wildtype controls) were supplied by the animal facility of the Charité (Berlin, Seja Lehnardt). All animals were kept in the animal facility of the MPIEM (Göttingen). In general, they were housed in groups of 2 – 4 animals in standard cages at a 12 hours light-dark cycle. They had access to food and water ad libitum.

Animals for the immunohistochemistry were 18 days, 75 days or 30 – 34 weeks old. Animals for the RNA-Seq. analysis, qRT-PCRs and Western blots were 18, 20 or 75 days old.

All experiments were conducted according to the Lower Saxony State regulations for the use of experimental animals in Germany as approved by the Niedersächsische Landesamt für Verbraucherschutz und Lebensmittelsicherheit (LAVES). The animal experiment proposal is listed under 33.19-42502-04-17/2409.

#### 2.2.1.2 Genetics

##### 2.2.1.2.1 CNP1 null mutant mice

The coding region including most of exon 1 – 3 of 2',3'-Cyclic-nucleotide 3'-phosphodiesterase (CNP1) on chromosome 11 was replaced with a Cre recombinase (Lappe-Siefke et al. 2003). The CNP1 deficient animals develop an astrogliosis and microgliosis as well as axonal degeneration (Lappe-Siefke et al. 2003). The animals start to develop symptoms such as a hind limb paralysis and kyphosis at around 4 months and die prematurely at around one year (Lappe-Siefke et al. 2003).

##### 2.2.1.2.2 MyD88 null mutant and CNP1-MyD88 double knockout mice

The MyD88 and CNP1-MyD88 deficient mice were generously provided by Prof. Dr. Seija Lehnardt (Charité, Berlin). The animals were designed in Japan by Shizuo Akira (Department of Biochemistry, Hyogo College of Medicine, 1-1 Mukogawa-cho, Nishinomiya, Hyogo, 663-8501,

Japan). The mice do not develop a pathology until 20 weeks of age (Adachi et al. 1998). Nevertheless, abnormalities in behavior and brain development are described (Schroeder et al. 2021). To my knowledge, no data have been published with CNP1-MyD88 double knockout mice so far. The animals came from two different cohorts. Göttingen animals are depicted in blue, Berlin animals are depicted in black.

### 2.2.2 Genotyping

In order to validate the animals' genotypes, all animals were genotyped at least twice. Mostly, a small piece of the ear and/or the tail were used, in some cases we also used material embedded in paraffin.

#### 2.2.2.1 DNA digestion

For the deoxyribonucleotide acid (DNA) digestion, the "nexttec"-kit was used in the vast majority of cases. The digestion of the murine material was done according to the manufacturers protocol with 265 µl G1 buffer, 10 µl G2 buffer, 25 µl G3 buffer for approx. 60 min at 62°C on 1200 revolutions per minute (rpm). The extraction columns were equilibrated with buffer for 5 min at room temperature. 120 µl of the digestion mix was filtrated through the column with a centrifuge and the DNA was stored at 4°C.

#### 2.2.2.2 DNA isolation from paraffin embedded tissue

The DNA isolation from paraffin embedded tissue was done according to the manufacturers protocol. The embedded tissue was mixed with 1 ml Octane and vortexed to dissolve the paraffin. The solution was centrifuged for 2 min at 12000 rpm, the supernatant discarded and the pellet was washed again with 1 ml Octane. Afterwards, the pellet was mixed with 100% ethanol (EtOH), shortly centrifuged, the EtOH aspirated and the pellet was dried at 52°C. Afterwards, 1 ml PBS buffer with 2 mM DTT were added to the DNA solution and mixed for 20 min at 99°C. The probe was centrifuged at 12000 rpm, the supernatant was discarded, 1ml of PBS was added, centrifugation for 1 min at 12000 rpm was performed and the supernatant was discarded again. 1 mM DTT in lysis buffer was added, vortexed and incubated at 52°C for at least 120 min. Then, 400 µl lysis buffer and 40 µl proteinase K were added and incubated for approx. 15 min. 200 µl of binding buffer were added and the probe was vortexed. The solution was spin filtered, the column was washed with EtOH, the DNA was eluted with prewarmed (52°C) elution buffer and stored at 4°C.

#### 2.2.2.3 Polymerase chain reaction (PCR)

For the Polymerase chain reactions, the DNA was mixed with primers, desoxyNucleosidTriPhosphates (dNTPs), Taq polymerase, buffer and water. First, the primers annealed to the complementary DNA segment, afterwards, the oligomers were elongated enzymatically by the polymerase and finally, the DNA was heated again and the two strands separate from each other (denaturation). This enables a specific and exponential amplification of the gene region of interest.

**Table 11: Procedure of CNP1-PCR**

| Components | Reaction conditions |
|---|---|
| 9.9 µl H2O (Millipore)<br>0.5 µl puro3 (10pmol/µl stock)<br>0.5 µl CNP1-E3sense (10pmol/µl stock)<br>1.0 µl CNP1-E3antisense (10pmol/µl stock)<br>2.0 µl dNTPs<br>4 µl Go Taq Buffer<br>0.1 µl Go Taq Polymerase<br>2 µl tail DNA | Annealing 56°C (30 sec)<br>Elongation 72°C (90 sec)<br>Denaturation 95°C (60 sec)<br>35 cycles |

**Table 12: Procedure of MyD88-PCR**

| Components | Reaction conditions |
|---|---|
| MyD88 WT<br>10.9 µl H2O (Millipore)<br>1.0 µl Primer 1 #19809 (10 pmol/µl)<br>1.0 µl Primer 2 #19810 (10 pmol/µl)<br>1.0 µl dNTPs (2.5 mM)<br>4 µl Go Taq Buffer<br>0.1 µl Go Taq Polymerase<br>1 µl tail DNA | 95°C (5 min)<br>95°C (30 sec)<br>69°C (30 sec)<br>72°C (30 sec)<br>72°C (8 min)<br>35 cycles |
| MyD88 NEO<br>10.9 µl H2O (Millipore)<br>1.0 µl Primer 1 #19809 (10 pmol/µl)<br>1.0 µl Primer 3 #19811 (10 pmol/µl)<br>1.0 µl dNTPs<br>4 µl Go Taq Buffer<br>0.1 µl Go Taq Polymerase<br>1 µl tail DNA | 95°C (5 min)<br>95°C (30 sec)<br>69°C (30 sec)<br>72°C (30 sec)<br>72°C (8 min)<br>35 cycles |

Afterwards, 5 µl GelRed (1:2500 diluted in $H_2O$) was added to each DNA sample. The DNA was applied on a 2% agarose gel (agarose in TBE buffer) and gel electrophoresis was performed with 120 Volt (V) for approx. 20 – 30 min.

### 2.2.3 Histology and immunohistochemistry

#### 2.2.3.1 Animal perfusion

The mice were anesthetized with 0.5 – 0.6 ml Avertin based on their individual weight. The anesthesia was controlled with pain stimuli at the toes of the animals. When the animal did not react to the stimuli, the abdomen and chest were opened in order to get access to the left heart chamber. The animals were perfused with Hank´s balanced salt solution (HBSS). This procedure prevents coagulation and ensures a distribution of the fixative PFA. After approx. 10 min, they were perfused with 4% PFA in order to fixate all structures and enable a staining. The brain was dissected and post-fixated in 4% PFA for 2 – 4 hours. Afterwards it was transferred in PBS solution or directly embedded in paraffin (50% EtOH 1 h, 70% EtOH 2 h, 70% EtOH 2 h, 96% EtOH 1 h, 96% EtOH 1 h, 100% EtOH 1 h, 100% EtOH 1 h, Isopropanol 1 h, Xylol 2 h, Xylol 2 h, Paraffin 2 h, Paraffin 2 h).

#### 2.2.3.2 Paraffin sections

The paraffin sections were obtained from the paraffin blocks with a sledge microtome. Each slide was 5 µm thick. According to the standard procedure, the slices were put into cold water and afterwards they relaxed in a 40°C water bath. There they were brought up onto a glass slide and dried over night at 37°C.

#### 2.2.3.3 Chromogenic immunohistochemistry with Dako-LSAB2 and DAB

Chromogenic immunohistochemistry was carried out according to a standard procedure. The slides were incubated at 60°C for 10 min in order to melt the paraffin. Afterwards, the remaining paraffin was removed by an incubation in xylol, xylol, xylol/isopropanol (each for 10 min), 100% EtOH, 90% EtOH, 70% EtOH, 50% EtOH, $H_2O$ (each for 5 min). The slides were incubated for 5 min in citrate buffer and cooked for 10 min in cooking citrate buffer (600 W). A possible loss of liquid was settled, so that the slides did not dry out. For the CD3 staining, TE buffer was used instead of the citrate buffer. Otherwise, the procedure is the same.

The slides cooled down in the citrate buffer at room temperature for approx. 20 min. Afterwards, the slides were blocked with 2% low fat milk powder in Tris buffer for 5 min. The slides were put on coverplates, where they were flushed and controlled for air bubbles. The peroxidase was inactivated for 5 min with 3% $H_2O_2$. Afterwards, the slides were flushed again with Tris buffer. They were blocked for 10 min with 20% goat or horse serum in PBS/BSA in order to prevent an unspecific background staining. Afterwards, the primary antibody was applied (diluted in PBS/BSA) and the slides were stored overnight at 4°C. At the next day, the slides were rinsed with 2% low

fat milk powder in Tris buffer. 100 µl $LSAB_2$ per slide were applied and incubated for 10 min at room temperature. The slides were rinsed again with 2% low fat milk powder in Tris buffer and the horseradish-peroxidase-streptavidin-complex was incubated for 10 min at room temperature. The slides were rinsed in Tris buffer. Then 10 µl substrate buffer + 0.5 µl Diaminobenzidine (DAB) per slide were mixed and incubated for 10 min. The slides were rinsed two times with $H_2O$ for approx. 5 min and stained in Haemalaun (filtered shortly before used; 30 sec). After rinsing them in *aqua dest.* (approx. 10 sec), they were shortly incubated in HCl-alcohol, *aqua dest.* (approx. 10 sec), Scott's solution (5 min), *aqua dest.* (approx. 10 sec), 50% EtOH, 70% EtOH, 90% EtOH, 100% EtOH (each for 5 min), xylol/isopropanol, xylol, xylol (each for 10 min). The slides were covered with cover slips with Eukitt.

The analysis of immunohistochemistry was performed on Corpus Callosum (Bregma 0.5 to 0.74 regarding Allen Brain Atlas), anterior commissure (Bregma: 0.5 to 0.74 regarding Allen Brain Atlas) and fimbriae (Bregma -1.46 to -1.70 regarding Allen Brain Atlas).

#### 2.2.3.4 Chromogenic immunohistochemistry with Vector Elite ABC and DAB

The procedure was exactly the same as immunohistochemistry with the Dako-$LSAB_2$ system. Instead of the $LSAB_2$ and the horseradish-peroxidase-streptavidin-complex, 2.5 ml 1xPBS was mixed with one drop of solution A and one drop of solution B and incubated for approx. 30 min at room temperature.

#### 2.2.3.5 Histology analysis

Light microscope images were captured in 20x (Mac3, Iba1, CD3) or 40x (APP). For the MyD88-CNP1 project, corpus callosum (Mac3, APP, CD3, Iba1) and anterior commissure (Mac3, APP, Iba1) were analyzed. For the CNP1 P18 vs. P75 project, corpus callosum (Mac3, APP, Gfap, Iba1) and fimbriae (Mac3, APP, Gfap, Iba1) were analyzed. Analysis of the immunohistochemistry was conducted manually with Image J and Fiji. The counting of cells and APP-positive swellings was performed under blinded conditions. Mostly, two areas of one animal were counted and the mean value was included into the statistical analysis.

### 2.2.4 Myelin preparation

Myelin preparation was done according to a standard procedure (Smith 1969; Norton and Poduslo 1973) and adapted for RNA analysis according to a protocol published by our lab in 2016 (Thakurela et al. 2016). The myelin was purified with two sucrose gradients. One day in advance, the RNAse free sucrose was prepared: For the 0.32 M sucrose, 27.38 g RNase and DNase-free sucrose

were diluted and the solution was filled up to 250 ml of DEPC water. For the 0.85 M sucrose, 72.75 g of RNase and DNase-free sucrose were used. After the solutions were sterile filtered, they were stored at 4°C over night. The sucrose was always prepared freshly. In a first step, the brains were homogenized with an Ultraturrax in 5 ml of the 0.32 M sucrose for 30 – 40 sec. The sucrose contains a proteinase inhibitor. Afterwards, 200 µl of the brain lysate were frozen away for later analysis and the brain lysate was added onto 6 ml of the 0.85 M sucrose very carefully without mixing the phases. The centrifugation was carried out with Sorval ultracentrifuge (TH641 rotor). For the first step, the brain lysate in sucrose was centrifuged at 24400 rpm for 30 min with a slow acceleration and deceleration. The myelin concentrates in the interphase. The interphase was taken up with a Pasteur pipette and washed with DEPC water in the second centrifugation step (24400 rpm, 15 min, acceleration and deceleration at maximum). The pellet was resuspended in water and centrifuged for 15 min at 9800 rpm at maximum acceleration and deceleration. The washing step was repeated once. Now the pellet was resuspended in 5 ml 0.32 M sucrose and again placed on top of 6 ml 0.85 M sucrose. After the centrifugation (24400 rpm, 30 min, slow acceleration and deceleration), the interphase was washed once more with DEPC water (24400 rpm, 15 min, acceleration and deceleration at maximum) and the pellet was taken up in 300 µl Quiazol and stored at -80°C. The Quiazol prevents a possible degradation of RNA. Since the brain of 20 days old animals is smaller and contains less myelin due to the ongoing developmental myelination, two brains of these animals were taken together. The brains of the 75 days old animals were taken individually.

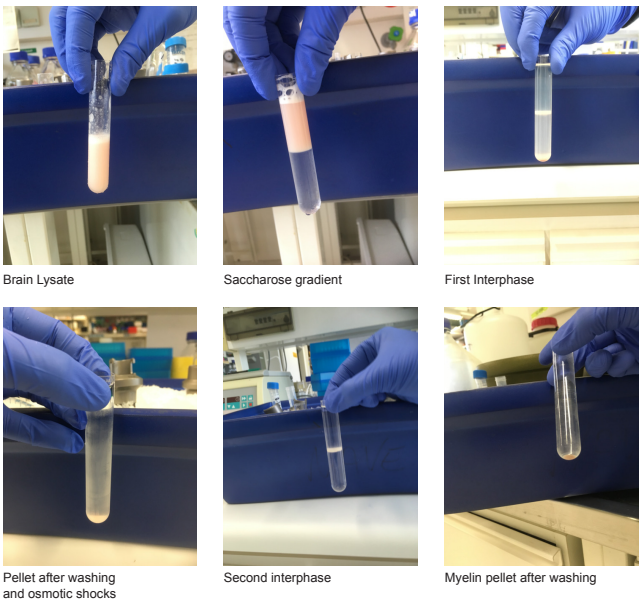


**Figure 2: Myelin preparation**

### 2.2.5 RNA isolation, cDNA synthesis and qRT-PCRs

#### 2.2.5.1 RNA isolation

In order to isolate RNA out of the purified myelin, the lipid-rich compact material had to be broken up mechanically. The myelin was lysed by mixing it for 10 min on a vortex machine. RNA was then isolated with the RNeasy mini kit according to the manufactures protocol. Afterwards, chloroform was added and the probe was stirred again. The homogenate was centrifuged and the upper aqueous phase was mixed with 70% EtOH and pipetted onto the column. The solution was washed with RW1- and RPE buffer and DNase (10 µl in 70 µl RDD) was applied in order to ensure the purity of the RNA. Elution was carried out two times with 30 ml RNase free water and the RNA was stored at -80°C. RNA from the brain lysates was isolated according to the manufactures protocol.

RNA concentration was measured with the Agilent system. This was not only important for the cDNA synthesis, but also to compare the RNA-amount of the different tissues (myelin vs. brain lysate), ages (P20 vs. P75) and genotypes (CNP1 null mutant vs. wildtype). The quality of isolated RNA was measured with RNA integrity number (RIN) analysis. All probes had RIN levels between 2.9 and 9.5, on average the RIN was 8.23 (CNP1 null mutant P20), 7.845 (CNP1 null mutant P75), 7.833 (wildtype P20) and 8.24 (wildtype P75).

#### 2.2.5.2 RNA precipitation

The isolated RNA was precipitated with Co-precipitant pink in order to increase its concentration. 0.5 volume (30 µl) of 7 M ammoniumacetate was added to the RNA in water (60 µl) together with 0.05 volume (3 µl) and the probe was vortexed. 2.5 volume (225 µl) of 100% EtOH were added, mixed and centrifuged for approx. 30 min at 12000 rpm and 4°C. The supernatant was immediately suspended and the small pellet with RNA was washed with 200 µl 70% EtOH. It was centrifuged for 10 min at 12000 rpm and 4°C. The supernatant was sucked off again and the pellet was dried on ice until the rest of the EtOH was vaporized and the pellet had turned beamless. The pellet was resuspended in approx. 10 µl $H_2O$ and stored at -20°C or -80°C.

#### 2.2.5.3 cDNA synthesis

For the quantitative RT-PCR, cDNA was synthesized according to the manufactures protocol. RNA, #9578 Anchored oligo dT-Mix and #4542 N9 were mixed and incubated for 2 min at 70°C (PCR machine). The Master Mix was prepared by mixing first strand buffer, DTT, dNTPs and Superscript III reverse transcriptase. Master Mix was added to the RNA-primer-solution, briefly

spun down and the reverse transcriptase process was started. The cDNA was stored at -80°C or at -20°C.

**Table 13: Procedure of cDNA synthesis**

| | |
|---|---|
| 4 µl (8 µl) RNA<br>1 µl (2 µl) primer-mix (0.6 pmol/µl)<br>1 µl (2 µl) N9 primer (120 pmol/µl) | 70°C for 2min |
| 2 µl (4 µl) 5x strand buffer<br>1 µl (2 µl) 0.1 M DTT<br>0.5 µl (1µl) dNTPs (10 mM)<br>1 µl (2 µl) Superscript III (200 U/µl) | 25°C for 10 min<br>50°C for 45 min<br>55°C for 45 min |

2.2.5.4 q-RT-PCR

In order to compare the amount of RNA in the different genotypes, tissues and ages, we performed quantitative real time PCRs (qRT-PCRs). 2 µl cDNA were pipetted into the 384 well plates. Afterwards, 8 µl of master mix, consisting of 5 µl 2xSYBR Green, 0.2 µl forward and 0.2 µl reverse primer and 2.6 µl RNAse free water were added. The plate was covered, the solution spun down and the qRT-PCR was started.

**Table 14: Procedure of qRT-PCR**

| | |
|---|---|
| Warm up | 1 cycle<br>50°C for 2 min<br>ramp rate (°C/s) 4.8 = max |
| Activation | 1 cycle<br>95°C for 10 min<br>ramp rate (°C/s) 4.8 |
| Amplification and quantification | 45 cycles<br>95°C for 15 sec (ramp rate (°C/s) 4.8)<br>60°C for 1 min (ramp rate (°C/s) 2.5) |

The qRT-PCRs are normalized with housekeeper genes. There are very few papers published with RT-PCRs based on myelin. Therefore, there are no standard housekeeper genes for myelin and we had to define own criteria and find suitable genes. According to the myelin transcriptome and the qRT-PCRs, we defined several prerequisites for these genes. First, the genes should have high reads in myelin as well as a similar concentration in myelin compared to brain lysate. Moreover, the reads had to be similar in wildtype and CNP1 null mutant mice as well as at both ages (P20 and P75). Atp1a1, Hprt and Rplp0 fulfilled these criteria.

### 2.2.6 Western Blot

To analyze the impact of loss of CNP1 on the abundance of the transporter MCT1 in the myelin, Western blot analysis of MCT1 was performed. The number of tested animals was three per group (CNP1 null mutants and wildtype controls both at P75).

#### 2.2.6.1 Brain lysate

Half of a brain was homogenized with an Ultraturrax and 200 µl were mixed with proteinase inhibitor in TBS. The proteinase inhibitor was dissolved in 25 ml of TBS at 4°C under rotation.

#### 2.2.6.2 Protein concentration and sample preparation

Protein concentration was determined using the Bio-Rad DC Protein Assay according to the manufacturer's protocol. A standard protein concentration curve was prepared using BSA (0, 1, 1.5, 2, 2.5, 3 µg/µl in TBS). 5 µl sample or standard were added to 25 µl protein assay reagent A and 200 µl protein assay reagent B. The solutions were incubated for approx. 10 min on a shaker at room temperature. The concentration was measured at the Platereader Eon. Protein samples were diluted in 1x SDS to a concentration of 0.75 µg/µl by adding $H_2O$. If the samples were tested under reduced conditions 5% ß-mercaptoethanol was added. Before loading the SDS gel, samples were heated for 15 min at 40°C.

#### 2.2.6.3 Electrophoresis

The electrophoresis was performed with NuPAGE 4 – 12% Bis-Tris Gel according to the manufacturer's protocol. The chamber was filled with 1x MOPS buffer and the wells were washed with a pipette. 5 µg of marker were loaded and 20 µg of the samples. The voltage was set to 130 V for 90 min.

#### 2.2.6.4 Wet Blot

Wet blot was performed using the Invitrogen X-Cell II Blot Module (EI9051) according to the manufacturer's protocol. Sponges and 3 mm Whatman filter papers were pre-soaked with transfer buffer. The gel was placed in Transfer Buffer for 10 min. The PVDF membrane was activated for 60 sec in MeOH, briefly rinsed in deionized water and also placed in the transfer buffer. Three sponges and two filter papers were placed in the bottom chamber. The PVDF membrane and the gel were placed on top. Any bubbles were carefully removed. Two more filter papers and three sponges were placed on top. The blot was carried out with 35 V for 60 min.

#### 2.2.6.5 Protein staining with Fast Green

For the Fast Green staining, the membrane was washed in water and incubated for approx. 10 min in 1x Fast Green solution. Afterwards, the membrane was washed with washing buffer and a fluorescent image was taken with Intas ECL ChemoStar. Then the membrane was destained with destaining solution for 10 min and two times for 5 min in water until the pH was no longer acidic.

#### 2.2.6.6 Staining

The membrane was blocked for 60 min in 5% low fat milk powder in TBST at room temperature on the shaker. The primary antibody was diluted in 5 ml of 5% low fat milk powder in TBST and the membrane was incubated in a 50 ml Falcon tube over night at 4° on the rotator. Afterwards, the membrane was washed three times for 5 min in TBST. The secondary antibody was also diluted 5 ml of 5% low fat milk powder in TBST and applied for 60 min at room temperature on the shaker. The membrane was again washed three times for 5 min in TBST and developed.

#### 2.2.6.7 Developing

Staining was visualized using Western Lightning Plus-ECL. 500 µl of reagent 1 were mixed with 500 µl of reagent 2 and the ECL solution was applied to the membrane. Images were acquired using the Intas ECL ChemoStar. For Western blots with a very low signal, Infinity Flash ECL was used instead.

### 2.2.7 RNA-Sequencing

The RNA-Sequencing (RNA-Seq.) was generated by Hauke Werner and Ramona Jung in cooperation with Sudhir Thakurela and Vijay Tiwari (Mainz) by following Illumina HiSeq protocols. Three animals per group (CNP1 null mutants and wildtype each P18 and P75) were used.

#### 2.2.7.1 Differential Gene Expression Analysis of RNA-Sequencing

A raw sequencing data alignment was conducted by Thakurela and Tiwari. Gene expression metrics was normalized using FPKM (Fragments per kilo base per million mapped reads). Gene differential expression analysis was performed in R (version 3.0.5) with the well-established DESeq2 R package (Love et al. 2014). Genes with less than 5 reads were filtered out and genes with adjusted P value $< 0.05$ were considered as differentially expressed (DEGs). DESeq2 uses negative binomial distribution and gene-specific variance to calculate p-values. Love et al. have explained the normalization and statistical analysis performed by DESeq2 in detail (Love et al. 2014).

#### 2.2.7.2 RNA-Sequencing data – Volcano plots

Volcano Plots were generated with GraphPad. Genes with log2 fold change (log2FC) $< -1, > 1$ and p adj $< 0.05$ were considered statistically significant. The volcano plots visualize significantly up- and downregulated genes of the RNA-Seq. analysis. All genes with p adj $< 0.05$ are depicted in blue, all genes with log2FC $< -1$ or $> 1$ are depicted in green and genes that fulfilled both criteria are depicted in red.

#### 2.2.7.3 RNA-Sequencing data – Gene ontology pathway analysis (GSEA)

Pathway analysis was performed according to a published protocol by Reimand et al. using free available and approved programs (Reimand et al. 2019). In detail, a ranked gene list was created by sorting the RNA-Seq. results by log2FC. All not identified genes were removed prior to the ranking (CNP1 null mutant P18 vs. P75 6401 genes; P75 CNP1 null mutant vs. wildtype 6393 genes; wildtype P18 vs. P75 6761 genes; P18 CNP1 null mutant vs. wildtype 3637 genes). A Gene Set Enrichment Analysis (GSEA) was performed on the ranked gene list using the Broad Institute GSEA software (GSEA v4.1.0, 2003 – 2019 Broad Institute, Inc., Massachusetts Institute of Technology, and Regents of the University of California) (Subramanian et al. 2005). The following ontologies and pathways were searched: GO:Biological Process, GO:Molecular Function, GO:Cellular Component, Reactome, Panther, using the most current .gmt file from August 2020 Bader Lab: Mouse_GO_AllPathways_no_GO_iea_August_01_2020_symbol, downloaded from Bader Lab (internet source 1) (Merico et al. 2010). The number of permutations was set to 1000. Only gene sets with 10 to 500 genes were tested.

### 2.2.8 Statistical analysis

The statistical analysis was performed and processed using the software program GraphPad. Probability values (p-value) or adjusted p values (p adj) of less than 0.05 (*$p < 0.05$, **$p < 0.01$, ***$p < 0.001$, ****$p < 0.0001$) were considered significant if not otherwise stated. Ordinary One-way analysis of variance (ANOVA) tests were conducted with the assumption of a normal distribution of the data. The experiments consist of rather low number of data points per group due to the usage of animals in consistence with the 3R rule. Consequently, the distribution of data points could not be tested in every group for its own. ANOVA-tests show, that there is at least one significant difference in the analyzed sample. In order to find out, where the differences are, post hoc multiple comparison tests such as Tukey's test, when every group was compared to every group, or Bonferroni's test in case of two-way ANOVA were performed. Moreover, the ANOVA test has the advantages of being robust, if the number of animals is similar in each group even if the variance is not homogeneous (Field 2013). If the variance is higher in groups with more animals compared to groups with less animals, ordinary one-way ANOVA test has been shown to produce conservative results and does not overestimate the significance. Therefore, this test can be considered as robust (Field 2013).

#### 2.2.8.1 Weight analysis MyD88 null mutants, CNP1 null mutants and MyD88-CNP1-double knockout mice

For the weight analysis, statistical analysis was conducted with One-way-ANOVA-analysis and Tukey's tests with multiple comparisons. The number of animals was five to nine animals per group. Since the variance is not clearly higher in groups with higher sample size (9 MyD88-CNP1 double knockout mice) compared to groups with lower sample size (wildtype, MyD88 null mutants CNP1 null mutants) consisting of five to six animals, ordinary one-way ANOVA test has been shown to not overestimate the significance (Field 2013). Quantile-Quantile (Q-Q) plots, which test for a normal distribution of the residuals containing all data points, formed a straight line. Therefore, these data can be considered as normally distributed residuals (University of Virginia Library, internet source 2). The mean with standard deviation (SD) is depicted.

#### 2.2.8.2 Immunohistochemistry

For the immunohistochemistry experiments, the technical and biological results were excluded when they were more than two standard deviations apart from the mean. The number of animals for the comparison of P18 and P75 CNP1 null mutants vs. wildtype animals was three to four per group. One-way ANOVA-analysis and Tukey's post hoc test with multiple comparisons were performed. The sample size with three or four animals per group is quite equal and therefore, ordinary one-way ANOVA test can be considered as robust (Field 2013). Immunohistochemical analyses with the markers GFAP, Mac3, Iba1, CD3 and APP are usually evaluated with t-tests also assuming normal distribution comparable to ordinary one-way ANOVA (Wieser et al. 2013). Hence, the usage of such a statistical method enables simpler comparisons of my data to other data. The mean with SD is depicted.

For the MyD88-CNP1 experiment, the number of animals was four to nine animals. One-way-ANOVA-analysis and Tukey with multiple comparisons were performed. The variance is higher in groups with eight to nine animals (CNP1 null mutants, double knockout animals) compared to the control groups wildtype and MyD88 null mutants consisting of four to five animals. Under these prerequisites, ordinary one-way ANOVA test has been shown to produce conservative results and does not overestimate the significance. Therefore, this test can be considered as robust (Field 2013). The mean with SD is depicted.

#### 2.2.8.3 RNA-Sequencing data – Bar diagrams

For comparing the four groups (CNP1 null mutants and wildtype mice both at P18 and P75), FPKM values were taken and ordinary One-way ANOVA and Tukey's multiple comparisons were

conducted. Since the sample size was three per group, ordinary one-way ANOVA test can be considered as robust even if the variance is not homogeneous (Field 2013). The Q-Q plots indicated a normal distribution of residuals. Hence, the usage of such a statistical method enables simpler comparisons of my data to other data. The mean with SD is depicted. For the comparison of cell markers at P18 and P75 CNP1 null mutants vs. wildtype, unpaired two-sided Student´s t-tests were conducted. The mean with SD is depicted. RNA-Seq. analysis data can be evaluated with t-tests also assuming normal distribution comparable to ordinary one-way ANOVA (Zhong et al. 2020).

#### 2.2.8.4 qRT-PCRs

The qRT-PCR results consisted of multiple groups, because of the three variables genotype, tissue and age. The number of animals was seven to nine per group. Technical and biological results were excluded, when they were more than two standard deviations apart from the mean. For the statistical analysis of the analysis of myelin (P20, P75, CNP1 null mutants and wildtype), two-way ANOVA-test was used with Bonferroni's multiple comparisons. Two-way ANOVA was used because of two independent variables genotype (CNP1 null mutant vs. wildtype) and sample (myelin vs. brain lysate). The ANOVA indicates, whether the variable genotype or the variable sample makes the difference. In order to find out the differences in the analyzed groups, a Bonferroni post hoc multiple comparison test was conducted. The ordinary one-way ANOVA test can be considered as robust even if the variance is not homogeneous (Field 2013). QRT-PCR data are usually evaluated with t-tests (Berghoff et al. 2021) that are comparable to ordinary one-way ANOVA. Hence, the usage of such a statistical method enables simpler comparisons of my data to other data. For the comparison of myelin vs. brain lysate (P75, wildtype mice) unpaired t-tests were conducted. The mean with standard error of the mean (SEM) is depicted.

# 3 Results

## 3.1 CNP1 null mutant mice depict a normal postnatal development in addition to an inflammatory reaction according to the RNA-Sequencing of purified myelin.

Although many features of CNP1 null mutant mice were already investigated, the causal relationship between the loss of CNP1 and neurodegeneration as well as reactions that drive the disease pathology at the very beginning, remain unresolved. We chose to investigate myelin, because it can be isolated biochemically quite easily and specifically (Jahn et al. 2009). Second, the CNP1 protein is a myelin protein and CNP1 null mutant animals primarily show a neuronal degeneration most likely due to the defect myelin sheath. Third, myelin is built exclusively by oligodendrocytes and it is in a continuous contact with the oligodendroglial soma via cytosolic channels, so that it appeared to be suitable to also investigate possible oligodendroglial reactions to the loss of CNP1 as well as the ongoing neuroinflammation and degeneration in mice deficient for CNP1. It has been shown previously, that myelin contains a plethora of oligodendrocyte enriched RNAs (Thakurela et al. 2016).

### 3.1.1 At P18 myelination is in progress, therefore two different ages (P18 and P75) were examined.

Since we were interested in early changes of CNP1 null mutant mice that might cause or drive the initial disease pathology, we decided to investigate the myelin of young animals. Because of suggested alterations due to maturation and myelination at P18, we looked at the process of maturation in wildtype animals first and compared the abundances of RNAs found in the myelin of wildtype mice at the age of 18 days (hereafter termed P18) and to mice at the age of 75 days (hereafter termed P75) in a transcriptome analysis. 260 RNAs were significantly downregulated in the myelin of P75 animals compared to P18 and 339 RNAs were significantly upregulated in the differential gene expression analysis with a p adj $< 0.05$ and log2FC $< -1$ and $> 1$. The analysis of RNA-Seq. (RNA-Sequencing) data revealed further that significantly downregulated genes at P75 were involved in myelination (Sirt2, Mbp, Srd5a1), OPC differentiation (Sirt2, Srd5a1) and CNS development (Marcksl1, Bmp4, Cdk5r2, Gsx1, Nr4a3) (**Fig. 3 a**). Significantly upregulated genes were linked to steroid metabolism (Scd3, Abca8a) amongst others (**Fig. 3 a**). The differences result from the fact, that oligodendrocytes and myelin are not fully developed but immature at the age of P18.

In order to exploit the significantly dysregulated genes in further detail, a gene ontology pathway analysis was performed (**Fig. S1 a**). 89 gene sets were significantly downregulated upon maturation (P18 > P75, negative normalized enrichment score (NES)) and 435 gene sets were significantly upregulated (P75 > P18, positive NES). The pathway analysis also revealed that many gene sets significantly downregulated at P75 were associated with DNA transcription ("PID_FOXM1_PATHWAY"; "ATF-2 transcription factor network"), cell cycle ("G1 Phase"; "regulation of attachment of spindle microtubules to kinetochore"; "PID_PI3KCI_PATHWAY"; "BIOCARTA_RACCYCD_PATHWAY"; "BIOCARTA_CELLCYCLE_PATHWAY"; "Cyclin D associated events in G1") and cytoskeleton ("actin polymerization or depolymerization"; "regulation of actin filament depolymerization"; "actin filament polymerization"; "negative regulation of microtubule depolymerization"). At P75 upregulated gene sets included genes involved in the immune system ("antigen processing and presentation of peptide antigen"; "MHC protein complex"), ion channels ("transmitter-gated ion channel activity"; "solute:sodium symporter activity"; "anion channel activity"), translation ("cytosolic large ribosomal subunit"; "cytosolic small ribosomal subunit") and lipids ("lipid translocation").

We decided to investigate CNP1 null mutant myelin at the very same two timepoints, P18 and P75, in comparison to the data obtained from wildtype mice in order to distinguish differences upon maturation and myelination from differences upon the progressive course of disease.

### 3.1.2 CNP1 null mutant mice exhibit a progressive phenotype and the myelin is contaminated with many immunomodulatory molecules at P75.

The volcano plot analysis of the RNA-Seq. analysis of myelin of CNP1 null mutant mice at P18 vs. P75 (**Fig. 3 b**) and P75 CNP1 null mutants vs. wildtype (**Fig. 3 c**) revealed many immunomodulatory RNAs significantly higher expressed in CNP1 null mutants at P75. A lot more RNAs were higher expressed (464 genes in the analysis CNP1 null mutants P18 vs. P75 and 116 genes in the analysis P75 CNP1 null mutants vs. wildtype) than lower expressed (33 genes in the analysis CNP1 null mutants P18 vs. P75 and 203 genes in the analysis P75 CNP1 null mutants vs. wildtype) upon the ongoing pathology (compare also **Fig. 3 d**). Amongst the higher expressed RNAs in both comparisons (CNP1 null mutants P75 vs. P18 and P75 CNP1 null mutants vs. wildtype) were pro-inflammatory RNAs associated with astrocytes (Gfap, Serpina3n, Aspg), microglia (Clec7a, Cd68, Cd14) and the NF-κB pathway (Tlr1, Tlr2, Cd86, Trem2). In the P75 CNP1 null mutant animals some further typical cell markers of inflammatory cells were significantly higher expressed in RNA-Seq. analysis (Aif1, Aqp4) (**Fig. 3 b, c**) and qRT-PCR (compare **Fig. 8 c**) compared to wildtype mice, which reflects the on-going inflammation and recruitment of immune cells into the myelin. Moreover, Interleukin (Il)-33 was significantly upregulated in the myelin of CNP1 null mutants at

P75 compared to P18 (**Fig. 3 b**). IL-33 is described as a cytokine that alerts the immune systems upon inflammatory processes and activates NF-κB and MAPK signaling pathways (Miller 2011). We also found Il-33 significantly higher expressed in CNP1 null mutants compared to wildtype controls in qRT-PCR at P20 (see **Fig. 6 d**). Interestingly, also anti-inflammatory RNAs such as Tnfaip6, Cd44, Cst7, Fcgr2b, Slamf8 and Trem2 were higher expressed in the myelin of P75 CNP1 null mutant mice compared to P18 (**Fig 3 b**) and wildtype controls (**Fig. 3 c**). We could confirm the higher expression of Tnfaip6 in CNP1 null mutants by qRT-PCR (compare **Fig. 6 a**). These findings at P75 are in line with the inflammatory reaction of the progressive phenotype of CNP1 null mutant mice. The dysregulated genes in the myelin of CPN1 null mutant mice at P75 compared to P18 were composed of changes due to development similar to the changes upon maturation in wildtype mice (compare **Fig. 3 a**) and inflammatory reaction comparable to the differential gene expression of P75 CNP1 null mutants vs. wildtype (compare **Fig. 3 c**) (**Fig. 3 d**). Furthermore, the results indicated that myelin purifications are co-enriched for RNAs of closely associated other cells such as microglia and astrocytes. Amongst the significantly lower expressed genes in CNP1 null mutant myelin at P75 compared to P18 were many RNAs associated with myelination and brain development comparable to wildtype animals (Mbp, Sirt2, Marcksl1, Bmp4, Cdk5r2, Gsx1, Nr4a3) (**Fig. 3 b**). This finding suggests that the early development of CNP1 null mutant mice is comparable to the development of wildtype animals and not strongly dysregulated.

A subsequently performed gene ontology pathway analysis of the RNA-Seq. data of myelin of CNP1 null mutant mice at P18 vs. P75 (**Fig. S1 b**) revealed 11 gene sets significantly downregulated (P18 > P75, negative NES) and 689 gene sets significantly upregulated (P75 > P18, positive NES), which clearly outnumbers the gene sets of wildtype animals. Gene ontology pathway analysis of P75 CNP1 null mutants vs. wildtype animals (**Fig. S1 c**) revealed 17 gene sets significantly lower expressed (wildtype > CNP1 null mutants, negative NES) and 570 gene sets enriched (CNP1 null mutants > wildtype, positive NES). Most of the enriched gene sets (184 of the top 200 regarding NES) in the myelin of CNP1 null mutant mice at P75 were involved in inflammation and immune system including glial cell activation. Both the cellular immune system ("leukocyte activation involved in inflammatory response"; "macrophage activation"; "microglial cell activation"; "neutrophil chemotaxis"; "glial cell activation"; "Immunoregulatory interactions between a Lymphoid and a non-Lymphoid cell"; "lymphocyte migration") as well as the humoral immune system (cytokines/chemokines ("positive regulation of interleukin-1 beta production"; "positive regulation of response to cytokine stimulus"; "Interleukin-10 signaling") and antigen presentation ("antigen processing and presentation of peptide antigen")) were involved. Moreover, the pathway analysis revealed gene sets associated with astrocytes ("astrocyte development"; "astrocyte cell migration") including typical general astrocyte markers such as Gfap and Vim. Significantly lower expressed

gene sets were linked to the cytoskeleton ("negative regulation of microtubule polymerization or depolymerization"), cell cycle ("regulation of attachment of spindle microtubules to kinetochore") and translation ("cytosolic small ribosomal subunit"; "Eukaryotic Translation Termination") amongst others.

These results suggest, that CNP1 null mutant mice develop normally compared to wildtype animals during the first 18 days. Moreover, the transcriptome analysis revealed an inflammatory reaction in the myelin of P75 CNP1 null mutant mice represented by an upregulation of many immunomodulatory RNAs. Those RNAs encode for immunomodulatory molecules that drive the disease pathology. Since those RNAs are most likely derived from microglia and astrocytes, the myelin transcriptome at P75 seems to be contaminated with RNAs from other cell types than oligodendrocytes.

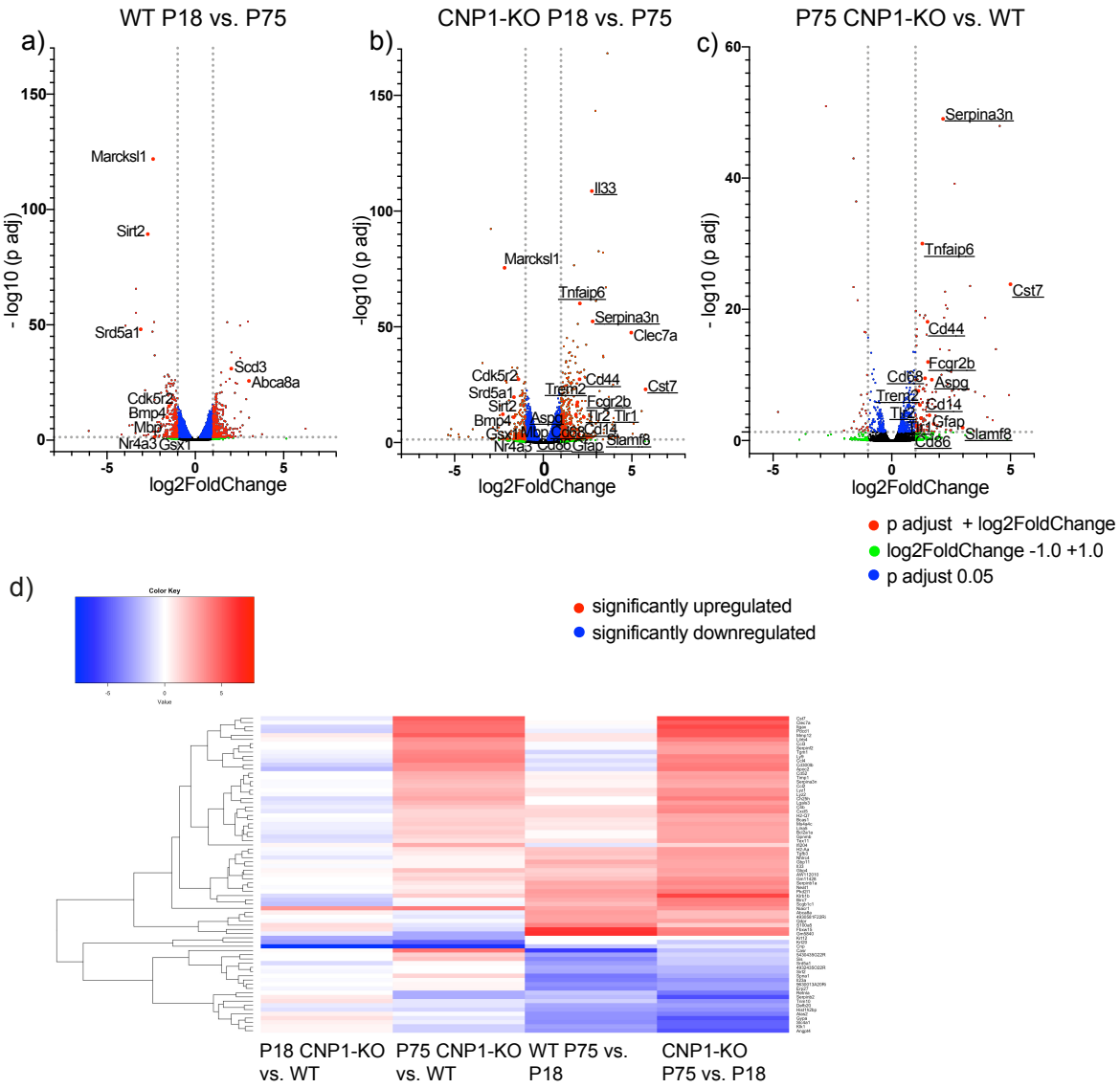


**Figure 3: RNA-Seq. of purified myelin from CNP1 null mutant mice: normal postnatal development at P18 and inflammatory phenotype at P75.**

Many RNAs associated with myelination (Sirt2, Mbp) and brain development (Marcksl1, Bmp4, Cdk5r2, Gsx1, Nr4a3) are downregulated in myelin of WT (a) and CNP1-KO animals (b) at P75 compared to P18. CNP1-KO animals show an upregulation of genes associated with inflammation/ immune system (RNAs underlined) (astrocyte activation: Gfap, Serpina3n, Aspg; microglia activation: Clec7a, Cd68, Cd14; activation of NF-κB pathway: Tlr1, Tlr2, CD86) as well as anti-inflammatory molecules (Tnfaip6, Cd44, Cst7, Fcgr2b, Slamf8, Trem2) (b, c). CNP1-KO mice show only very few genes dysregulated at P18 especially when compared to P75 (d). CNP1-KO P18 vs. P75 reflects changes upon development (compare WT P75 vs. P18) and inflammation (compare P75 CNP1-KO vs. WT) (d). CNP1-KO animals show more significant dysregulated genes at P18 vs. P75 compared to WT animals (d). Volcano plots were generated with Prism 8 from RNA-Seq. data. Genes with p adj. < 0.05 are depicted in blue, genes with a log2FC < - 1 or > 1 are depicted in green and genes that fulfill both criteria are depicted in red. Genes higher expressed in WT P75 (a), CNP1-KO P75 (b) and P75 CNP1-KO (c) are displayed on the right side. The heatmap depicts genes that are at least in one way (p-adj < 0.01 and/ or log2FC > 2.6 or < - 2.6) significantly up- (red) or downregulated (blue). The heatmap was generated with R from RNA-Seq. data. RNA-Seq. data: n = 3 per group, gene differential expression was performed with R (DeSeq2 package).

## 3.2 Attempt to define a prodromal phase without inflammation in the myelin that allows the detection of oligodendrocyte-derived molecules mediating the early disease pathology of CNP1 null mutants at P20.

We found CNP1 null mutant myelin contaminated with astroglial and microglial RNAs at P75. In order to distinguish causes from effects in the vicious cycle of neuronal degeneration and neuroinflammation both observed in the disease pathology of CNP1 null mutants, we attempted to identify a prodromal stage of disease. In such a phase, every dysregulated gene expression in CNP1 null mutants may represent early changes in oligodendrocytes themselves as a reaction to the loss of CNP1 instead of a representation of the reaction of immune cells.

There were only three significantly downregulated genes in the differential expression analysis of RNA-Seq. data of myelin of P18 CNP1 null mutant mice compared to P18 wildtype mice (**Fig. 4 a**). That the myelin of CNP1 null mutants and wildtype mice is very similar was also visible in the heatmap, especially when compared to the high amount of differences between CNP1 null mutants and wildtype mice at P75 (**Fig. 3 d**). This implies that there is not much pathology or immune reaction in the myelin of CNP1 null mutant mice at P18. The three dysregulated RNAs (Krt12, Krt20 and Srd5a1), all significantly downregulated in the mutant animals, are not described to be involved in neurodegeneration, immune system or inflammatory reaction. Summarized, we could neither detect an upregulation of microglial genes in the myelin of P18 CNP1 null mutants by RNA-Seq. (Cd68, Itgam, Aif1) (**Fig. 4 b**) nor in myelin and brain lysates of P20 CNP1 null mutants by qRT-PCR analysis (Aif, iNOS, Cd16, Cd206, Il-1β, TNFα, Cxcl10, Ccl4) (**Fig. 4 f**). Second, we could also not detect an increased abundance of astroglial markers (Aldh1l1, Aqp4, Gfap) in myelin of CNP1 null mutant mice compared to wildtype mice at P18 (**Fig. 4 c**). Neither in P18 nor in P75 CNP1 null mutant animals, typical endothelial (Ocln, Fn1, Cldn5) or neuronal markers (Rbfox3, Eno2, Tubb3) were upregulated. The downregulation of Keratin 12 (Krt12) and Keratin 20 (Krt20) might result from a contamination of the myelin of wildtype animals, since those RNAs are almost not expressed in the brain (Zhang et al. 2014). However, Keratin 12 has been shown to be significantly downregulation in CNP1 null mutant animals previously (Wichert 2009; McKenzie et al. 2017). The significance of this observation remains to be investigated in further studies. Steroid 5-alpha reductase (Srd5a1), which is mainly expressed in myelinating oligodendrocytes and newly formed oligodendrocytes (Zhang et al. 2014), is an enzyme involved in steroid metabolism, oligodendroglial differentiation and myelination (Melcangi et al. 1988). This is in line with our finding, that Srd5a1 is downregulated upon maturation from P18 to P75 in wildtype and CNP1 null mutant mice (**Fig. 3 a, 3 b**). The observed significantly lower expression of Srd5a1 in myelin of CNP1 null mutant mice compared to wildtypes at P18 could in turn indicate a shift in the chronological order of myelination.

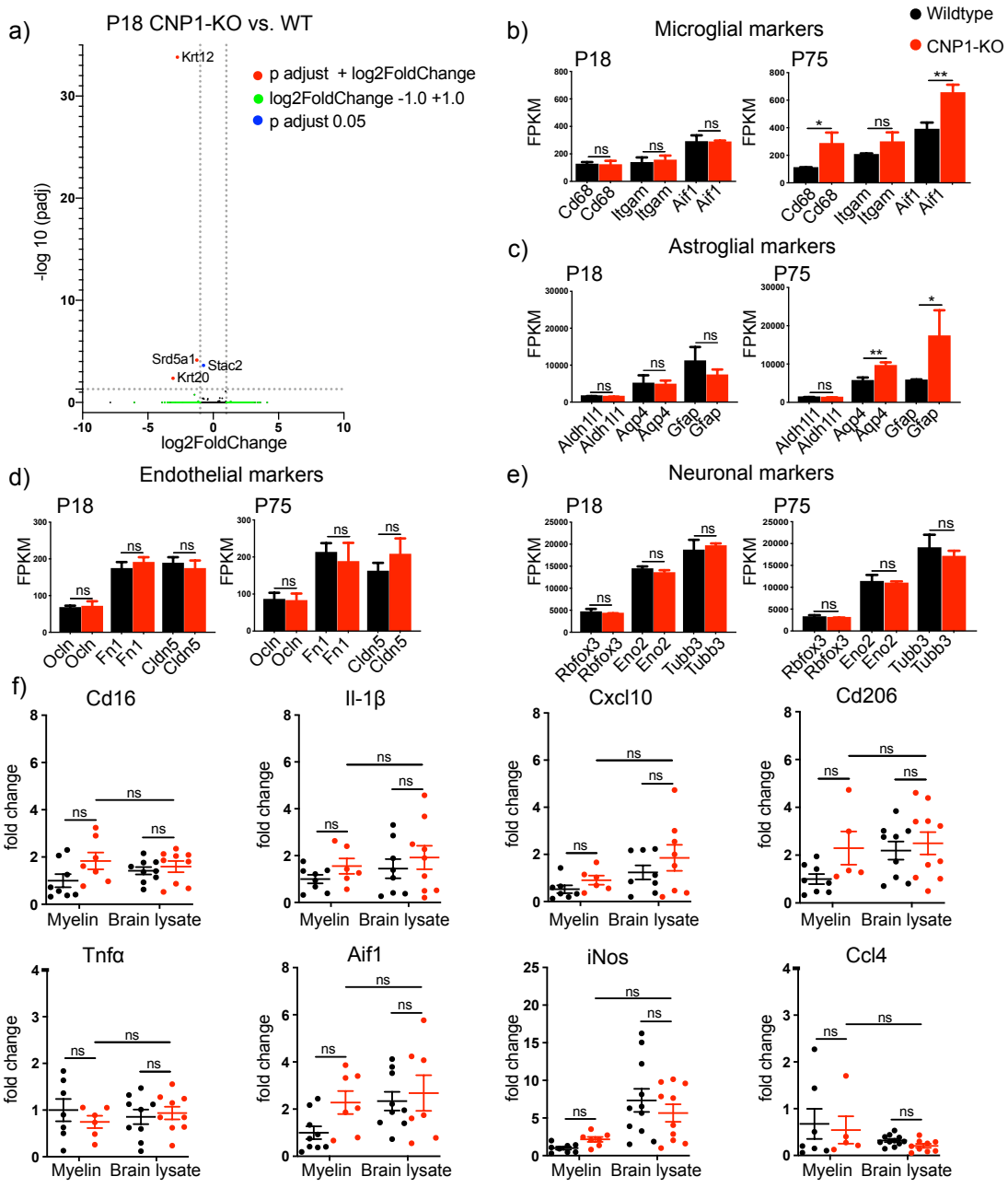


**Figure 4: A prodromal phase in CNP1 null mutant mice as defined by RNA-Seq. and qRT-PCR of purified myelin at P18/P20.**

Only 3 RNAs (Krt12, Krt20, Srd5a1) are significantly dysregulated in myelin of CNP1-KO mice compared to WT at P18 (a). At P18, there are no different relative expression levels of RNAs typical for microglia (Cd68, Itgam, Aif1) (b), astrocytes (Aldh1l1, Aqp4, Gfap) (c), endothelia (Ocln, Fn1, Cldn5) (d) or neurons (Rbfox3, Eno2, Tubb3) (e) in myelin of CNP1-KO mice compared to WT. In contrast, some microglial (Cd68, Aif1) (b) and astroglial (Aqp4, Gfap) (c) markers are higher expressed at P75 in mutants compared to controls. Relative expression of microglia marker genes (CD16, IL-1β, TNFα, Aif1, Cxcl10, CD206, iNOS and Ccl4) is unaltered in myelin and brain lysate of CNP1-KO mice compared to WT at P20 in qRT-PCR (f). Volcano plot was generated with Prism 8 from RNA-Seq. data. Genes with a p adj. < 0.05 are depicted in blue, genes with a log2FC < - 1 or > 1 are depicted in green and genes that fulfill both criteria are depicted in red. Genes lower expressed in CNP1-KO P18 (a) are displayed on the left side. RNA-Seq.: n = 3 per group, normalized gene expression values (FPKM), unpaired tow-sided Student's t-test, mean ± SD depicted. qRT-PCR: All individual data points are normalized to the mean of P20 wildtype myelin (set to 1), n = 7 – 9 per group, two-way ANOVA and Bonferroni multiple comparisons post hoc test, mean ± SEM depicted. *p value < 0.05, **p < 0.01, ***p < 0.001, ****p < 0.0001.

RNA-Seq. analysis and qRT-PCR suggested that P18/P20 are a prodromal disease stage. We confirmed this finding by quantitative immunohistochemical analysis at P18. Immunostaining for specific marker antigens revealed, that at P18 inflammatory signs such as microgliosis (Mac3, Iba1) (**Fig. 5 a, b**), astrogliosis (Gfap) (**Fig. 5 c**) or neurodegenerative signs like APP swellings (**Fig. 5 d**) were indeed absent from corpus callosum (**Fig. 5 e**) and fimbriae (**Fig. 5 f**), two typical white matter tracts of the brain that are later heavily affected reflected in an astrogliosis and microgliosis as well as a neurodegeneration in CNP1 null mutants at P75 (Lappe-Siefke et al. 2003) (**Fig. 5 a – f**).

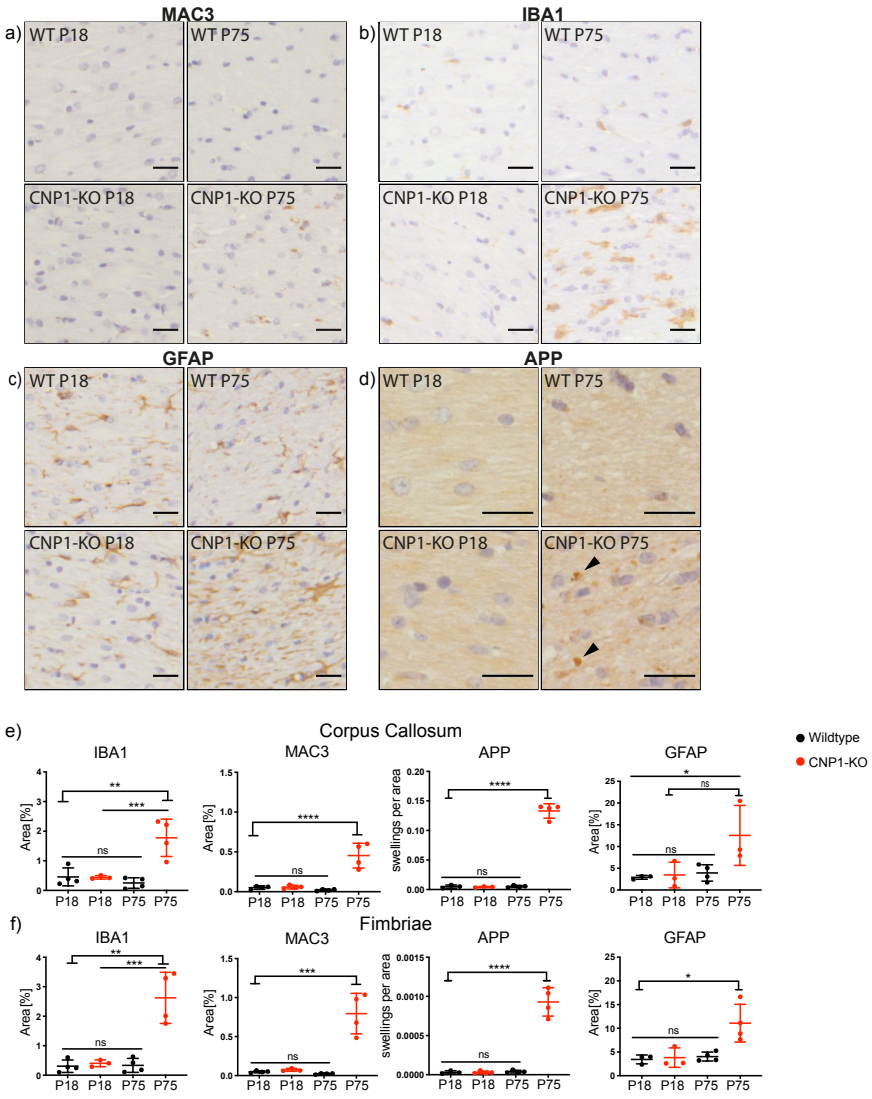


**Figure 5: A prodromal phase in CNP1 null mutant mice as defined by immunohistochemistry at P18.**

Representative light microscope images immunostained for Mac3 (a), Iba1 (b), GFAP (c) and APP (arrowheads) (d) of white matter tracts of CNP1-KO mice at P18 and P75. Scale bar 25 µm. At P18 CNP1-KO mice are undistinguishable from WT regarding the number of microglia (Iba1), activation of microglia (Mac3, labelling CD107b), astrocytes (GFAP) and signs of neuronal degeneration (APP positive spheroids) in corpus callosum (e) and fimbriae (f) (both Bregma -1.34). In contrast, at P75 CNP1-KO mice exhibit a significantly enhanced axonal pathology and inflammation. (n = 4 for P18 WT, P75 WT and P75 CNP1-KO; n = 3 for P18 CNP1-KO; one-way ANOVA and Tukey's multiple comparison post hoc test (*p value < 0.05, **p < 0.01, ***p < 0.001, ****p < 0.0001), mean ± SD depicted. Results were obtained in collaboration with Chalid Hasan.

Taken together, these results support the finding, that the early development of CNP1 null mutants is comparable to wildtype mice. Considering the absence of inflammatory or immune markers at P18 and P20, this age seems to represent a prodromal stage of disease of the CNP1 null mutant phenotype. Thus, we chose this time point for further investigation to identify potential immunomodulatory molecules derived from oligodendrocytes in CNP1 null mutant mice that modulate the early phase of disease.

RNA-Seq. analysis of myelin of CNP1 deficient mice at P75 revealed Tumor Necrosis Factor alpha induced protein 6 (Tnfaip6) as one of the significantly higher expressed genes compared to wildtype animals (**Fig. 3 b, 3 c, 6 b**). Interestingly, we found Tnfaip6 significantly higher expressed in the more sensitive qRT-PCR of myelin but not of brain lysate of CNP1 deficient mice at P20 (**Fig. 6 a**). The progressive disease course of CNP1 deficient mice is reflected by the fact, that Tnfaip6 is even higher expressed in the mutant myelin at P75 compared to P18 and higher expressed in the mutant whole brain lysate of mice at P75 compared to brain lysate of wildtype mice (**Fig. 6 b**). Tnfaip6 is mainly expressed in oligodendrocyte lineage cells and astrocytes in the brain (Zhang et al. 2014) (**Fig. 6 c**).

RNA-Seq. analysis also demonstrated Il-33, another secreted immunomodulatory molecule, significantly higher expressed in myelin of P75 CNP1 deficient mice (**Fig. 6 e**). IL-33 has been described to be expressed by oligodendrocytes in patients with MS (Allan et al. 2016). In the more sensitive qRT-PCR analysis we identified a significant higher expression in myelin of P20 CNP1 deficient mice compared to wildtype mice (**Fig. 6 d**), which suggests a role in the early pathogenesis of the pathology similar to Tnfaip6. However, although the upregulation at P75 is visible in RNA-Seq. analysis and not in qRT-PCR, there is much more Il-33-RNA in myelin of animals at P75 compared to P20. This makes it an interesting molecule for the investigation of the further pathology of CNP1 null mutant mice. IL-33 is mainly expressed in OPCs and astrocytes in the brain (Zhang et al. 2014) (**Fig. 6 f**).

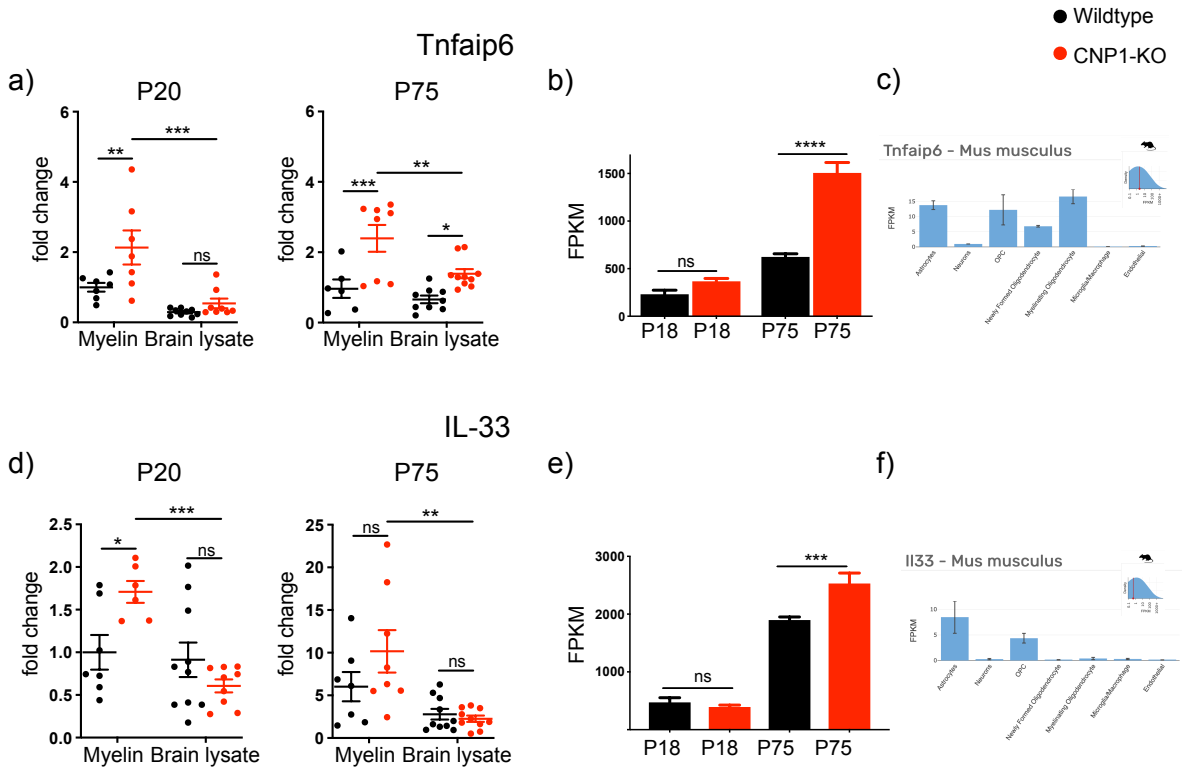


**Figure 6: Early upregulation of immunomodulatory markers potentially derived from oligodendrocytes by qRT-PCR at P20.**

Tnfaip6 is significantly higher expressed in myelin of CNP1-KO animals than in control myelin at P20 when quantified by qRT- PCR (a). Tnfaip6 is mainly expressed in oligodendrocyte lineage cells and astrocytes in the brain (c) (Zhang, The Journal of Neuroscience, 2014). The effect strengthens at P75 and is even significant in whole brain lysate at this age. Unexpected from RNA Seq. analysis (e), qRT-PCR analysis indicates that also Il-33 is transiently higher expressed in myelin of P20 CNP1-KO animals compared to WT (d). Il-33 is mainly expressed in OPCs and astrocytes in the brain (f) (Zhang et al. 2014). At P75, there is significantly more Il-33-RNA in myelin compared to P20 (different scale). qRT-PCR: All individual data points are normalized to the mean of P20 wildtype myelin (set to 1), n = 7-9 per group, two-way ANOVA and Bonferroni multiple comparisons post hoc test, mean ± SEM depicted. RNA-Seq.: n = 3 per group, normalized gene expression values (FPKM), one-way ANOVA and Tukey's multiple comparisons post hoc test, mean ± SD depicted. *p value < 0.05, **p < 0.01, ***p < 0.001, ****p < 0.0001.

Both TNFAIP6 and IL-33 might be secreted as an early immunomodulatory reaction of oligodendrocytes to the loss of CNP1. A validation of the enhancement of Tnfaip6 provided no further evidence, because we did not achieve convincing results with the antibodies for immunohistochemistry and Western blot. Further experiments are required in the future.

## 3.3 Sensitive qRT-PCR analysis casted doubt on the existence of a prodromal phase in CNP1 null mutants at P20.

Further attempts to verify that P18/P20 is a prodromal disease stage in CNP1 null mutants by subsequent qRT-PCR, a much more sensitive method compared to RNA-Seq. analysis, raised doubt on our first conclusions.

Since TNFAIP6 and IL-33 could be also derived from astrocytes according to Barres database (Zhang et al. 2014), we investigated the myelin of CNP1 null mutant mice at P20 in more detail. Unexpectedly, we detected a significantly higher expression of typical astroglial markers (Gfap, Aldh1l1) in purified myelin but not brain lysate at P20 in qRT-PCR (**Fig. 7 a, c**), which was not evident from RNA-Seq. analysis (**Fig. 7 b, d**). Because of this discovery, we revaluated the myelin for two more typical microglial RNAs. Both, the transmembrane glycoprotein Cd68 and the pro-inflammatory cytokine Ccl6 were significantly higher expressed in the myelin of CNP1 null mutants at P20 in qRT-PCR, which was again not evident from RNA-Seq. analysis (**Fig. 7 f, h**). The early upregulation of astroglial and microglial RNAs most likely represents an early immigration of these cells into the disturbed myelin of CNP1 null mutants. Since not all typical cell markers of microglia were upregulated, it cannot formally be excluded, although it is highly unlikely, that CD68, Ccl6, Gfap and Aldh1l1 are expressed by oligodendrocytes as an early pro-inflammatory reaction.
Unexpectedly, the myelin of CNP1 null mutant animals contained several immunomodulatory molecules most likely secreted from astrocytes and microglia at a very early time point, which could be partly detected by RNA-Seq. analysis and mainly by the more sensitive qRT-PCR analysis. P20 is not a prodromal phase as previously suggested. Hence, the upregulated immunomodulatory RNAs Tnfaip6 and Il-33 might be derived from oligodendrocytes or from astrocytes or microglia, which immigrated early into the myelin of CNP1 null mutant mice.

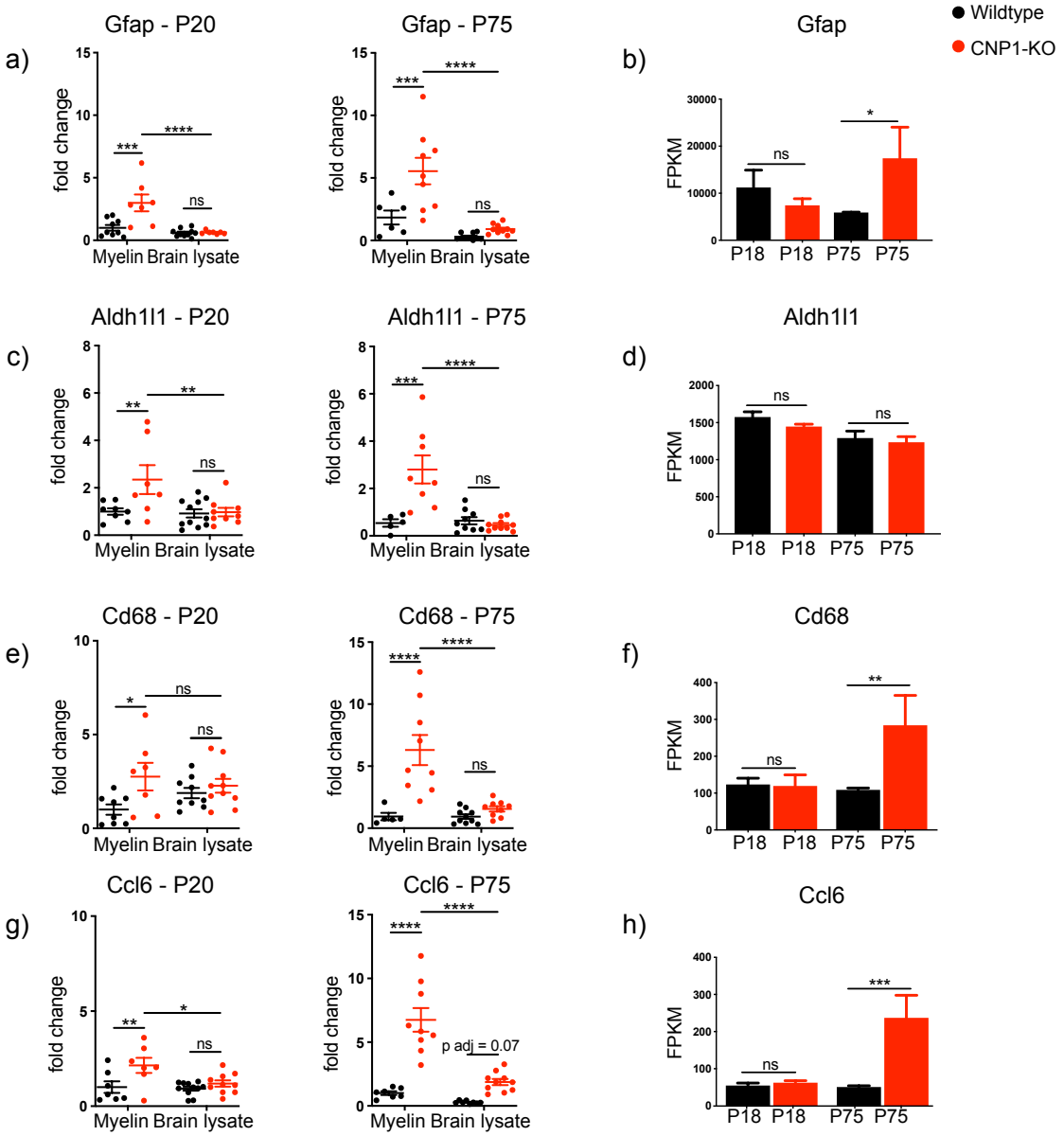


**Figure 7: Unexpected early upregulation of some astroglial and microglial markers in qRT-PCR at P20.**

Both astroglial markers GFAP (a) and Aldh1l1 (c) are already higher expressed in myelin but not in brain lysates of P20 CNP1-KO mice in qRT-PCR analysis but not in less sensitive RNA-Seq. analysis (b, d). At P75, Aldh1l1 is even higher expressed in myelin of CNP1-KO mice (c). Interestingly, also two microglial markers Cd68 (e) and Ccl6 (g) already show an increased abundance in myelin but not in brain lysates of CNP1-KO animals compared to WT at P20 by qRT-PCR with both RNAs even higher expressed at P75. This early effect is not detected by RNA-Seq. data (f, h). qRT-PCR: All individual data points are normalized to the mean of P20 wildtype myelin (set to 1), n = 7 – 9 per group, two-way ANOVA and Bonferroni multiple comparisons post hoc test, mean ± SEM depicted. RNA-Seq.: n = 3 per group, normalized gene expression values (FPKM), one-way ANOVA and Tukey's multiple comparisons post hoc test, mean ± SD depicted. *p value < 0.05, **p < 0.01, ***p < 0.001, ****p < 0.0001.

## 3.4 Characteristics of astrocytes and microglia in CNP1 null mutant mice at P75.

Because of the relevance of loss of function mutations of CNP1 for human health and the significance of the extensive crosstalk of cells in the CNS, we characterized astrocytes and microglia as the main local immune cells of the brain in more detail in CNP1 null mutants at P75.

### 3.4.1 Loss of CNP1 induces cytotoxic (A1) and neuroprotective (A2) astrocytes at P75.

Due to a concept from Liddelow et al., astrocytes can exhibit different states of activation. A1 astrocytes are cytotoxic whereas A2 astrocytes are rather neuroprotective (Liddelow et al. 2017). CNP1 null mutant mice are reportedly affected by astrogliosis and microglia activation at P75 and older (Lappe-Siefke et al. 2003). None of the suggested typical A1 or A2 genes was significantly lower expressed in RNA-Seq. data of myelin of CNP1 null mutant mice at P75. We found many (Gfap, Timp1, Cxcl10, Cd44, Osmr, Serpina3n and Aspg) but not all so-called pan-reactive genes higher expressed in CNP1 null mutants compared to wildtype mice in the RNA-Seq. data. My analysis revealed, that typical A1 RNAs (C3, Ggta1, Gbp2) as well as typical A2 RNAs (Cd109, Cd14, Emp1) were higher expressed in CNP1 null mutants compared to wildtype mice at P75 (**Fig. 8 a**). This finding suggests, that there are more activated astrocytes in CNP1 null mutant mice compared to wildtype animals and that there are not only cytotoxic astrocytes activated by pro-inflammatory microglia. In fact, the astrocytes seem to be more diverse and maybe some of the astrocytes exhibiting typical features of A2 astrocytes try to limit the neuronal damage due to the progressive inflammatory reaction.

### 3.4.2 Loss of CNP1 induces proinflammatory and phagocytic microglia with a DAM-like phenotype at P75.

Previous results have shown an essential role of microglia in the pathology of CNP1 null mutant mice (Lappe-Siefke et al. 2003; Janova et al. 2018). The myelin and brain lysate of P75 CNP1 null mutant mice contained only significantly higher expressed or not dysregulated microglial markers and no significantly lower expressed markers compared to wildtype animals (**Fig. 8 b – d**). Microglia exhibited a pro-inflammatory phenotype with typical M1 and pro-inflammatory markers (Cd86, Ccl6, Fcgr3 (**Fig. 8 b**) and CD16, Il-1β, Ccl6, Tnfα (**Fig. 8 c**), but unexpectedly not iNOS (**Fig. 8 c**)), pan-reactive/ general microglial markers (Cd68, Ptprc, Cd14) (**Fig. 8 b**) and markers of phagocytotic activity (C1qa, C1qc, C3) (**Fig. 8 b**) in myelin of CNP1 null mutants at P75. None of the investigated M2 genes (CD206, Arg1, CD163) was significantly higher expressed in myelin

or whole brain lysate in qRT-PCR (**Fig. 8 d**), whereas RNA-Seq. analysis revealed a higher expression of two typical M2 markers (Trem2, Clec7a) (**Fig. 8 b**). Since both are also typically expressed by disease-associated microglia (DAM), a specific subpopulation of microglia detected in neurodegenerative diseases with phagocytic, pro-inflammatory and probably also anti-inflammatory capacities, we investigated our differential gene expression analysis of CNP1 null mutant myelin. Interestingly, the analysis revealed a higher expression of many typical DAM-markers (Aif1/Iba1, Trem2, Clec7a, Lyz2, Gpnmb, Itgax, Cst7, Tyrobp, Ccl6, Lilrb4, Cd74) compared to wildtype myelin at P75 (**Fig. 8 b**). The upregulation of microglial RNAs was restricted to myelin and not visible in whole brain lysate at P75 (**Fig. 8 c, d**), a finding that supports the hypothesis, that the inflammation is predominantly in myelin due to the loss of CNP1.

At P75, we also found RNAs encoding for two of the microglially expressed toll like receptors (Tlr), Tlr1 and Tlr2 (**Fig. 8 e**), enriched in the mutant myelin compared to wildtype myelin (**Fig. 8 b**). Binding of ligands to Tlr1 and Tlr2 leads to a switch from resting, homeostatic microglia to activated microglia via a recruitment of the adaptor molecule MyD88, which results in an activation of NF-κB and the transcription of pro-inflammatory molecules. This pathway plays an important role in M1 polarization (Toshchakov et al. 2002) and is typical for M1 microglia (Liu et al. 2018; Huang et al. 2019). Il-33, which is higher expressed in the myelin of CNP1 null mutants (compare **Fig. 6 d, e**) is also described to activate NF-κB via MyD88 (Miller 2011). Since activated microglia drive the disease pathology of CNP1 null mutants reportedly and since we predominantly identified microglial RNAs typical for M1 and DAM microglia in the myelin of CNP1 null mutant mice in addition to an upregulation of Tlr1, Tlr2 and a trend for upregulation of one further RNA Mal, whose protein is involved in the MyD88 pathway, we considered it possible that CNP1 loss of function activates the MyD88 pathway in microglia.

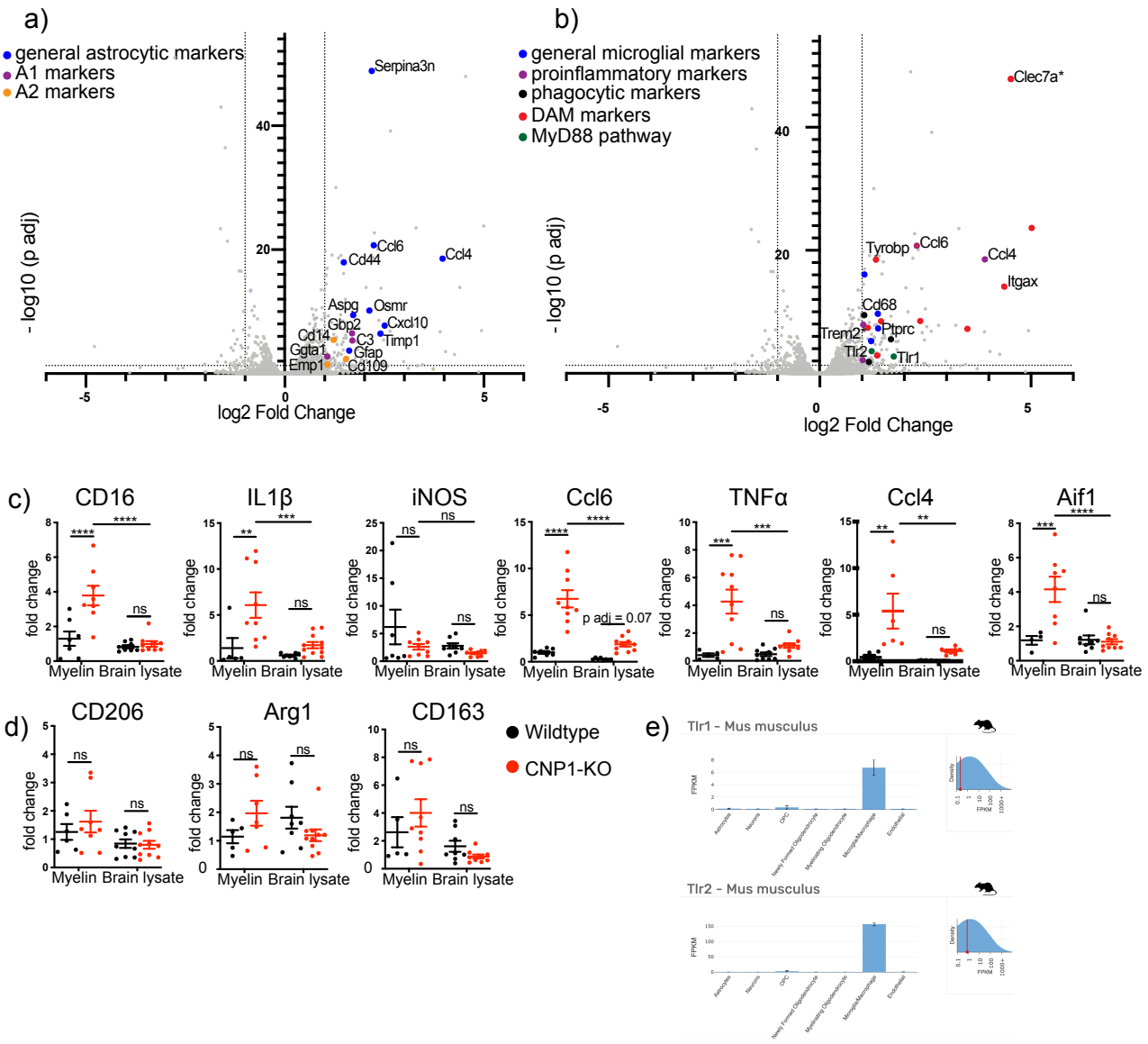


**Figure 8: Loss of CNP1 induces cytotoxic and neuroprotective astrocytes and proinflammatory and phagocytic microglia with a DAM-phenotype.**

Upregulation of general/pan-reactive (Serpina3n, Gfap, Ccl6, Ccl4, Cd44, Aspg, Osmr, Cxcl10, Timp1; depicted in blue), typical A1 (Gbp2, C3, Ggta1; depicted in purple) and typical A2 (Cd14, Cd109, Emp1; depicted in orange) astroglial markers in RNA-Seq. of myelin of CNP1-KO animals compared to WT at P75. Upregulation of general microglial (Cd68, Ptprc, Cq14; depicted in blue), proinflammatory (Ccl4, Ccl6, Fcgr3, Cd86; depicted in purple) and phagocytic markers (C3, C1qca, C1qc; depicted in black) in addition to DAM markers (Clec7a, Trem2, Ccl6, Tyrobp, Cd74, Lyz2, Cst7, Itgax, Lilrb4, Gpnmb; depicted in red) in RNA-Seq. of myelin of CNP1-KO animals compared to WT at P75. Significantly upregulated genes involved in MyD88 pathway activating microglia are depicted in green. Genes with asterisk (Trem2, Clec7a) are also associated with M2 microglia phenotype according to literature. The pro-inflammatory phenotype of microglia is confirmed by qRT-PCRs as represented in an upregulation of typical M1 markers in myelin but not in brain lysate of CNP1-KO mice (c). Prototypical M2 markers are not significantly different in myelin between CNP1-KO and WT animals (d). Tlr1 and Tlr2 are mainly expressed in microglia in the brain (e) (Zhang et al. 2014). Volcano plots were generated with Prism 8 from RNA-Seq. data (n = 3 per group, gene differential expression was performed with R (DeSeq2 package)). Only genes with p adj < 0.05 are depicted, log2FC is set to < - 1 and > + 1 (grey axes). qRT-PCR: All groups are normalized to P20 wildtype myelin, n = 7 – 9 per group, two-way ANOVA and Bonferroni multiple comparisons post hoc test (*p value < 0.05, **p < 0.01, ***p < 0.001, ****p < 0.0001), mean ± SEM depicted. DAM = disease-associated microglia.

### 3.4.3 Deletion of the adaptor molecule MyD88 of the NF-κB pathway leads to an amelioration of neurodegeneration, but this pathway is not (exclusively) responsible for the recruitment and activation of immune cells in CNP1 null mutant mice.

In order to test whether the MyD88 pathway in microglia drives the pathology in CNP1 null mutant mice, we investigated MyD88-CNP1-double knockout mice in comparison to CNP1 and MyD88 single mutants and wildtype controls. A loss of body weight is unsubtle evidence for illness in mice. We detected no significant difference in body weight between CNP1 deficient and CNP1-MyD88-double knockout animals at the age of 30 – 34 weeks, whereas the weight of CNP1 null mutants and double knockout animals was significantly reduced compared to wildtype animals (**Fig. 9 a**). My immunohistochemical analysis of frontal corpus callosum detected no differences in the number of microglia (Mac3) (**Fig. 9 b**), activated microglia (Iba1) (**Fig. 9 c**) and T-cells (CD3) in CNP1-MyD88-double knockout animals compared to CNP1 null mutant animals. (**Fig. 9 d**). Nevertheless, there was a significant reduction of axonal swellings (APP) in the corpus callosum of CNP1-MyD88-double knockout mice compared to CNP1 null mutants (**Fig. 9 e**). Consequently, a depletion of MyD88 has indeed neuroprotective capacity to a limited extend and therefore might serve as potential therapeutic target in neurodegenerative and neuroinflammatory diseases.

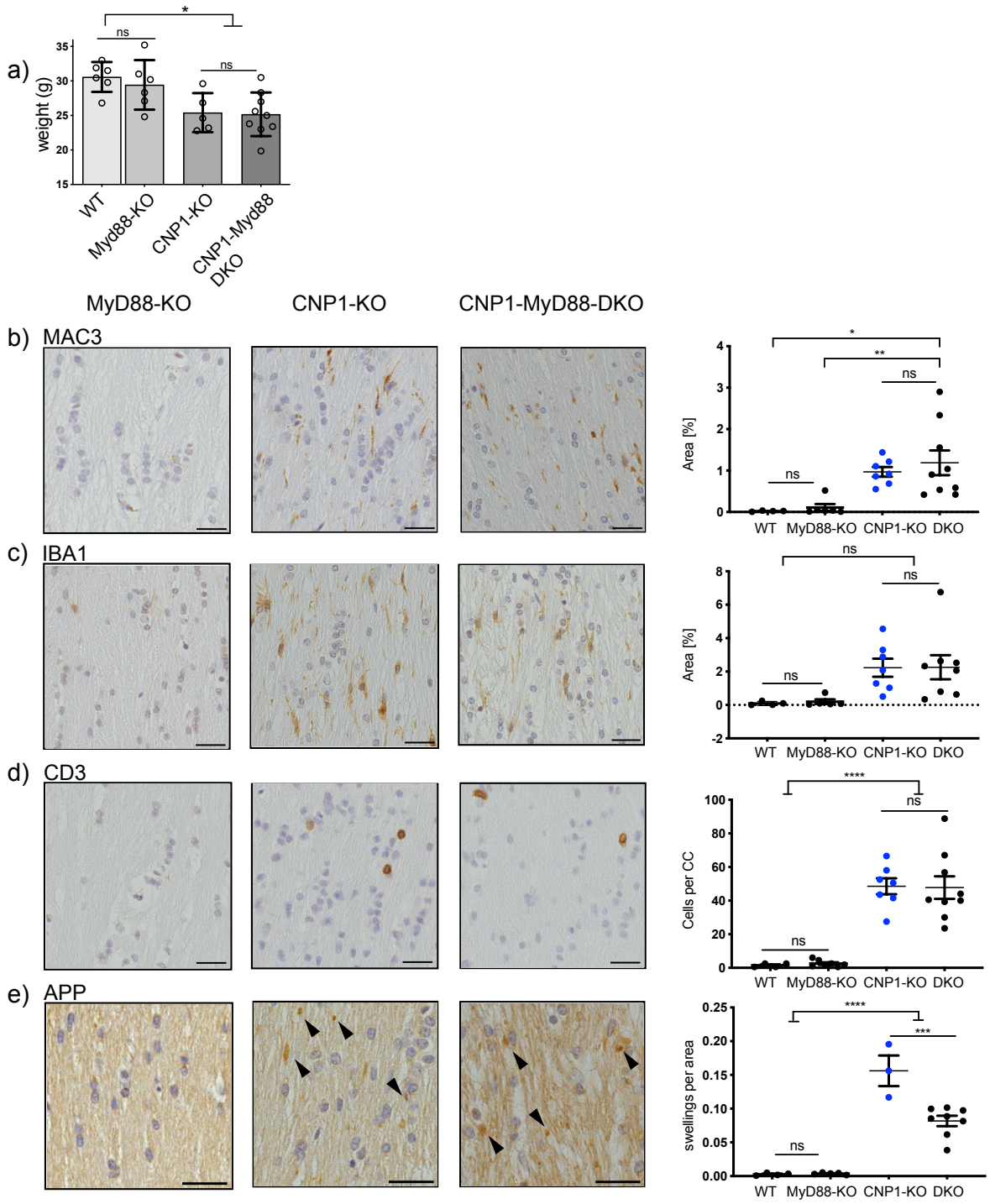


**Figure 9: Deletion of MyD88 leads to an amelioration of neurodegeneration, but this pathway is not (exclusively) responsible for the recruitment and activation of immune cells in CNP1 null mutant mice.**

Body weight is similar between CNP1-KO and CNP1-MyD88-DKO animals, whereas the weight of animals of both genotypes is significantly reduced compared to WT and MyD88-KO animals at the age of 30 – 34 weeks (a). The number of microglia (MAC3) (b), activated microglia (IBA1) (c) and T-cells (CD3) (d) is similar in CNP1-MyD88-DKO animals compared to CNP1-KO in immunohistochemical analysis of frontal corpus callosum. However, the number of axonal swellings (APP, arrowheads) (e) is significantly reduced in CNP1-MyD88-DKO animals compared to CNP1-KO. Scale bar 25 µm. The animals came from two different cohorts (Göttingen animals are depicted in blue, Berlin animals are depicted in black). N = 7 – 9. Weight analysis: Ordinary one-way ANOVA with Tukey's multiple comparison post hoc test. Histological analysis: Ordinary one-way-ANOVA-analysis with Tukey's multiple comparison post hoc test. *p value < 0.05, **p < 0.01, ***p < 0.001, ****p < 0.0001, mean ± SD is depicted. DKO = double knockout. CC = corpus callosum.

All in all, the glial cells showed an activated state of function in CNP1 null mutant mice at P75. Whereas astrocytes exhibited cytotoxic and neurotrophic features, microglia were pro-inflammatory and phagocytotic. The depletion of the adaptor molecule MyD88 led to a significant reduction of neurodegeneration in the white matter of CNP1-MyD88 double mutant mice, even if this pathway was not exclusively responsible for the recruitment of microglia and T-cells. Further pathways of microglial cell activation remain to be elucidated in future studies.

## 3.5 Altered RNA composition and MCT1 protein abundance in myelin of CNP1 null mutant mice.

CNP1 null mutant mice have been previously described to exhibit less cytosolic channels within compact myelin compared to wildtype animals throughout the early development (Snaidero et al. 2017). At least some of the RNA molecules found in the myelin transcriptome such as Mbp (Trapp et al. 1987; Ainger et al. 1993; Müller et al. 2013), Mobp and Fth1 (Holz et al. 1996; Gould et al. 2000) are actively transported into the myelin sheath. Therefore, we investigated the functional integrity of cytosolic channels in CNP1 null mutant mice by analyzing differences on RNA (RNA-Seq. and qRT-PCR) and protein (Western blot) level.

### 3.5.1 qRT-PCR analysis as a readout for the integrity of cytoplasmic channels in myelin of CNP1 null mutant mice.

In line with published data (Thakurela et al. 2016), qRT-PCR analysis confirmed a strong enrichment of Mbp-, Mobp- and Fth1-mRNA in the biochemically isolated myelin of wildtype animals compared to whole brain lysate at P75 (**Fig. 10 a**). RNA of PLP, the most abundant myelin protein, was also enriched in myelin compared to brain lysate, but less strongly than Mbp, Mobp or Fth1, most likely because Plp-RNA is translated in the oligodendroglial soma and the protein is transported into the myelin (Colman et al. 1982). Moreover, the analysis revealed, that the lack of CNP1 has an impact on the presence of RNAs enriched in myelin (**Fig. 10 b**). First, the abundance of Mbp-RNA was significantly higher in myelin of P20 CNP1 null mutant animals. Since MBP is the reported essential protein for myelin compaction in the CNS (Snaidero et al. 2017), local translation of this enriched RNA could be the cause for a previously reported, yet unexplained earlier or stronger closure of cytosolic channels in CNP1 null mutant mice (Snaidero et al. 2017). In contrast to that, we found a significant diminution of Fth1-RNA in myelin of P75 CNP1 null mutant animals, which was also visible in the RNA-Seq. analysis (**Fig. 10 c**). This might indicate that the previously reported reduction of cytosolic channels in CNP1 null mutant mice indeed has physiological consequences, since oligodendroglially derived Fth1 is important for axonal health (Mukherjee et al. 2020) (**Fig. 10 c**). Since Mobp-RNA is not significantly altered in myelin of CNP1 null

mutant mice at P75 (**Fig. 10 b**), even if the dispersion here is quite large, we have evidence, that there is an impact of the null mutation for some but not all oligodendroglial factors with regard to transport into the myelin sheath. Abundance of Plp-RNA is also not significantly altered in CNP1 null mutants according to our expectations (**Fig. 10 b**, **c**).

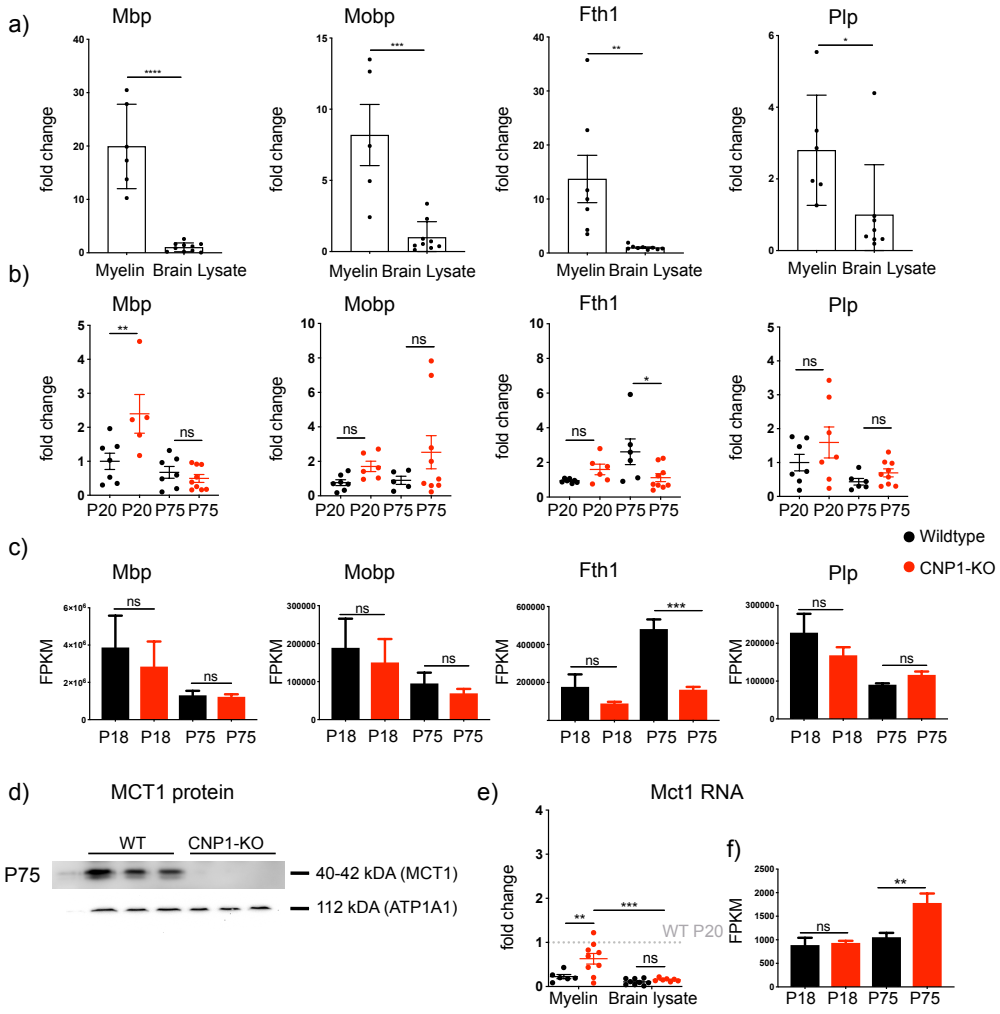


**Figure 10: Altered RNA composition and MCT1 protein abundance in myelin of CNP1 null mutant mice.**

Mbp-, Mobp- and Fth1-RNA are strongly enriched in myelin compared to whole brain lysate by qRT-PCR analysis at P75, which indicates an active transport into the myelin sheath. Plp-RNA, that encodes for the most abundant myelin protein, is less strongly enriched in myelin (a). Abundance of Mbp-RNA is significantly increased in myelin of P20 CNP1-KO mice, whereas Fth1-RNA is significantly diminished in myelin of P75 CNP1-KO mice (b). The latter finding is verified by RNA-Seq. analysis (c). MCT1-protein, previously shown to be located at the adaxonal membrane, is clearly downregulated in Western blot analysis of myelin of CNP1-KO mice compared to WT at P75 (d). In contrast, Mct1-RNA is of higher abundance in myelin of CNP1-KO compared to WT mice at P75 when analyzed by qRT-PCR (e) and RNA-Seq. (f), which might reflect a compensatory mechanism. qRT-PCR (b, e) normalized to the mean of P20 wildtype myelin (set to 1), n = 7 – 9 per group, two-way ANOVA with Bonferroni multiple comparisons post hoc test. qRT-PCR (a) normalized to the mean of P75 wildtype brain lysate (set to 1), n = 7 – 9 per group, unpaired t-test, mean ± SEM is depicted. RNA-Seq. (c, f): n = 3 per group, normalized gene expression values (FPKM), one-way ANOVA and Tukey's multiple comparisons post hoc test, mean ± SD is depicted. Western blot: n = 3 (in collaboration with Dr. Kathrin Kusch). *p value < 0.05, **p < 0.01, ***p < 0.001, ****p < 0.0001.

### 3.5.2 The decreased abundance of MCT1 protein in myelin of CNP1 null mutants might result from an altered transport along cytoplasmic channels and might contribute to the observed dysfunction and degeneration of axons.

Not only are mRNAs transported along microtubules but also other molecules such as proteins, peroxisomes (Islinger et al. 2018) and extracellular vesicles/exosomes (Frühbeis et al. 2020). This seems to be a prerequisite for the support and long-term integrity of neurons. While exosomes are secreted from oligodendrocytes via exocytosis, some molecules are also transported via carrier. An example for a transporter found to be located at the adaxonal membrane is the monocarboxylic acid transporter 1 (MCT1, also called SLC16A1). MCT1 transports molecules such as lactate and pyruvate from glycolytic oligodendrocytes to neurons (Fünfschilling et al. 2012).

I found MCT1-protein clearly downregulated in Western blot analysis of purified myelin of CNP1 null mutant mice compared to wildtype animals at P75 (**Fig. 10 d**). This finding is compatible with the idea that CNP1 mutant myelin may have an impaired support of axons as MCT1 has an instrumental role in metabolic support (Lee et al. 2012; Saab et al. 2013) and a loss of oligodendroglial MCT1 has been shown to cause neurodegeneration and hypomyelination recently (Philips et al. 2021). In contrast to this, I detected more Mct1-RNA in myelin of CNP1 null mutants compared to wildtype mice at P75 in qRT-PCR and RNA-Seq. analysis, which might reflect a compensatory mechanism by oligodendrocytes (**Fig. 10 e, f**).

Taken together, the loss of CNP1 affects the transport of some RNA molecules (Mbp, Fth1) and MCT1-protein into the myelin of CNP1 null mutant mice. The increase of Mbp-RNA in young CNP1 null mutants could explain the earlier/ stronger channel closure causing myelin dysfunction. The decrease of Fth1-RNA and MCT1-protein could both represent pathological consequences of the channel closure resulting in a disturbed axono-glial communication and impaired trophic support of axons causing the observed neurodegeneration in CNP1 null mutant mice.

# 4 Discussion

## 4.1 Characterization of neuroinflammation in CNP1 null mutant mice, a disease model of neurologic and psychiatric condition in humans.

The causal link between the lack of CNP1 and the associated progressive neuroinflammation and neurodegeneration is not fully understood yet. The recently described homozygous missense variant of CNP1 causing a lethal leukodystrophy in humans (Al-Abdi et al. 2020) as well as a decrease of CNP1 in various neurological and psychiatric diseases (Aston et al. 2005; Peirce et al. 2006; Mitkus et al. 2008) require to further uncover insights into oligodendroglial, myelin and axonal dysfunctions in CNP1 null mutant mice and the glial crosstalk including the molecular expression patterns of microglial and astroglial cells and their pathways of activation.

The investigation of RNAs isolated from purified myelin has shown that myelin contains numerically comparable RNAs (21939 in myelin of P75 wildtype mice) to RNAs isolated from myelinating oligodendrocytes (22462) (Zhang et al. 2014). Additionally, the myelin transcriptome is enriched for oligodendroglial transcripts and even further enriched for some mRNAs such as Mbp, Mobp and Fth1, that are most likely actively transported into the myelin (Thakurela et al. 2016). Moreover, the myelin transcriptome has been shown to correlate with the myelin proteome, since 88% of all proteins were represented in the transcriptome (Thakurela et al. 2016). Thus, we hypothesized that myelin is a valid source for oligodendroglial and myelin-enriched RNAs, and conducted a transcriptomic analysis of myelin for the characterization of the pathology of CNP1 null mutant mice. In our analyses we also found, that purified myelin-enriched fractions of CNP1 mutants at P75 are contaminated with many different microglial and astroglial mRNAs, which is in line with published proteomic data sets of other myelin mutant mice (Patzig et al. 2011; de Monasterio-Schrader et al. 2012; Jahn et al. 2020; Siems et al. 2020). This is most likely due to a close interaction of microglia and astrocytes with the disturbed myelin and allows a characterization of the expression patterns of these cells and hence of the neuroinflammatory reaction.

In order to better understand the initial sequence of events causing inflammation, degeneration and symptoms in CNP1 mutants, we were moreover interested in dysregulations that occur before the mice suffer from extensive neuroinflammation causing neurodegeneration and oligodendroglial dysfunction itself. Therefore, we investigated CNP1 null mutant myelin not only at P75 but also at the early age of P20.

The reported points in time whereby neuroinflammation starts in CNP1 null mutants are inconclusive so far and region-dependent starting from P28 in the brain hemispheres by immunohistochemistry (Wieser et al. 2013) to later than 3.5 months in the optic nerve (Rasband et al. 2005). Although we could neither detect any signs of neurodegeneration and neuroinflammation by immunohistochemistry nor any signs of neuroinflammation by RNA-Seq. analysis at P18, qRT-PCR revealed first evidence for enhanced activity of inflammatory cells (Gfap and Aldh1l1 for astrocytes and Ccl6 and Cd68 for microglia) in myelin of CNP1 null mutant mice as early as P20 with a progressive development of immune cell activation and neuroinflammation also visible in RNA-Seq. and immunohistochemistry at P75. Since this is still a very early stage and clinical symptoms are absent at P75 (Lappe-Siefke et al. 2003), we chose to characterize the neuroinflammatory reaction of CNP1 null mutants at the age of P75.

By qRT-PCR analysis I could demonstrate that the inflammatory reaction is largely restricted to purified myelin-enriched fractions at P75 and not visible in brain lysate, composed of grey and white matter, which suits previous histopathological analyses (Wieser et al. 2013). In the course of the progressive disease at around six months, the inflammation has been shown to spread into grey matter (Janova et al. 2018) and an increase of inflammatory and immunomodulatory markers in myelin and brain lysates can be expected.

When analyzing microglial gene expression in detail at the age of P75, we found a proinflammatory (Ccl4, Ccl6, Fcgr3, Cd86) expression profile with a DAM-like (Itgax, Cst7, Trem2, Clec7a, Gpnmb, Lyz2, Tyrobp, Ccl6, Lilrb4, Cd74) expression pattern, which is in line with another study of our lab (Depp et al. 2021). The characterization of DAM-like microglia is rather new and has been firstly performed in a murine model of Alzheimer's disease (5xFAD mice) and brains of patients diagnosed with Alzheimer's disease (Keren-Shaul et al. 2017). Similar to Depp et al., we found that the higher expressed DAM-like genes have both an anti-inflammatory pattern (Itgax, Tyrobp, Clec7a, Cst7), which argues for the presence of anti-inflammatory molecules that try to limit the neuroinflammation and the resulting damage, and a pro-inflammatory pattern (Tlr2, Cd44, Il-1β) (Rangaraju et al. 2018; Gao et al. 2019) in null mutant myelin at P75. In contrast to Depp et al., I did not find an enhancement of some typical DAM associated RNAs (Lpl, Spp1, Ms4a7, Apoe) and no downregulation of homeostatic genes (P2ry12, Cx3cr1, Tmem119) (Keren-Shaul et al. 2017) in my analysis. Although the data come from the same lab, these discrepancies may be explained by differences in the investigated material (Magnetic activated cell sorting (MACS) of microglia in grey and white matter and single cell analysis of microglia from cortex and corpus callosum vs. purified myelin) and ages (three and six months vs. P75). Importantly, the major finding that microglia express a phagocytic and DAM-like expression pattern is concordant and may help

to identify potential therapeutic targets in future experiments, that could enhance anti-inflammatory functions or dampen pro-inflammatory reactions and ameliorate the disease. Moreover, the role of DAM-like microglia and their functions upon neurodegeneration remain to be further characterized in future studies. Since these concepts are rather new and further findings are published regularly, the concepts are likely to get adapted and even further subdivided in the next years.

DAM-like microglia express pro-inflammatory molecules such as Ccl6 and Aif1/Iba1 as well as anti-inflammatory molecules such as Clec7a and Trem2 (Keren-Shaul et al. 2017; Xue and Du 2021), that were all higher expressed in myelin of CNP1 null mutants at P75. I also found Tyrobp, one of the Trem2 regulators, higher expressed in myelin of CNP1 null mutants, however not Apoe, a second Trem2 regulator, although this can be expected in the further course of the disease, since Apoe, Trem2 and Tyrobp have been also shown enhanced in CNP1 null mutants at six months of age in MACS analysis and three months of age in single-cell analysis of microglia (Depp et al. 2021) and in gene array analysis of six month CNP1 null mutants after UCMS (Edgar et al. 2011). Microglial Trem2 has been demonstrated to be involved in myelin debris clearance and remyelination (Cantoni et al. 2015; Cignarella et al. 2020) and may be involved in phagocytosis of pathological myelin outfouldings, that are increased in mice deficient for myelin genes including CNP1 (Patzig et al. 2016). Indeed, microglia of CNP1 null mutants express also phagocytotic markers (C3 and C1q), which is in line with previous results that microglia engulf myelin debris in CNP1 null mutants as identified by single cell transcriptome analysis of microglia (Depp et al. 2021) and suggested by electron microscopy (Edgar et al. 2009).

Upon inflammation, brain injury or neurodegeneration, DAM-like microglia can get activated via pathogen-associated molecular pattern (PAMP) and damage-associated molecular pattern (DAMP) molecules binding to pattern-recognition-receptors such as TLR (García-Revilla et al. 2019), of which I found Tlr1 and Tlr2 higher expressed in RNA-Seq. of CNP1 null mutant myelin. The DAMP IL-33 (Wicher et al. 2017), which I also found upregulated in RNA-Seq. analysis and qRT-PCR, is a potent driver of the MyD88 dependent activation of the transcription factor NF-κB via binding on its receptor ST2 (Schmitz et al. 2005). Since MyD88 is involved in microglia activation (Deguine and Barton 2014), we analyzed CNP1-MyD88 double knockout mice, in order to investigate the relevance of MyD88 dependent activation of NF-κB in CNP1 null mutants. The analysis revealed an amelioration of axonal pathology as shown by a significant reduction of APP positive spheroids in immunohistochemistry of double mutant mice compared to single CNP1 null mutants implying that neurons are less attacked in the double mutants. Hence, the MyD88-NF-κB-pathway is at least partially involved in the activation of microglia in CNP1 null mutant mice. Unexpectedly, there was no reduced recruitment of activated microglia (Iba1, Mac3) and T-cells (CD3) in MyD88-CNP1 double knockout animals. A possible explanation might be that microglia in CNP1-MyD88

double knockout mice are only less aggressive towards axons, however, this is speculative and needs to be investigated in further studies. Since Iba1, a marker of activated microglia, is not a target gene of the transcription factor NF-κB (Boston University Biology, internet source 3), it is likely, that there are further pathways of microglia activation in CNP1 null mutants that remain to be elucidated. Concludingly, neurodegeneration and neuroinflammation are at least partially uncoupled from each other in CNP1 null mutant mice at the age of 30 – 34 weeks and the activation of microglia is not solely dependent on MyD88. However, since the number of axonal spheroids as signs of axonal pathology is decreased in CNP1-MyD88 double mutants, the pathway appears to be relevant for microglial attack of axons in diseases associated with CNP1 deficiency and in order to investigate the significance of this finding, additional experiments such as behavioral and cognitive testing could be performed with CNP1-MyD88 double knockout mice.

A limiting factor of our study is that we had to complement CNP1 null mutants from Göttingen to the Berlin cohort of CNP1-MyD88 double knockout and MyD88 knockout animals for immunohistochemistry experiments due to incorrect genotyping. Since differences due to the transport of CNP1-MyD88 double knockout mice from Berlin to Göttingen would expect to cause more rather than less stress, resulting in an enhanced neuroinflammation and neurodegeneration compared to CNP1 null mutant animals from Göttingen, the finding that CNP1-MyD88 double knockout animals are equal in most parameters and exhibited less and not more neurodegeneration, allows to interpret this as a valid readout.

My study also revealed an involvement of activated astrocytes in CNP1 null mutant mice as shown by RNA-Seq., qRT-PCR and immunohistochemistry, which has been demonstrated previously (Lappe-Siefke et al. 2003; Wieser et al. 2013). Astrocytes are known to be highly diverse upon development and aging (Matias et al. 2019), brain localization, displaying different morphologies and protein expression in grey matter and white matter for instance (Sofroniew and Vinters 2010; Li et al. 2016), and they can exert a plethora of specific functions. Astrocytes also dynamically adapt gene expression upon neuroinflammation (Hasel et al. 2021), hence actively influencing neuroinflammation and neurodegeneration. My RNA-Seq. analysis of CNP1 null mutant myelin revealed that the activated astrocytes express typical features of both neurotoxic A1 (Gbp2, C3, Ggta1) and neuroprotective A2 (Cd14, Cd109, Emp1) astrocytes (Liddelow et al. 2017), which is the first characterization of the molecular pattern of activated astrocytes in CNP1 null mutant mice to my knowledge. Since the concept of A1/A2 polarization of activated astrocytes upon neuroinflammation (Liddelow et al. 2017) is rather new and further insights into the complex biology of astrocytes will arise in the future, the characterization will likely be adapted and subdivided similar to microglia. My data reveal also enhanced expression of Timp1, Gfap, H2-K1, H2-D1, Aqp4 and Vim in myelin of CNP1 null mutants, markers that have been shown to define a specialized subset of

astrocytes associated with white matter in a murine model of neuroinflammation (Hasel et al. 2021). Aqp4 encodes a water channel on astrocytes and anti-AQP4 antibodies are found in most patients with Neuromyelitis optica spectrum disorder (Kawachi and Lassmann 2017; Carnero Contentti and Correale 2021), demonstrating that astrocytes are also directly involved in causing white matter diseases. Some further higher expressed genes in null mutant myelin such as components of the complement system (C1qa and C1qc) or Cxcl10 are known to be involved in the complex crosstalk between glial cells upon neuroinflammation (Reid and Kuipers 2021). The specific functions and molecular patterns of astrocytes in the pathophysiology of neuroinflammation and neurodegeneration in general and in CNP1 null mutant mice specifically are not fully understood so far and need to be elucidated in further studies, since this may provide diagnostic and prognostic biomarkers as well as therapeutic targets for a variety of diseases.

According to my data, a lack of CNP1 causes an early inflammatory reaction with pro- and anti-inflammatory features and an activation of microglia that exhibit a DAM-like phagocyting pattern and are activated at least partially via MyD88, as well as an activation of astrocytes with an A1 and A2 signature. Since we were also interested in dysregulations that occur in early stages of the disease before neurodegeneration and oligodendroglial dysfunction due to the neuroinflammatory response itself, we also investigated myelin of CNP1 null mutants at the age of P18. This allows an investigation of early consequences of the lack of CNP1 as well as the potential immunomodulatory role of oligodendrocytes, which are increasingly known to display a relevant dysfunction in neurological and psychiatric diseases (Walsh et al. 2002; Nasrabady et al. 2018; Bøstrand and Williams 2021; Sams 2021), at a point in time resembling preclinical stages, that is difficult to investigate in humans. Although we identified two interesting immunomodulatory molecules, Tnfaip6 and Il-33, we could not finally prove their oligodendroglial origin.

## 4.2 Oligodendrocytes as potentially early immunomodulatory cells in CNP1 null mutant mice.

The finding, that oligodendroglial cells exhibit specific and heterogeneous gene expression subsets in single cell and single nucleus transcriptome analyses of murine MS models (Falcão et al. 2018), patients with MS (Jäkel et al. 2019; Schirmer et al. 2019) and Alzheimer's disease patients (Mathys et al. 2019) lead to the assumption, that oligodendrocytes themselves contribute actively to disease pathology or even etiology. Although multiple risk factors for MS have been found, the etiology and initial events leading to an attack of immune cells towards the myelin sheath are largely unknown (Reich et al. 2018). Also the reasons for a failure of sufficient remyelination in MS are unknown and oligodendrocyte-extrinsic dysfunctions (Starost et al. 2020) are discussed just as oligodendrocyte-intrinsic dysfunctions (Factor et al. 2020). Interestingly, there are some reports that

suggest oligodendroglial dysfunction as the initial cause of MS (Traka et al. 2016). Moreover, oligodendrocytes of experimental autoimmune encephalomyelitis (EAE) mice (Falcão et al. 2018) and MS patients (Schirmer et al. 2019) have been shown to express a lot of MS susceptibility genes/ gene homologues. Jäkel et al. even defined a subset of so-called immune oligodendroglia (imOLG) in single-nucleus transcriptome analysis of MS patients that share some expressional features with microglia (Jäkel et al. 2019). Therefore, the suggestion arises, that oligodendrocytes act immunomodulatory by themselves due to genetic alterations and a dysfunction of myelin. Hence, CNP1 null mutant mice, which are characterized by an activation of microglia, astrocytes and T-cells and neurodegeneration after the inactivation of an oligodendrocyte-specific gene (Lappe-Siefke et al. 2003; Wieser et al. 2013) are a valid model to study this hypothesis in more detail.

The *in-vivo* functions of CNP1 and direct consequences of a loss of CNP1 for oligodendrocytes, the primary affected cells in CNP1 null mutant mice, are not fully understood yet. Moreover, early signals initiating the inflammatory reaction in CNP1 null mutants are unknown so far. Thus, we intended to investigate the role of oligodendrocytes in the disease pathology of CNP1 null mutant mice and analyze, whether there is evidence for immunomodulation by oligodendrocytes present in myelin. The loss of CNP1 seems to shift oligodendrocytes towards imOLG, as we could detect an upregulated abundance of some typical genes of imOLG in the purified CNS myelin-enriched fractions of CNP1 null mutants including Ly86, Cd74, Serpina3n and major histocompatibility complex (MHC)-I and MHC-II related genes (Jäkel et al. 2019; Schirmer et al. 2019) similar to results from EAE mice (Falcão et al. 2018), which experience an immune attack against myelin (Constantinescu et al. 2011). The presence of MHC-I and -II related genes argues for a direct crosstalk between oligodendrocytes and immune cells such as T-cells, providing further evidence for an active immunomodulation of oligodendrocytes in white matter diseases. However, since we demonstrated an infiltration of immune cells into white matter tracts of CNP1 null mutants at P75 by immunohistochemistry, which is in line with previous results (Lappe-Siefke et al. 2003), immune cells such as astrocytes and microglia may be a source of contamination of the purified myelin and it can thus not be formally excluded that these proteins have a different source. Indeed, isolated myelin has been shown previously to be moderately contaminated with non-myelinic and non-oligodendroglial proteins (Patzig et al. 2011; de Monasterio-Schrader et al. 2012; Jahn et al. 2020; Siems et al. 2020) and mRNAs (Thakurela et al. 2016).

As a next step and in order to distinguish oligodendroglially expressed genes from those of other cells, we aimed to define a prodromal phase that allows conclusions about early oligodendroglial reactions to the loss of CNP1 without contaminating RNAs. Although CNP1 null mutant mice are known to exhibit ultrastructural alterations at paranodal loops and increased neurodegeneration in certain areas of the CNS from a very early time point on (Edgar et al. 2009), there was no evidence

for immune cell activation before the age of P28 (Wieser et al. 2013) so far. In accordance with these data, we could also define such a prodromal phase successfully by immunohistochemistry and RNA-Seq., which both gave no evidence for an immigration of astrocytes or microglia into the myelin of CNP1 null mutant mice at P18. When investigating this age by qRT-PCR, we identified Tnfaip6 and Il-33 higher expressed in the null mutant mice. The early presence of Tnfaip6, which encodes for the secreted, anti-inflammatory TSG-6 (Lee et al. 1992; Wisniewski and Vilček 1997; Dyer et al. 2016) and the cytokine IL-33 (Miller 2011) in myelin indicate, that those molecules are oligodendroglially derived and play a central role in the early disease pathology of CNP1 null mutants. Tnfaip6 is even further upregulated at P75 in myelin and brain lysate, whereas Il-33 is upregulated at P20 in qRT-PCR and at P75 in RNA-Seq. A possible explanation, why we did not find Il-33-mRNA upregulated in myelin of P75 mice in qRT-PCR may be the high distribution in our analysis.

A previous finding of Tnfaip6 expression in single cell transcriptome analyses of oligodendrocyte lineage cells (Zhang et al. 2014; Falcão et al. 2018) and the early presence in myelin provide support for an oligodendroglial source of Tnfaip6 in CNP1 null mutants. Similarly, IL-33 has been repeatedly shown to be expressed by oligodendrocyte lineage cells in health and disease (Zhang et al. 2014; Gadani et al. 2015; Allan et al. 2016; Zarpelon et al. 2016; Wicher et al. 2017; Falcão et al. 2018; Ljunggren-Rose et al. 2020). Tnfaip6 exerts several anti-inflammatory functions (Wisniewski et al. 1996; Fries and Kaczmarczyk 2003; Cao et al. 2004; Szántó et al. 2004; Milner et al. 2006) including a shift of microglia towards an anti-inflammatory phenotype (Li et al. 2018) comparable to Il-33 (Gadani et al. 2015; Pomeshchik et al. 2015), as well as a binding of chemokines such as Ccl2 and Ccl5 (Dyer et al. 2014; Dyer et al. 2016). This binding prevents the chemokines to bind to glycosaminoglycans and reduces immune cell immigration. As Ccl2 and Ccl5 were both higher expressed in RNA-Seq. of CNP1 null mutant mice at P75 compared to P18, this may be an early mechanism to prevent an extensive inflammatory reaction in CNP1 null mutants. While Tnfaip6 decreases TLR2/MyD88/NF-κB signaling (Choi et al. 2011; Mittal et al. 2016; Tang et al. 2021), a pathway of microglia activation that we have shown at least partially responsible for neurodegeneration in CNP1 null mutant mice at later stages, Il-33 leads to an activation of NF-κB via MyD88 (Schmitz et al. 2005; Li et al. 2021). Since both are already upregulated in the prodromal phase it remains open, which effect overrides the other in the early stage of disease in CNP1 null mutants. Next to the function of IL-33 as a DAMP (Klegeris 2021) activating microglia and inducing them to produce pro-inflammatory cytokines (Xu et al. 2008; Gadani et al. 2015; Wicher et al. 2017; Cao et al. 2018), IL-33 has also anti-inflammatory (Kurowska-Stolarska et al. 2008) and tissue reparative effects in the CNS (Molofsky et al. 2015). IL-33 secreted from oligodendrocytes in the spinal cord of mice has been also demonstrated to cause increased levels of the pro-inflammatory molecules

TNFα and IL-1β (Zarpelon et al. 2016), both inducing the secretion TSG-6 (Lee et al. 1992; Wisniewski et al. 1993). In combination with the anti-inflammatory properties of TSG-6 this suggests a negative feed-back loop preventing or dampening inflammation (Wisniewski and Vilček 1997) in order to reduce the resulting damage, which is highly relevant in the CNS due to its low regenerative capacities. TNFα is not only neurotoxic but it causes also oligodendroglial cell death and myelin damage (Selmaj and Raine 1988; D'Souza et al. 1995; Jurewicz et al. 2005), hence, oligodendrocytes may secret Tnfaip6 upon defect myelin in order to protect themselves and their surroundings. Tnfaip6 acts partly through the cell-surface receptor CD44 (Choi et al. 2011), which we also found significantly upregulated in RNA-Seq. of myelin of CNP1 null mutants at P75 and which is expressed by astrocytes (Zhang et al. 2014; Coulson-Thomas et al. 2016; Liddelow et al. 2017) and other cells (Choi et al. 2011; Piao et al. 2013; Zhang et al. 2014). TSG-6 and CD44 have been repeatedly demonstrated to play a role in various animal models of inflammation and CNS injury (Bertling et al. 2016; Coulson-Thomas et al. 2016; Reinbach et al. 2020; Wan et al. 2021) similar to Il-33 (Li et al. 2012; Gadani et al. 2015; Pomeshchik et al. 2015; Wicher et al. 2017; Yang et al. 2017; Gao et al. 2018; Li et al. 2021). Importantly, Tnfaip6 and Cd44 as well as Il-33 and St2 are also higher expressed in several human CNS diseases such as Alzheimer's disease (Du et al. 2018; Reed et al. 2019; Damodarasamy et al. 2020; Saresella et al. 2020; Sun et al. 2021) and MS (Chang et al. 2012; Lieury et al. 2014; Allan et al. 2016; Nataf et al. 2017; Schirmer et al. 2019), reinforcing the important roles of TSG-6 and IL-33 in white matter dysfunction as it is present in CNP1 null mutants.

In agreement with my results, Tnfaip6 has been found in another transcriptome analysis of the frontal cortex of CNP1 null mutant mice at P20 (McKenzie et al. 2017), although the authors had a different approach and statistical criteria (false discovery rate = 0.3, p adj < 0.05) than we had (log2FC < - 1/ > 1, p adj < 0.05). Moreover, this study found homologous dysregulations to early disease stages of Alzheimer's disease in CNP1 null mutants (McKenzie et al. 2017), which underlines the important role of CNP1 in or at least similarities regarding the pathophysiology of neurodegenerative diseases. The finding, that Tnfaip6 is significantly higher expressed in further young murine transgenic models missing PLP, UGT8 (UDP glycosyltransferase 8) (McKenzie et al. 2017) and MBP (Aaker et al. 2016) and which all display primary oligodendroglial and/ or myelin pathology similar to CNP1 null mutant mice, provides additional support for the hypothesis that Tnfaip6 is verifiable connected to oligodendrocyte pathology, which makes it an interesting diagnostic and therapeutic target for a wide range of diseases. However, since Tnfaip6 was only upregulated in whole brain analysis but not in primary cell cultures of oligodendrocytes and OPC of shiverer mice lacking MBP (Aaker et al. 2016), Tnfaip6 can also to be secreted from other cells than oligodendrocytes.

Indeed, Tnfaip6 and Il-33 are not only expressed by oligodendrocytes but also by astrocytes (Gadani et al. 2015; Allan et al. 2016; Coulson-Thomas et al. 2016) and further peripheral immune cells (Liew et al. 2010; Day and Milner 2019). Hence, we followed the possibility that the purified myelin could be already contaminated with immigrated glial cells at P20, even though to a lesser extent that at P75, as suggested by the finding of higher expression of pro-inflammatory, typical microglial (Cd68, Ccl6) and astroglial (Gfap, Aldh1l1) mRNAs in my qRT-PCR. The higher expression of Gfap, Aldh1l1, Cd68 and Ccl6 at P18/P20 could also result from closely attached cells to the myelin sheath such as physiologically present perinodal astrocytes (Dutta et al. 2018) and microglia (Wlodarczyk et al. 2017), which are involved in the still on-going myelination at P20 for instance (Bennett and Barres 2017; Hagemeyer et al. 2017; Wlodarczyk et al. 2017). These cells may be more present and/ or activated in CNP1 null mutants for unknown reasons so far, however, not enough to be detected by immunohistochemistry. Cd68 positive microglia have been described to be predominantly found in white matter regions upon neuroinflammation (Raj et al. 2017), which argues for an involvement of microglia in the pathology of CNP1 null mutants at that early age. Therefore, it is most likely, that the upregulation of Cd68, Ccl6, Gfap and Aldh1l1 results from microglia and astrocytes. Consequently, the existence of a prodromal phase and the conclusion, that the immunomodulatory molecules Tfnaip6 and Il-33 are secreted by oligodendrocytes and not by other cells, has to be questioned. Generally, qRT-PCR is used to validate results from transcriptome analyses, since it is still considered as gold standard for measuring gene expression (Corchete et al. 2020), and in our hands, qRT-PCR results were more sensitive than RNA-Seq. and immunohistochemistry. That the differences between the analyses of RNA-Seq. and qRT-PCR data result from the different ages (P18 in RNA-Seq. data and P20 in qRT-PCR data) is highly unlikely, since these are only two days.

Independently from the initial source of Tnfaip6 and Il-33, both molecules may depict a primary or early secondary response to the loss of CNP1 modulating the disease pathology. Since immunohistochemistry validated that axonal pathology is minor at early ages, TSG-6 and IL-33 may serve as diagnostic or therapeutic markers. Tnfaip6 has a diagnostic potential as biomarker (Wisniewski et al. 2014; Yu et al. 2016) and it has been investigated in several studies as a possible therapeutic molecule in animal models of various diseases (Mindrescu et al. 2000; Bárdos et al. 2001; Day and Milner 2019). In the CNS, the administration of recombinant TSG-6 or stem cells, which have immunomodulatory abilities that have been demonstrated to be at least partially dependent on the secretion of Tnfaip6 (Liu et al. 2014a; Liu et al. 2014b; Xu et al. 2017; Hu et al. 2018; Yang et al. 2020), led to an amelioration of various traumatic CNS diseases (Li et al. 2018; Jha et al. 2019; Xu et al. 2020) and memory function (Watanabe et al. 2013) and is suggestively neuroprotective (Bertling et al. 2016; Morioka et al. 2017). Several studies have also investigated the capacities of

IL-33 as a therapeutic target in CNS diseases with conflicting observations (Li et al. 2012; Pomeshchik et al. 2015; Yang et al. 2017; Gao et al. 2018; Xiao et al. 2018; Gao et al. 2020; Li et al. 2021). In contrast to Tnfaip6, the properties of IL-33 seem to be more diverse and therefore, further experiments are required to better understand the functions of IL-33 and identify therapeutic targets to develop potential therapies for white matter diseases.

Taken together, my results demonstrate that the loss of CNP1 has very early impacts on mRNAs isolated from myelin including evidence for an inflammatory reaction already at P20. Whether a prodromal phase in terms of an absence of any immune reaction exists at earlier stages of the disease or whether the lack of CNP1 induces an immediate immune cell activation, needs to be investigated in further studies and will require other experiments than myelin purification, since therefore a sufficient number of axons needs to be myelinated. For instance, one could perform single-cell or single-nucleus transcriptome analyses of glial cells isolated from white matter tracts of CNP1 null mutant mice at different ages. In the light of the emerging knowledge about the active role of oligodendrocytes in inflammation and immune processes, oligodendrocytes may – despite the early presence of typical astroglial and microglial genes in the disturbed myelin of CNP1 null mutants – release the immunomodulatory molecules IL-33 and TSG-6 in order to alarm the immune system on the one hand and calm down the inflammatory reaction on the other hand. However, we could not finally prove a clear oligodendroglial origin of Tnfaip6 and Il-33, since we were neither able to detect TSG-6 in immunohistochemistry, a difficult that has been reported previously (Bertling et al. 2016), nor by Western Blot so far. Such a validation of the oligodendroglial origin of TSG-6 and IL-33 is the next step. With regard to the emerging knowledge about the role of CNP1 in human diseases, CNP1 null mutant mice treated with TSG-6 could be analyzed for an amelioration of neuroinflammation, neurodegeneration and the clinical phenotype. Another promising approach could be the development of an inducible construct of Tnfaip6-overexpression in oligodendrocytes of CNP1 null mutants, with the aim to protect the mice from neurodegeneration. Chandra et al. have published proof of principle evidence of this kind of transgenic rescue approach (Chandra et al. 2005). The comparison of our myelin transcriptome with transcriptome data of oligodendrocyte lineage cells provides an interesting tool for the discovery of further oligodendroglial reactions to the loss of CNP1, however, the different experimental approaches, methods and statistics have to be considered. It must be also noted, that the analysis of single cell transcriptomes may lead to falsified results due to the complex cytological architecture of oligodendrocytes, since a cell purification disrupts the delicate connections between the oligodendroglial soma and its processes ensheathing axons (Colonna and Brioschi 2020), which could result especially in a loss of oligodendroglial mRNAs in the non-compact myelin parts. Single-nucleus transcriptome analyses of myelinating oligodendrocytes in CNP1 null mutant mice would circumvent

this problem; nevertheless, these would not allow the detection of myelin enriched mRNAs that are possibly involved in the pathogenesis of this myelin disease.

## 4.3 RNA expression analysis provides evidence for a perturbed function of cytosolic channels in CNP1 mutant mice.

My results from qRT-PCR analysis indicate that mRNAs encoding Mbp, Mobp and Fth1 are strongly enriched in myelin compared to brain lysate, which confirms that they are likely being actively transported into the myelin sheath (Colman et al. 1982; Trapp et al. 1987, Holz et al.1996, Carson et al. 1998; Gould et al. 2000). Although this process has been described in detail only for Mbp-mRNA and it is strongly suggested for Mobp- and Fth1-mRNA, an active transport into the myelin sheath has been recently suggested to apply for many more RNAs (Yergert et al. 2021).
In qRT-PCR analysis we found, that CNP1 null mutant myelin contains significantly more Mbp-mRNA compared to wildtype myelin at the age of P20. A direct interference of CNP1 and MBP has been suggested earlier, since CNP1 overexpression induces more non-compact myelin and a decrease of MBP-mRNA and protein (Gravel et al. 1996). In contrast, a lack of CNP1 has been demonstrated to cause a reduction of cytosolic channels in myelin (Snaidero et al. 2017). Furthermore, Mbp-mRNA transport has been suggested to be influenced by CNP1 (Yin et al. 1997). These findings suggested a model of CNP1 antagonizing the compaction function of MBP mechanically (Snaidero et al. 2017). Hence, the increased abundance of Mbp-mRNA in the myelin of CNP1 null mutants at P20 in my qRT-PCR analyses provides a possible mechanistical explanation for the observation of an earlier or stronger closure of cytosolic channels in CNP1 null mutants, since MBP is the instrumental protein for myelin membrane compaction and translated locally at the axon-glia contact site (Müller et al. 2013). Interestingly, I found that Mbp-mRNA concentration in myelin of CNP1 null mutants was not significantly altered anymore at P75 when compared to wildtype mice. We hypothesize that the earlier presence of Mbp-mRNA in high abundance induces preferential, fast and/or more dense closure of channels in CNP1 mutant mice. Upon this enhanced closure the transport of Mbp-mRNA within the channels normalizes with age.
We hypothesized that an earlier and/or stronger closure of cytosolic channels in CNP1 mutant myelin influences the transport of proteins necessary for axonal support. One of the relevant molecules is MCT1, a monocarboxylate transporter involved in the transport of energetic metabolites lactate and pyruvate from oligodendrocytes to axons (Fünfschilling et al. 2012; Lee et al. 2012; Saab et al. 2013). Indeed, at P75 my Western blot analysis demonstrated that MCT1 is significantly reduced in CNP1 null mutant myelin when compared to control animals. Could this loss of MCT1 be a direct cause of the axonal pathology in CNP1 null mutant mice? Experimental evidence from the analysis of MCT1 null mutant mice are compatible with this idea, since oligodendroglial MCT1

has been recently demonstrated to be required for the long-term well-being of axons (Philips et al. 2021). A loss of MCT1 in mature oligodendrocytes causes hypomyelination and axonal degeneration with signs of energy failure such as swollen and atypically shaped axonal mitochondria at about 12 months of age (Philips et al. 2021). Thus, the identified loss of MCT1 may indeed be causatively linked to the pathology in CNP1 mutant mice. Contrary to our results of MCT1 protein, we detected significantly more Mct1-mRNA in myelin of CNP1 null mutants, which could be interpreted as reactive attempt of compensation.

Next to MCT1, another oligodendroglial protein with a suggested role for axonal support is Fth1. My analyses revealed that Fth1-mRNA is extremely abundant in myelin of wildtype mice compared to brain lysate (Mukherjee et al. 2020). In contrast, we found FTH1 protein rather enriched in brain lysate compared to myelin (Mukherjee et al. 2020). These and additional findings by the collaborating group of Mikael Simons (Institute of Neuronal Cell Biology, TU Munich and German Center for Neurodegenerative Diseases Munich) supported the idea that Fth1 is secreted from oligodendrocytes in extracellular vesicles and serves as an antioxidant to protect neurons against iron-mediated toxicity (Mukherjee et al. 2020). Interestingly, myelin of CNP1 null mutants contained significantly less Fth1-mRNA than wildtype myelin, which might result from the disturbed transport of this mRNA. Given the newly defined role of FTH1 we hypothesize that this may have severe consequences to brain homeostasis and iron metabolism in the CNP1 mutant brain. One consequence might be a reduced capacity to store iron, which enhances neurodegeneration, since iron in its free from is neurotoxic and can increase free radicals, as shown in mice with Fth1 deficient oligodendrocytes or a disruption of oligodendroglial Fth1 release in extracellular vesicles (Mukherjee et al. 2020).

Interestingly, we did not have evidence that the reduced amount of Fth1-mRNA in CNP1 mutant myelin is directly caused by the proposed defects in the cytosolic channel system through myelin. On the contrary, other mRNAs that are known to be actively transported into the myelin sheath such as those encoding for MBP or MOBP, were not significantly decreased at the age of P75 in CNP1 null mutant myelin. Hence, the effect is specific to Fth1-mRNA and further studies are required to elucidate, why one or more mRNAs and proteins are lower concentrated in the myelin of CNP1 mutant mice.

Based on the current literature, both the decreased amount of Fth1-mRNA and Mct1 protein in CNP1 null mutant myelin can be linked to disturbances of myelinic support of axons causing the suggested energy failure and axonal degeneration associated to CNP loss of function mutations. In the future, patients with the lethal leukodystrophy caused by a homozygous missense variant of CNP1 (Al-Abdi et al. 2020) could be also investigated histologically for axonal degeneration as well as for the abundances of Fth1 and MCT1 in *post-mortem* CNS myelin. Moreover, CNP1 null mutants

could be further investigated regarding the mechanisms and involved cellular structures and pathways of the suggested energy failure in axons. In order to shed light on further functional consequences of CNP1 deficiency on axons next to APP swellings indicating transport perturbation and neurodegeneration, one could investigate, whether CNP1 null mutants exhibit a decrease of transported mRNAs in axons and measuring the conduction velocity at various ages of CNP1 null mutant mice could be performed since previous findings are inconclusive so far (Kolaric et al. 2013) in order to determine the point in time of axonal dysfunction.

# 5 Supplement

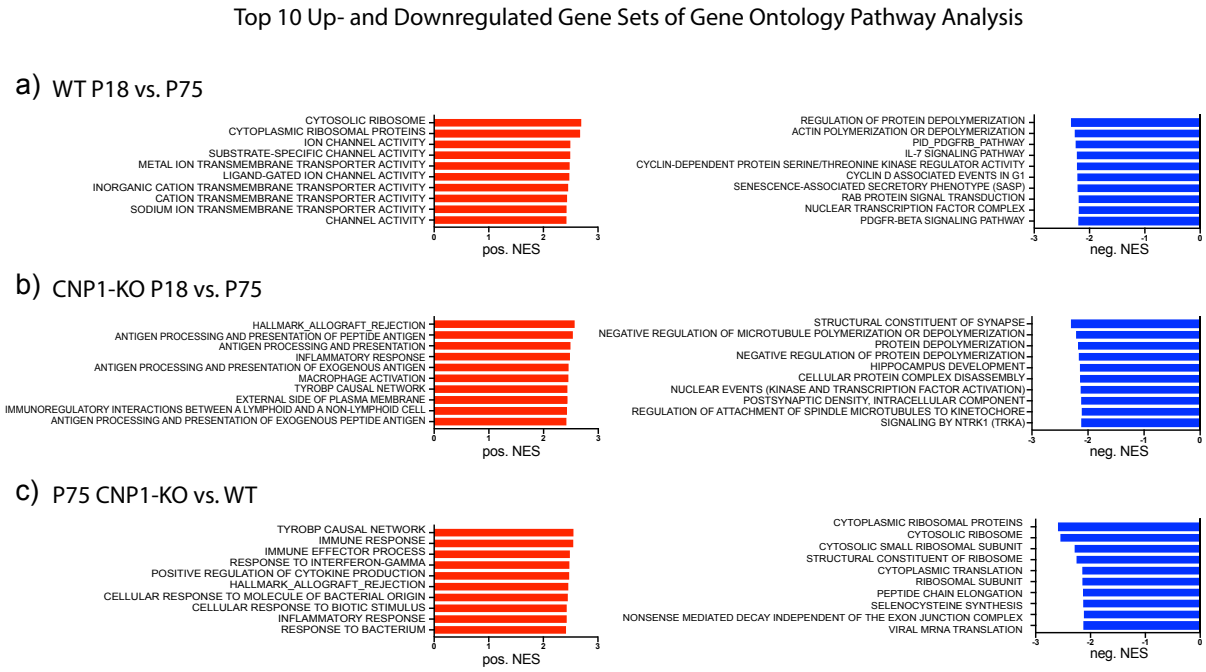


**Figure S1: Gene ontology pathway analysis**

Gene ontology pathway analysis (GSEA) was performed with gene sets with 10–500 genes utilizing log2FC. Exemplary, the top ten dysregulated pathways are listed. Upregulated pathways (pos. NES) are depicted in red and represent higher expressed genes at P75 compared to P18 (a, b) and higher expressed genes in null mutants compared to wildtype mice (c). Downregulated pathways (neg. NES) are depicted in blue, respectively. In total, the analysis of differentially expressed genes revealed 435 pathways upregulated due to development and 89 pathways downregulated in WT P18 vs. P75 (a). For CNP1 P18 vs. P75 (b) 689 pathways were upregulated, of which most are involved in immune reactions and development, and 11 pathways were downregulated. At P75 CNP1-KO vs. WT (c) most of the 570 upregulated pathways were also inflammation-associated, and 17 pathways were downregulated. The analysis of P18 CNP1-KO vs. WT revealed no significantly dysregulated pathways. Visualization was performed with GraphPad. NES = Normalized enrichment score.

# 6 References

Aaker JD, Elbaz B, Wu Y, Looney TJ, Zhang L, Lahn BT, Popko B (2016): Transcriptional Fingerprint of Hypomyelination in *Zfp191* $^{null}$ and *Shiverer* (*Mbp* $^{shi}$) Mice. ASN Neuro 8, 1759091416670749

Adachi O, Kawai T, Takeda K, Matsumoto M, Tsutsui H, Sakagami M, Nakanishi K, Akira S (1998): Targeted Disruption of the MyD88 Gene Results in Loss of IL-1- and IL-18-Mediated Function. Immunity 9, 143–150

Afridi R, Lee W-H, Suk K (2020): Microglia Gone Awry: Linking Immunometabolism to Neurodegeneration. Front Cell Neurosci 14, 246

Aggarwal S, Snaidero N, Pähler G, Frey S, Sánchez P, Zweckstetter M, Janshoff A, Schneider A, Weil M-T, Schaap IAT, et al. (2013): Myelin Membrane Assembly Is Driven by a Phase Transition of Myelin Basic Proteins Into a Cohesive Protein Meshwork. PLoS Biol 11, e1001577

Ainger K, Avossa D, Morgan F, Hill SJ, Barry C, Barbarese E, Carson JH (1993): Transport and localization of exogenous myelin basic protein mRNA microinjected into oligodendrocytes. J Cell Biol 123, 431–441

Al-Abdi L, Al Murshedi F, Elmanzalawy A, Al Habsi A, Helaby R, Ganesh A, Ibrahim N, Patel N, Alkuraya FS (2020): CNP deficiency causes severe hypomyelinating leukodystrophy in humans. Hum Genet 139, 615–622

Allan D, Fairlie-Clarke KJ, Elliott C, Schuh C, Barnett SC, Lassmann H, Linnington C, Jiang H-R (2016): Role of IL-33 and ST2 signalling pathway in multiple sclerosis: expression by oligodendrocytes and inhibition of myelination in central nervous system. Acta Neuropathol Commun 4, 75

Amor S, Puentes F, Baker D, van der Valk P (2010): Inflammation in neurodegenerative diseases. Immunology 129, 154–169

Amor S, Peferoen LAN, Vogel DYS, Breur M, van der Valk P, Baker D, van Noort JM (2014): Inflammation in neurodegenerative diseases - an update. Immunology 142, 151–166

Arroyo EJ, Scherer SS (2000): On the molecular architecture of myelinated fibers. Histochem Cell Biol 113, 1–18

Aston C, Jiang L, Sokolov BP (2005): Transcriptional profiling reveals evidence for signaling and oligodendroglial abnormalities in the temporal cortex from patients with major depressive disorder. Mol Psychiatry 10, 309–322

Bachiller S, Jiménez-Ferrer I, Paulus A, Yang Y, Swanberg M, Deierborg T, Boza-Serrano A (2018): Microglia in Neurological Diseases: A Road Map to Brain-Disease Dependent-Inflammatory Response. Front Cell Neurosci 12, 488

Bader Lab (internet source 1): http://download.baderlab.org/EM_Genesets/, accessed on August 15, 2020

Balabanov R, Strand K, Goswami R, McMahon E, Begolka W, Miller SD, Popko B (2007): Interferon- -Oligodendrocyte Interactions in the Regulation of Experimental Autoimmune Encephalomyelitis. J Neurosci 27, 2013–2024

Barbarese E, Koppel DE, Deutscher MP, Smith CL, Ainger K, Morgan F, Carson JH (1995): Protein translation components are colocalized in granules in oligodendrocytes. J Cell Sci 108, 2781–2790

Bárdos T, Kamath RV, Mikecz K, Glant TT (2001): Anti-inflammatory and chondroprotective effect of TSG-6 (tumor necrosis factor-alpha-stimulated gene-6) in murine models of experimental arthritis. Am J Pathol 159, 1711–1721

Barnett MH, Prineas JW (2004): Relapsing and remitting multiple sclerosis: Pathology of the newly forming lesion. Ann Neurol 55, 458–468

Baumann N, Pham-Dinh D (2001): Biology of Oligodendrocyte and Myelin in the Mammalian Central Nervous System. Physiol Rev 81, 871–927

Bennett ML, Barres BA (2017): A genetically distinct microglial subset promotes myelination. EMBO J 36, 3269–3271

Berghoff SA, Spieth L, Sun T, Hosang L, Depp C, Sasmita AO, Vasileva MH, Scholz P, Zhao Y, Krueger-Burg D, et al. (2021): Neuronal cholesterol synthesis is essential for repair of chronically demyelinated lesions in mice. Cell Rep 37, 109889

Bergles DE, Richardson WD (2015): Oligodendrocyte Development and Plasticity. Cold Spring Harb Perspect Biol 8, a020453

Bertling F, Bendix I, Drommelschmidt K, Wisniewski HG, Felderhoff-Mueser U, Keller M, Prager S (2016): Tumor necrosis factor-inducible gene 6 protein: A novel neuroprotective factor against inflammation-induced developmental brain injury. Exp Neurol 279, 283–289

Bifulco M, Laezza C, Stingo S, Wolff J (2002): 2',3'-Cyclic nucleotide 3'-phosphodiesterase: A membrane-bound, microtubule-associated protein and membrane anchor for tubulin. Proc Natl Acad Sci USA 99, 1807–1812

Boston University Biology (internet source 3): https://www.bu.edu/nf-kb/gene-resources/target-genes/, accessed on September 26, 2021

Bøstrand SMK, Williams A (2021): Oligodendroglial Heterogeneity in Neuropsychiatric Disease. Life 11, 125

Bradl M, Lassmann H (2010): Oligodendrocytes: biology and pathology. Acta Neuropathol 119, 37–53

Braun E, Sandillon F, Edwards A, Matthieu JM, Privat A (1988): lmmunocytochemical Localization by Electron Microscopy of 2',3'-Cyclic Nucleotide 3'-Phosphodiesterase in Developing Oligodendrocytes of Normal and Mutant Brain. J Neurosci 8, 1057–1066

Buscham T, Eichel M, Siems S, Werner H (2019): Turning to myelin turnover. Neural Regen Res 14, 2063–2066

Cannella B, Raine CS (2004): Multiple sclerosis: Cytokine receptors on oligodendrocytes predict innate regulation. Ann Neurol 55, 46–57

Cantoni C, Bollman B, Licastro D, Xie M, Mikesell R, Schmidt R, Yuede CM, Galimberti D, Olivecrona G, Klein RS, et al. (2015): TREM2 regulates microglial cell activation in response to demyelination in vivo. Acta Neuropathol 129, 429–447

Cao K, Liao X, Lu J, Yao S, Wu F, Zhu X, Shi D, Wen S, Liu L, Zhou H (2018): IL-33/ST2 plays a critical role in endothelial cell activation and microglia-mediated neuroinflammation modulation. J Neuroinflammation 15, 136

Cao TV, La M, Getting SJ, Day AJ, Perretti M (2004): Inhibitory Effects of TSG-6 Link Module on Leukocyte–Endothelial Cell Interactions *In Vitro* and *In Vivo*. Microcirculation 11, 615–624

Carnero Contentti E, Correale J (2021): Neuromyelitis optica spectrum disorders: from pathophysiology to therapeutic strategies. J Neuroinflammation 18, 208

Carson JH, Kwon S, Barbarese E (1998): RNA trafficking in myelinating cells. Curr Opin Neurobiol 8, 607–612

Cathomas F, Azzinnari D, Bergamini G, Sigrist H, Buerge M, Hoop V, Wicki B, Goetze L, Soares S, Kukelova D, et al. (2019): Oligodendrocyte gene expression is reduced by and influences effects of chronic social stress in mice. Genes Brain Behav 18, e12475

Chandra S, Gallardo G, Fernández-Chacón R, Schlüter OM, Südhof TC (2005): α-Synuclein Cooperates with CSPα in Preventing Neurodegeneration. Cell 123, 383–396

Chang A, Staugaitis SM, Dutta R, Batt CE, Easley KE, Chomyk AM, Yong VW, Fox RJ, Kidd GJ, Trapp BD (2012): Cortical remyelination: A new target for repair therapies in multiple sclerosis. Ann Neurol 72, 918–926

Chapuis J, Hot D, Hansmannel F, Kerdraon O, Ferreira S, Hubans C, Maurage CA, Huot L, Bensemain F, Laumet G, et al. (2009): Transcriptomic and genetic studies identify IL-33 as a candidate gene for Alzheimer's disease. Mol Psychiatry 14, 1004–1016

Che R, Tang W, Zhang J, Wei Z, Zhang Z, Huang K, Zhao X, Gao J, Zhou G, Huang P, et al. (2009): No relationship between 2',3'-cyclic nucleotide 3'-phosphodiesterase and schizophrenia in the Chinese Han population: an expression study and meta-analysis. BMC Med Genet 10, 31

Cherry JD, Olschowka JA, O'Banion M (2014): Neuroinflammation and M2 microglia: the good, the bad, and the inflamed. J Neuroinflammation 11, 98

Choi H, Lee RH, Bazhanov N, Oh JY, Prockop DJ (2011): Anti-inflammatory protein TSG-6 secreted by activated MSCs attenuates zymosan-induced mouse peritonitis by decreasing TLR2/NF-κB signaling in resident macrophages. Blood 118, 330–338

Cignarella F, Filipello F, Bollman B, Cantoni C, Locca A, Mikesell R, Manis M, Ibrahim A, Deng L, Benitez BA, et al. (2020): TREM2 activation on microglia promotes myelin debris clearance and remyelination in a model of multiple sclerosis. Acta Neuropathol 140, 513–534

Clarke LE, Liddelow SA, Chakraborty C, Münch AE, Heiman M, Barres BA (2018): Normal aging induces A1-like astrocyte reactivity. Proc Natl Acad Sci USA 115, E1896–E1905

Colman DR, Kreibich G, Frey AB, Sabatini DD (1982): Synthesis and incorporation of myelin polypeptides into CNS myelin. J Cell Biol 95, 598–608

Colonna M, Brioschi S (2020): Neuroinflammation and neurodegeneration in human brain at single-cell resolution. Nat Rev Immunol 20, 81–82

Constantinescu CS, Farooqi N, O'Brien K, Gran B (2011): Experimental autoimmune encephalomyelitis (EAE) as a model for multiple sclerosis (MS): EAE as model for MS. Br J Pharmacol 164, 1079–1106

Corchete LA, Rojas EA, Alonso-López D, De Las Rivas J, Gutiérrez NC, Burguillo FJ (2020): Systematic comparison and assessment of RNA-seq procedures for gene expression quantitative analysis. Sci Rep 10, 19737

Coulson-Thomas VJ, Lauer ME, Soleman S, Zhao C, Hascall VC, Day AJ, Fawcett JW (2016): Tumor Necrosis Factor-stimulated Gene-6 (TSG-6) Is Constitutively Expressed in Adult Central Nervous System (CNS) and Associated with Astrocyte-mediated Glial Scar Formation following Spinal Cord Injury. J Biol Chem 291, 19939–19952

Damodarasamy M, Vernon RB, Pathan JL, Keene CD, Day AJ, Banks WA, Reed MJ (2020): The microvascular extracellular matrix in brains with Alzheimer's disease neuropathologic change (ADNC) and cerebral amyloid angiopathy (CAA). Fluids Barriers CNS 17, 60

Daniele SG, Béraud D, Davenport C, Cheng K, Yin H, Maguire-Zeiss KA (2015): Activation of MyD88-dependent TLR1/2 signaling by misfolded α-synuclein, a protein linked to neurodegenerative disorders. Sci Signal 8, ra45

Day AJ, Milner CM (2019): TSG-6: A multifunctional protein with anti-inflammatory and tissue-protective properties. Matrix Biol 78–79, 60–83

de Monasterio-Schrader P, Jahn O, Tenzer S, Wichert SP, Patzig J, Werner HB (2012): Systematic approaches to central nervous system myelin. Cell Mol Life Sci 69, 2879–2894

Deczkowska A, Keren-Shaul H, Weiner A, Colonna M, Schwartz M, Amit I (2018): Disease-Associated Microglia: A Universal Immune Sensor of Neurodegeneration. Cell 173, 1073–1081

Deguine J, Barton GM (2014): MyD88: a central player in innate immune signaling. F1000Prime Rep 6, 97

Depp C, Sun T, Sasmita AO, Spieth L, Berghoff SA, Steixner-Kumar AA, Subramanian S, Möbius W, Göbbels S, Saher G, et al. (2021): Ageing-associated myelin dysfunction drives amyloid deposition in mouse models of Alzheimer's disease. Biorxiv 2021

D'Souza S, Alinauskas K, McCrea E, Goodyer C, Antel J (1995): Differential susceptibility of human CNS-derived cell populations to TNF-dependent and independent immune-mediated injury. J Neurosci 15, 7293–7300

Du L-X, Wang Y-Q, Hua G-Q, Mi W-L (2018): IL-33/ST2 Pathway as a Rational Therapeutic Target for CNS Diseases. Neuroscience 369, 222–230

Dutta DJ, Woo DH, Lee PR, Pajevic S, Bukalo O, Huffman WC, Wake H, Basser PJ, SheikhBahaei S, Lazarevic V, et al. (2018): Regulation of myelin structure and conduction velocity by perinodal astrocytes. Proc Natl Acad Sci USA 115, 11832–11837

Dyer DP, Thomson JM, Hermant A, Jowitt TA, Handel TM, Proudfoot AEI, Day AJ, Milner CM (2014): TSG-6 Inhibits Neutrophil Migration via Direct Interaction with the Chemokine CXCL8. J Immunol 192, 2177–2185

Dyer DP, Salanga CL, Johns SC, Valdambrini E, Fuster MM, Milner CM, Day AJ, Handel TM (2016): The Anti-inflammatory Protein TSG-6 Regulates Chemokine Function by Inhibiting Chemokine/Glycosaminoglycan Interactions. J Biol Chem 291, 12627–12640

Edgar JM, Nave K-A (2009): The role of CNS glia in preserving axon function. Curr Opin Neurobiol 19, 498–504

Edgar JM, McLaughlin M, Werner HB, McCulloch MC, Barrie JA, Brown A, Faichney AB, Snaidero N, Nave K-A, Griffiths IR (2009): Early ultrastructural defects of axons and axon-glia junctions in mice lacking expression of *Cnp1*. Glia 57, 1815–1824

Edgar NM, Touma C, Palme R, Sibille E (2011): Resilient emotionality and molecular compensation in mice lacking the oligodendrocyte-specific gene Cnp1. Transl Psychiatry 1, e42

Factor DC, Barbeau AM, Allan KC, Hu LR, Madhavan M, Hoang AT, Hazel KEA, Hall PA, Nisraiyya S, Najm FJ, et al. (2020): Cell Type-Specific Intralocus Interactions Reveal Oligodendrocyte Mechanisms in MS. Cell 181, 382-395.e21

Falcão AM, van Bruggen D, Marques S, Meijer M, Jäkel S, Agirre E, Samudyata, Floriddia EM, Vanichkina DP, ffrench-Constant C, et al. (2018): Disease-specific oligodendrocyte lineage cells arise in multiple sclerosis. Nat Med 24, 1837–1844

Field A: Discovering Statistics Using IBM SPSS Statistics. 4th edition; Sage, London, 2013

Fields RD (2008): White matter in learning, cognition and psychiatric disorders. Trends Neurosci 31, 361–370

Fields RD (2015): A new mechanism of nervous system plasticity: activity-dependent myelination. Nat Rev Neurosci 16, 756–767

Filley CM, Fields RD (2016): White matter and cognition: making the connection. J Neurophysiol 116, 2093–2104

Francois C, Nguyen-Legros J, Percheron G (1981): Topographical and cytological localization of iron in rat and monkey brains. Brain Res 215, 317–322

Franklin RJM, ffrench-Constant C, Edgar JM, Smith KJ (2012): Neuroprotection and repair in multiple sclerosis. Nat Rev Neurol 8, 624–634

Fries E, Kaczmarczyk A (2003): Inter-a-inhibitor, hyaluronan and inflammation. Acta Biochim Pol 50, 735–742

Frühbeis C, Kuo-Elsner WP, Müller C, Barth K, Peris L, Tenzer S, Möbius W, Werner HB, Nave K-A, Fröhlich D, et al. (2020): Oligodendrocytes support axonal transport and maintenance via exosome secretion. PLoS Biol 18, e3000621

Fujita A, Yamaguchi H, Yamasaki R, Cui Y, Matsuoka Y, Yamada K, Kira J (2018): Connexin 30 deficiency attenuates A2 astrocyte responses and induces severe neurodegeneration in a 1-methyl-4-phenyl-1,2,3,6-tetrahydropyridine hydrochloride Parkinson's disease animal model. J Neuroinflammation 15, 227

Fünfschilling U, Supplie LM, Mahad D, Boretius S, Saab AS, Edgar J, Brinkmann BG, Kassmann CM, Tzvetanova ID, Möbius W, et al. (2012): Glycolytic oligodendrocytes maintain myelin and long-term axonal integrity. Nature 485, 517–521

Gadani SP, Walsh JT, Smirnov I, Zheng J, Kipnis J (2015): The Glia-Derived Alarmin IL-33 Orchestrates the Immune Response and Promotes Recovery following CNS Injury. Neuron 85, 703–709

Gao T, Jernigan J, Raza SA, Dammer EB, Xiao H, Seyfried NT, Levey AI, Rangaraju S (2019): Transcriptional regulation of homeostatic and disease-associated-microglial genes by IRF1, LXRβ, and CEBPα. Glia 67, 1958–1975

Gao Y, Zhang M, Wang T, Fan Y, Yu L, Ye G, Wang Z, Gao C, Wang H, Luo C, et al. (2018): IL-33/ST2L Signaling Provides Neuroprotection Through Inhibiting Autophagy, Endoplasmic Reticulum Stress, and Apoptosis in a Mouse Model of Traumatic Brain Injury. Front Cell Neurosci 12, 95

Gao Y, Luo C, Yao Y, Huang J, Fu H, Xia C, Ye G, Yu L, Han J, Fan Y, et al. (2020): IL-33 Alleviated Brain Damage via Anti-apoptosis, Endoplasmic Reticulum Stress, and Inflammation After Epilepsy. Front Neurosci 14, 898

García-Revilla J, Alonso-Bellido IM, Burguillos MA, Herrera AJ, Espinosa-Oliva AM, Ruiz R, Cruz-Hernández L, García-Domínguez I, Roca-Ceballos MA, Santiago M, et al. (2019): Reformulating Pro-Oxidant Microglia in Neurodegeneration. J Clin Med 8, 1719

Gibson EM, Purger D, Mount CW, Goldstein AK, Lin GL, Wood LS, Inema I, Miller SE, Bieri G, Zuchero JB, et al. (2014): Neuronal Activity Promotes Oligodendrogenesis and Adaptive Myelination in the Mammalian Brain. Science 344, 1252304

Ginhoux F, Greter M, Leboeuf M, Nandi S, See P, Gokhan S, Mehler MF, Conway SJ, Ng LG, Stanley ER, et al. (2010): Fate Mapping Analysis Reveals That Adult Microglia Derive from Primitive Macrophages. Science 330, 841–845

Gould RM, Freund CM, Palmer F, Feinstein DL (2000): Messenger RNAs Located in Myelin Sheath Assembly Sites. J Neurochem 75, 1834–1844

Gravel M, Peterson J, Yong VW, Kottis V, Trapp B, Braun PE (1996): Overexpression of 2',3'-Cyclic Nucleotide 3'-Phosphodiesterase in Transgenic Mice Alters Oligodendrocyte Development and Produces Aberrant Myelination. Mol Cell Neurosci 7, 453–466

Gravel M, Robert F, Kottis V, Gallouzi I-E, Pelletier J, Braun PE (2009): 2',3'-Cyclic nucleotide 3'-phosphodiesterase: A novel RNA-binding protein that inhibits protein synthesis. J Neurosci Res 87, 1069–1079

Hagemeyer N, Goebbels S, Papiol S, Kästner A, Hofer S, Begemann M, Gerwig UC, Boretius S, Wieser GL, Ronnenberg A, et al. (2012): A myelin gene causative of a catatonia-depression syndrome upon aging. EMBO Mol Med 4, 528–539

Hagemeyer N, Hanft K-M, Akriditou M-A, Unger N, Park ES, Stanley ER, Staszewski O, Dimou L, Prinz M (2017): Microglia contribute to normal myelinogenesis and to oligodendrocyte progenitor maintenance during adulthood. Acta Neuropathol 134, 441–458

Hartmann K, Sepulveda-Falla D, Rose IVL, Madore C, Muth C, Matschke J, Butovsky O, Liddelow S, Glatzel M, Krasemann S (2019): Complement 3+-astrocytes are highly abundant in prion diseases, but their abolishment led to an accelerated disease course and early dysregulation of microglia. Acta Neuropathol Commun 7, 83

Hasel P, Rose IVL, Sadick JS, Kim RD, Liddelow SA (2021): Neuroinflammatory astrocyte subtypes in the mouse brain. Nat Neurosci 24, 1475–1487

Holz A, Schaeren-Wiemers N, Schaefer C, Pott U, Colello R, Schwab M (1996): Molecular and developmental characterization of novel cDNAs of the myelin-associated/oligodendrocytic basic protein. J Neurosci 16, 467–477

Hu Y, Li G, Zhang Y, Liu N, Zhang P, Pan C, Nie H, Li Q, Tang Z (2018): Upregulated TSG-6 Expression in ADSCs Inhibits the BV2 Microglia-Mediated Inflammatory Response. Biomed Res Int 2018, 7239181

Huang M, Li Y, Wu K, Yan W, Tian T, Wang Y, Yang H (2019): Paraquat modulates microglia M1/M2 polarization via activation of TLR4-mediated NF-κB signaling pathway. Chem Biol Interact 310, 108743

Hudson CA, Christophi GP, Gruber RC, Wilmore JR, Lawrence DA, Massa PT (2008): Induction of IL-33 expression and activity in central nervous system glia. J Leukoc Biol 84, 631–643

Hughes EG, Appel B (2016): The cell biology of CNS myelination. Curr Opin Neurobiol 39, 93–100

Islinger M, Voelkl A, Fahimi HD, Schrader M (2018): The peroxisome: an update on mysteries 2.0. Histochem Cell Biol 150, 443–471

Jahn O, Tenzer S, Werner HB (2009): Myelin Proteomics: Molecular Anatomy of an Insulating Sheath. Mol Neurobiol 40, 55–72

Jahn O, Siems SB, Kusch K, Hesse D, Jung RB, Liepold T, Uecker M, Sun T, Werner HB (2020): The CNS Myelin Proteome: Deep Profile and Persistence After Post-mortem Delay. Front Cell Neurosci 14, 239

Jäkel S, Agirre E, Mendanha Falcão A, van Bruggen D, Lee KW, Knuesel I, Malhotra D, ffrench-Constant C, Williams A, Castelo-Branco G (2019): Altered human oligodendrocyte heterogeneity in multiple sclerosis. Nature 566, 543–547

Janova H, Arinrad S, Balmuth E, Mitjans M, Hertel J, Habes M, Bittner RA, Pan H, Goebbels S, Begemann M, et al. (2018): Microglia ablation alleviates myelin-associated catatonic signs in mice. J Clin Invest 128, 734–745

Jha KA, Pentecost M, Lenin R, Gentry J, Klaic L, Del Mar N, Reiner A, Yang CH, Pfeffer LM, Sohl N, et al. (2019): TSG-6 in conditioned media from adipose mesenchymal stem cells protects against visual deficits in mild traumatic brain injury model through neurovascular modulation. Stem Cell Res Ther 10, 318

Jian N, Dowle M, Horniblow RD, Tselepis C, Palmer RE (2016): Morphology of the ferritin iron core by aberration corrected scanning transmission electron microscopy. Nanotechnology 27, 46LT02

Jurewicz A, Matysiak M, Tybor K, Kilianek L, Raine CS, Selmaj K (2005): Tumour necrosis factor-induced death of adult human oligodendrocytes is mediated by apoptosis inducing factor. Brain 128, 2675–2688

Kaur C, Rathnasamy G, Ling E-A (2017): Biology of Microglia in the Developing Brain. J Neuropathol Exp Neurol 76, 736–753

Kawachi I, Lassmann H (2017): Neurodegeneration in multiple sclerosis and neuromyelitis optica. J Neurol Neurosurg Psychiatry 88, 137–145

Keren-Shaul H, Spinrad A, Weiner A, Matcovitch-Natan O, Dvir-Szternfeld R, Ulland TK, David E, Baruch K, Lara-Astaiso D, Toth B, et al. (2017): A Unique Microglia Type Associated with Restricting Development of Alzheimer's Disease. Cell 169, 1276-1290.e17

Klegeris A (2021): Regulation of neuroimmune processes by damage- and resolution-associated molecular patterns. Neural Regen Res 16, 423–429

Kolaric KV, Thomson G, Edgar JM, Brown AM (2013): Focal axonal swellings and associated ultrastructural changes attenuate conduction velocity in central nervous system axons: a computer modeling study. Physiol Rep 1, e00059

Krämer-Albers E-M (2020): Extracellular vesicles in the oligodendrocyte microenvironment. Neurosci Lett 725, 134915

Kurowska-Stolarska M, Kewin P, Murphy G, Russo RC, Stolarski B, Garcia CC, Komai-Koma M, Pitman N, Li Y, McKenzie ANJ, et al. (2008): IL-33 induced Ag-specific IL-5 $^{+}$ T cells and promotes allergic-induced airway inflammation independent of IL-4. J Immunol 181, 4780–4790

Lappe-Siefke C, Goebbels S, Gravel M, Nicksch E, Lee J, Braun PE, Griffiths IR, Nave K-A (2003): Disruption of Cnp1 uncouples oligodendroglial functions in axonal support and myelination. Nat Genet 33, 366–374

Lee J, Gravel M, Gao E, O'Neill RC, Braun PE (2001): Identification of Essential Residues in 2',3'-Cyclic Nucleotide 3'-Phosphodiesterase. J Biol Chem 276, 14804–14813

Lee J, Gravel M, Zhang R, Thibault P, Braun PE (2005): Process outgrowth in oligodendrocytes is mediated by CNP, a novel microtubule assembly myelin protein. J Cell Biol 170, 661–673

Lee TH, Wisniewski HG, Vilcek J (1992): A novel secretory tumor necrosis factor-inducible protein (TSG-6) is a member of the family of hyaluronate binding proteins, closely related to the adhesion receptor CD44. J Cell Biol 116, 545–557

Lee Y, Morrison BM, Li Y, Lengacher S, Farah MH, Hoffman PN, Liu Y, Tsingalia A, Jin L, Zhang P-W, et al. (2012): Oligodendroglia metabolically support axons and contribute to neurodegeneration. Nature 487, 443–448

Lehnardt S (2009): Innate immunity and neuroinflammation in the CNS: The role of microglia in Toll-like receptor-mediated neuronal injury. Glia 58, 253–263

LeVine SM, Macklin WB (1990): Iron-enriched oligodendrocytes: A reexamination of their spatial distribution. J Neurosci Res 26, 508–512

Li H-N, Yang Q-Q, Wang W-T, Tian X, Feng F, Zhang S-T, Xia Y-T, Wang J-X, Zou Y-W, Wang J-Y, et al. (2021): Red nucleus IL-33 facilitates the early development of mononeuropathic pain in male rats by inducing TNF-α through activating ERK, p38 MAPK, and JAK2/STAT3. J Neuroinflammation 18, 150

Li J, Zhang L, Chu Y, Namaka M, Deng B, Kong J, Bi X (2016): Astrocytes in Oligodendrocyte Lineage Development and White Matter Pathology. Front Cell Neurosci 10, 119

Li M, Li Y, Liu X, Gao X, Wang Y (2012): IL-33 blockade suppresses the development of experimental autoimmune encephalomyelitis in C57BL/6 mice. J Neuroimmunol 247, 25–31

Li R, Liu W, Yin J, Chen Y, Guo S, Fan H, Li X, Zhang X, He X, Duan C (2018): TSG-6 attenuates inflammation-induced brain injury via modulation of microglial polarization in SAH rats through the SOCS3/STAT3 pathway. J Neuroinflammation 15, 231

Liddelow SA, Guttenplan KA, Clarke LE, Bennett FC, Bohlen CJ, Schirmer L, Bennett ML, Münch AE, Chung W-S, Peterson TC, et al. (2017): Neurotoxic reactive astrocytes are induced by activated microglia. Nature 541, 481–487

Lieury A, Chanal M, Androdias G, Reynolds R, Cavagna S, Giraudon P, Confavreux C, Nataf S (2014): Tissue remodeling in periplaque regions of multiple sclerosis spinal cord lesions: Glia Remodeling in MS Spinal Cord. Glia 62, 1645–1658

Liew FY, Pitman NI, McInnes IB (2010): Disease-associated functions of IL-33: the new kid in the IL-1 family. Nat Rev Immunol 10, 103–110

Liu J-T, Wu S-X, Zhang H, Kuang F (2018): Inhibition of MyD88 Signaling Skews Microglia/Macrophage Polarization and Attenuates Neuronal Apoptosis in the Hippocampus After Status Epilepticus in Mice. Neurotherapeutics 15, 1093–1111

Liu Y, Zhang R, Yan K, Chen F, Huang W, Lv B, Sun C, Xu L, Li F, Jiang X (2014a): Mesenchymal stem cells inhibit lipopolysaccharide-induced inflammatory responses of BV2 microglial cells through TSG-6. J Neuroinflammation 11, 135

Liu Y, Yin Z, Zhang R, Yan K, Chen L, Chen F, Huang W, Lv B, Sun C, Jiang X (2014b): MSCs inhibit bone marrow-derived DC maturation and function through the release of TSG-6. Biochem Biophys Res Commun 450, 1409–1415

Ljunggren-Rose Å, Natarajan C, Matta P, Pandey A, Upender I, Sriram S (2020): Anacardic acid induces IL-33 and promotes remyelination in CNS. Proc Natl Acad Sci USA 117, 21527–21535

Love MI, Huber W, Anders S (2014): Moderated estimation of fold change and dispersion for RNA-seq data with DESeq2. Genome Biol 15, 550

Magistretti PJ, Allaman I (2018): Lactate in the brain: from metabolic end-product to signalling molecule. Nat Rev Neurosci 19, 235–249

Martinez FO, Gordon S (2014): The M1 and M2 paradigm of macrophage activation: time for reassessment. F1000 Prime Rep 6, 13

Mathys H, Davila-Velderrain J, Peng Z, Gao F, Mohammadi S, Young JZ, Menon M, He L, Abdurrob F, Jiang X, et al. (2019): Single-cell transcriptomic analysis of Alzheimer's disease. Nature 570, 332–337

Matias I, Morgado J, Gomes FCA (2019): Astrocyte Heterogeneity: Impact to Brain Aging and Disease. Front Aging Neurosci 11, 59

McKenzie AT, Moyon S, Wang M, Katsyv I, Song W-M, Zhou X, Dammer EB, Duong DM, Aaker J, Zhao Y, et al. (2017): Multiscale network modeling of oligodendrocytes reveals molecular components of myelin dysregulation in Alzheimer's disease. Mol Neurodegeneration 12, 82

Melcangi RC, Celotti F, Ballabio M, Castano P, Poletti A, Milani S, Martini L (1988): Ontogenetic development of the 5 alpha-reductase in the rat brain: cerebral cortex, hypothalamus, purified myelin and isolated oligodendrocytes. Brain Res Dev Brain Res 44, 181–188

Merico D, Isserlin R, Stueker O, Emili A, Bader GD (2010): Enrichment Map: A Network-Based Method for Gene-Set Enrichment Visualization and Interpretation. PLoS One 5, e13984

Miller AM (2011): Role of IL-33 in inflammation and disease. J Inflamm 8, 22

Milner CM, Higman VA, Day AJ (2006): TSG-6: a pluripotent inflammatory mediator? Biochem Soc Trans 34, 446–450

Mindrescu C, Thorbecke GJ, Klein MJ, Vilček J, Wisniewski H-G (2000): Amelioration of collagen-induced arthritis in DBA/1J mice by recombinant TSG-6, a tumor necrosis factor/interleukin-1-inducible protein. Arthritis Rheum 43, 2668–2677

Mitew S, Hay CM, Peckham H, Xiao J, Koenning M, Emery B (2014): Mechanisms regulating the development of oligodendrocytes and central nervous system myelin. Neuroscience 276, 29–47

Mitkus SN, Hyde TM, Vakkalanka R, Kolachana B, Weinberger DR, Kleinman JE, Lipska BK (2008): Expression of oligodendrocyte-associated genes in dorsolateral prefrontal cortex of patients with schizophrenia. Schizophrenia Res 98, 129–138

Mittal M, Tiruppathi C, Nepal S, Zhao Y-Y, Grzych D, Soni D, Prockop DJ, Malik AB (2016): TNFα-stimulated gene-6 (TSG6) activates macrophage phenotype transition to prevent inflammatory lung injury. Proc Natl Acad Sci USA 113, E8151–E8158

Möbius W, Nave K-A, Werner HB (2016): Electron microscopy of myelin: Structure preservation by high-pressure freezing. Brain Res 1641, 92–100

Molofsky AB, Savage AK, Locksley RM (2015): Interleukin-33 in Tissue Homeostasis, Injury, and Inflammation. Immunity 42, 1005–1019

Morioka C, Komaki M, Taki A, Honda I, Yokoyama N, Iwasaki K, Iseki S, Morio T, Morita I (2017): Neuroprotective effects of human umbilical cord-derived mesenchymal stem cells on periventricular leukomalacia-like brain injury in neonatal rats. Inflamm Regen 37, 1

Mukherjee C, Kling T, Russo B, Miebach K, Kess E, Schifferer M, Pedro LD, Weikert U, Fard MK, Kannaiyan N, et al. (2020): Oligodendrocytes Provide Antioxidant Defense Function for Neurons by Secreting Ferritin Heavy Chain. Cell Metab 32, 259-272.e10

Müller C, Bauer NM, Schäfer I, White R (2013): Making myelin basic protein -from mRNA transport to localized translation. Front Cell Neurosci 7, 169

Nasrabady SE, Rizvi B, Goldman JE, Brickman AM (2018): White matter changes in Alzheimer's disease: a focus on myelin and oligodendrocytes. Acta Neuropathol Commun 6, 22

Nataf S, Barritault M, Pays L (2017): A Unique TGFB1-Driven Genomic Program Links Astrocytosis, Low-Grade Inflammation and Partial Demyelination in Spinal Cord Periplaques from Progressive Multiple Sclerosis Patients. Int J Mol Sci 18, 2097

Natalia Silva P, Furuya TK, Sampaio Braga I, Rasmussen LT, de Labio RW, Bertolucci PH, Chen ES, Turecki G, Mechawar N, Payão SL, et al. (2013): CNP and DPYSL2 mRNA Expression and Promoter Methylation Levels in Brain of Alzheimer's Disease Patients. J Alzheimers Dis 33, 349–355

Nave K-A (2010): Myelination and the trophic support of long axons. Nat Rev Neurosci 11, 275–283

Nave K-A, Werner HB (2021): Ensheathment and Myelination of Axons: Evolution of Glial Functions. Annu Rev Neurosci 44, 197–219

Norton WT, Poduslo SE (1973): Myelination in rat brain: method of myelin isolation. J Neurochem 21, 749–757

Okun E, Griffioen KJ, Lathia JD, Tang S-C, Mattson MP, Arumugam TV (2009): Toll-like receptors in neurodegeneration. Brain Res Rev 59, 278–292

Olson JK, Miller SD (2004): Microglia Initiate Central Nervous System Innate and Adaptive Immune Responses through Multiple TLRs. J Immunol 173, 3916–3924

Patzig J, Jahn O, Tenzer S, Wichert SP, de Monasterio-Schrader P, Rosfa S, Kuharev J, Yan K, Bormuth I, Bremer J, et al. (2011): Quantitative and Integrative Proteome Analysis of Peripheral Nerve Myelin Identifies Novel Myelin Proteins and Candidate Neuropathy Loci. J Neurosci 31, 16369–16386

Patzig J, Erwig MS, Tenzer S, Kusch K, Dibaj P, Möbius W, Goebbels S, Schaeren-Wiemers N, Nave K-A, Werner HB (2016): Septin/anillin filaments scaffold central nervous system myelin to accelerate nerve conduction. Elife 5, e17119

Peferoen L, Kipp M, van der Valk P, van Noort JM, Amor S (2014): Oligodendrocyte-microglia cross-talk in the central nervous system. Immunology 141, 302–313

Peirce TR, Bray NJ, Williams NM, Norton N, Moskvina V, Preece A, Haroutunian V, Buxbaum JD, Owen MJ, O'Donovan MC (2006): Convergent Evidence for 2',3'-Cyclic Nucleotide 3'-Phosphodiesterase as a Possible Susceptibility Gene for Schizophrenia. Arch Gen Psychiatry 63, 18–24

Pellerin L, Magistretti PJ (1994): Glutamate uptake into astrocytes stimulates aerobic glycolysis: a mechanism coupling neuronal activity to glucose utilization. Proc Natl Acad Sci USA 91, 10625–10629

Pellerin L, Pellegri G, Bittar PG, Charnay Y, Bouras C, Martin J-L, Stella N, Magistretti PJ (1998): Evidence Supporting the Existence of an Activity-Dependent Astrocyte-Neuron Lactate Shuttle. Dev Neurosci 20, 291–299

Philips T, Rothstein JD (2017): Oligodendroglia: metabolic supporters of neurons. J Clin Invest 127, 3271–3280

Philips T, Mironova YA, Jouroukhin Y, Chew J, Vidensky S, Farah MH, Pletnikov MV, Bergles DE, Morrison BM, Rothstein JD (2021): MCT1 Deletion in Oligodendrocyte Lineage Cells Causes Late-Onset Hypomyelination and Axonal Degeneration. Cell Rep 34, 108610

Piao J-H, Wang Y, Duncan ID (2013): CD44 is required for the migration of transplanted oligodendrocyte progenitor cells to focal inflammatory demyelinating lesions in the spinal cord. Glia 61, 361–367

Pomeshchik Y, Kidin I, Korhonen P, Savchenko E, Jaronen M, Lehtonen S, Wojciechowski S, Kanninen K, Koistinaho J, Malm T (2015): Interleukin-33 treatment reduces secondary injury and improves functional recovery after contusion spinal cord injury. Brain Behav Immun 44, 68–81

Raj D, Yin Z, Breur M, Doorduin J, Holtman IR, Olah M, Mantingh-Otter IJ, Van Dam D, De Deyn PP, den Dunnen W, et al. (2017): Increased White Matter Inflammation in Aging- and Alzheimer's Disease Brain. Front Mol Neurosci 10, 206

Rangaraju S, Dammer EB, Raza SA, Rathakrishnan P, Xiao H, Gao T, Duong DM, Pennington MW, Lah JJ, Seyfried NT, et al. (2018): Identification and therapeutic modulation of a pro-inflammatory subset of disease-associated-microglia in Alzheimer's disease. Mol Neurodegener 13, 24

Ransohoff RM (2016): A polarizing question: do M1 and M2 microglia exist? Nat Neurosci 19, 987–991

Rasband MN, Tayler J, Kaga Y, Yang Y, Lappe-Siefke C, Nave K-A, Bansal R (2005): CNP is required for maintenance of axon-glia interactions at nodes of Ranvier in the CNS. Glia 50, 86–90

Reed MJ, Damodarasamy M, Pathan JL, Chan CK, Spiekerman C, Wight TN, Banks WA, Day AJ, Vernon RB, Keene CD (2019): Increased Hyaluronan and TSG-6 in Association with Neuropathologic Changes of Alzheimer's Disease. J Alzheimers Dis 67, 91–102

Reich DS, Lucchinetti CF, Calabresi PA (2018): Multiple Sclerosis. N Engl J Med 378, 169–180

Reid JK, Kuipers HF (2021): She Doesn't Even Go Here: The Role of Inflammatory Astrocytes in CNS Disorders. Front Cell Neurosci 15, 704884

Reimand J, Isserlin R, Voisin V, Kucera M, Tannus-Lopes C, Rostamianfar A, Wadi L, Meyer M, Wong J, Xu C, et al. (2019): Pathway enrichment analysis and visualization of omics data using g:Profiler, GSEA, Cytoscape and EnrichmentMap. Nat Protoc 14, 482–517

Reinbach C, Stadler M-S, Pröbstl N, Chrzanowski U, Schmitz C, Kipp M, Hochstrasser T (2020): CD44 expression in the cuprizone model. Brain Res 1745, 146950

Ribbe K, Friedrichs H, Begemann M, Grube S, Papiol S, Kästner A, Gerchen MF, Ackermann V, Tarami A, Treitz A, et al. (2010): The cross-sectional GRAS sample: A comprehensive phenotypical data collection of schizophrenic patients. BMC Psychiatry 10, 91

Rinholm JE, Hamilton NB, Kessaris N, Richardson WD, Bergersen LH, Attwell D (2011): Regulation of Oligodendrocyte Development and Myelination by Glucose and Lactate. J Neurosci 31, 538–548

Rosenberger K, Dembny P, Derkow K, Engel O, Krüger C, Wolf SA, Kettenmann H, Schott E, Meisel A, Lehnardt S (2015): Intrathecal heat shock protein 60 mediates neurodegeneration and demyelination in the CNS through a TLR4- and MyD88-dependent pathway. Mol Neurodegener 10, 5

Saab AS, Tzvetanova ID, Nave K-A (2013): The role of myelin and oligodendrocytes in axonal energy metabolism. Curr Opin Neurobiol 23, 1065–1072

Sams EC (2021): Oligodendrocytes in the aging brain. Neuronal Signal 5, NS20210008

Saresella M, Marventano I, Piancone F, La Rosa F, Galimberti D, Fenoglio C, Scarpini E, Clerici M (2020): IL-33 and its decoy sST2 in patients with Alzheimer's disease and mild cognitive impairment. J Neuroinflammation 17, 174

Schirmer L, Velmeshev D, Holmqvist S, Kaufmann M, Werneburg S, Jung D, Vistnes S, Stockley JH, Young A, Steindel M, et al. (2019): Neuronal vulnerability and multilineage diversity in multiple sclerosis. Nature 573, 75–82

Schmitz J, Owyang A, Oldham E, Song Y, Murphy E, McClanahan TK, Zurawski G, Moshrefi M, Qin J, Li X, et al. (2005): IL-33, an Interleukin-1-like Cytokine that Signals via the IL-1 Receptor-Related Protein ST2 and Induces T Helper Type 2-Associated Cytokines. Immunity 23, 479–490

Schroeder P, Rivalan M, Zaqout S, Krüger C, Schüler J, Long M, Meisel A, Winter Y, Kaindl AM, Lehnardt S (2021): Abnormal brain structure and behavior in MyD88-deficient mice. Brain Behabv Immun 91, 181–193

Selmaj KW, Raine CS (1988): Tumor necrosis factor mediates myelin and oligodendrocyte damage in vitro. Ann Neurol 23, 339–346

Seol Y, Ki S, Ryu HL, Chung S, Lee J, Ryu H (2020): How Microglia Manages Non-cell Autonomous Vicious Cycling of Aβ Toxicity in the Pathogenesis of AD. Front Mol Neurosci 13, 593724

Siems SB, Jahn O, Eichel MA, Kannaiyan N, Wu LMN, Sherman DL, Kusch K, Hesse D, Jung RB, Fledrich R, et al. (2020): Proteome profile of peripheral myelin in healthy mice and in a neuropathy model. Elife 9, e51406

Simons M, Nave K-A (2015): Oligodendrocytes: Myelination and Axonal Support. Cold Spring Harb Perspect Biol 8, a020479

Simpson IA, Carruthers A, Vannucci SJ (2007): Supply and Demand in Cerebral Energy Metabolism: The Role of Nutrient Transporters. J Cereb Blood Flow Metab 27, 1766–1791

Smith ME (1969): An in vitro system for the study of myelin synthesis. J Neurochem 16, 83–92

Snaidero N, Möbius W, Czopka T, Hekking LHP, Mathisen C, Verkleij D, Goebbels S, Edgar J, Merkler D, Lyons DA, et al. (2014): Myelin Membrane Wrapping of CNS Axons by PI(3,4,5)P3-Dependent Polarized Growth at the Inner Tongue. Cell 156, 277–290

Snaidero N, Velte C, Myllykoski M, Raasakka A, Ignatev A, Werner HB, Erwig MS, Möbius W, Kursula P, Nave K-A, et al. (2017): Antagonistic Functions of MBP and CNP Establish Cytosolic Channels in CNS Myelin. Cell Rep 18, 314–323

Snaidero N, Simons M (2017): The logistics of myelin biogenesis in the central nervous system: Myelin Biogenesis. Glia 65, 1021–1031

Sofroniew MV, Vinters HV (2010): Astrocytes: biology and pathology. Acta Neuropathol 119, 7–35

Stadelmann C, Timmler S, Barrantes-Freer A, Simons M (2019): Myelin in the Central Nervous System: Structure, Function, and Pathology. Physiol Rev 99, 1381–1431

Starost L, Lindner M, Herold M, Xu YKT, Drexler HCA, Heß K, Ehrlich M, Ottoboni L, Ruffini F, Stehling M, et al. (2020): Extrinsic immune cell-derived, but not intrinsic oligodendroglial factors contribute to oligodendroglial differentiation block in multiple sclerosis. Acta Neuropathol 140, 715–736

Subramanian A, Tamayo P, Mootha VK, Mukherjee S, Ebert BL, Gillette MA, Paulovich A, Pomeroy SL, Golub TR, Lander ES, et al. (2005): Gene set enrichment analysis: A knowledge-based approach for interpreting genome-wide expression profiles. Proc Natl Acad Sci USA 102, 15545–15550

Sun Y, Wen Y, Wang L, Wen L, You W, Wei S, Mao L, Wang H, Chen Z, Yang X (2021): Therapeutic Opportunities of Interleukin-33 in the Central Nervous System. Front Immunol 12, 654626

Suzuki A, Stern SA, Bozdagi O, Huntley GW, Walker RH, Magistretti PJ, Alberini CM (2011): Astrocyte-Neuron Lactate Transport Is Required for Long-Term Memory Formation. Cell 144, 810–823

Szántó S, Bárdos T, Gál I, Glant TT, Mikecz K (2004): Enhanced neutrophil extravasation and rapid progression of proteoglycan-induced arthritis in TSG-6-knockout mice: TSG-6/Tnfip6 Deficiency and Aggravation of Arthritis. Arthritis Rheum 50, 3012–3022

Tang B, Song M, Xie X, Le D, Tu Q, Wu X, Chen M (2021): Tumor Necrosis Factor-stimulated Gene-6 (TSG-6) Secreted by BMSCs Regulates Activated Astrocytes by Inhibiting NF-κB Signaling Pathway to Ameliorate Blood Brain Barrier Damage After Intracerebral Hemorrhage. Neurochem Res 46, 2387–2402

Tang Y, Le W (2016): Differential Roles of M1 and M2 Microglia in Neurodegenerative Diseases. Mol Neurobiol 53, 1181–1194

Tekkök SB, Brown AM, Westenbroek R, Pellerin L, Ransom BR (2005): Transfer of glycogen-derived lactate from astrocytes to axons via specific monocarboxylate transporters supports mouse optic nerve activity. J Neurosci Res 81, 644–652

Thakurela S, Garding A, Jung RB, Müller C, Goebbels S, White R, Werner HB, Tiwari VK (2016): The transcriptome of mouse central nervous system myelin. Sci Rep 6, 25828

Toshchakov V, Jones BW, Perera P-Y, Thomas K, Cody MJ, Zhang S, Williams BRG, Major J, Hamilton TA, Fenton MJ, Vogel SN (2002): TLR4, but not TLR2, mediates IFN-β–induced STAT1α/β-dependent gene expression in macrophages. Nat Immunol 3, 392–398

Traka M, Podojil JR, McCarthy DP, Miller SD, Popko B (2016): Oligodendrocyte death results in immune-mediated CNS demyelination. Nat Neurosci 19, 65–74

Trapp BD, Moench T, Pulley M, Barbosa E, Tennekoon G, Griffin J (1987): Spatial Segregation of mRNA Encoding Myelin-Specific Proteins. Proceedings of the National Academy of Sciences of the United States of America 84, 7773–7777

Trapp BD, Bernier L, Andrews SB, Colman DR (1988): Cellular and Subcellular Distribution of 2',3'-Cyclic Nucleotide 3'-Phosphodiesterase and Its mRNA in the Rat Central Nervous System. J Neurochem 51, 859–868

Trapp BD (2004): Pathogenesis of multiple sclerosis: The eyes only see what the mind is prepared to comprehend. Ann Neurol 55, 455–457

Tzartos JS, Friese MA, Craner MJ, Palace J, Newcombe J, Esiri MM, Fugger L (2008): Interleukin-17 Production in Central Nervous System-Infiltrating T Cells and Glial Cells Is Associated with Active Disease in Multiple Sclerosis. Am J Pathol 172, 146–155

University of Virginia Library (internet source 2): https://data.library.virginia.edu/understanding-q-q-plots/, accessed on November 9, 2021

Walsh DM, Klyubin I, Fadeeva JV, Cullen WK, Anwyl R, Wolfe MS, Rowan MJ, Selkoe DJ (2002): Naturally secreted oligomers of amyloid b protein potently inhibit hippocampal long-term potentiation in vivo. Nature 416, 535–539

Wan R, Cheli VT, Santiago-González DA, Rosenblum SL, Wan Q, Paez PM (2020): Impaired Postnatal Myelination in a Conditional Knockout Mouse for the Ferritin Heavy Chain in Oligodendroglial Cells. J Neurosci 40, 7609–7624

Wan Y, Song M, Xie X, Chen Z, Gao Z, Wu X, Huang R, Chen M (2021): BMSCs Regulate Astrocytes through TSG-6 to Protect the Blood-Brain Barrier after Subarachnoid Hemorrhage. Mediators Inflamm 2021, 1–18

Watanabe J, Shetty AK, Hattiangady B, Kim D-K, Foraker JE, Nishida H, Prockop DJ (2013): Administration of TSG-6 improves memory after traumatic brain injury in mice. Neurobiol Dis 59, 86–99

Wicher G, Wallenquist U, Lei Y, Enoksson M, Li X, Fuchs B, Abu Hamdeh S, Marklund N, Hillered L, Nilsson G, Forsberg-Nilsson K (2017): Interleukin-33 Promotes Recruitment of Microglia/Macrophages in Response to Traumatic Brain Injury. Journal Neurotrauma 34, 3173–3182

Wichert S: Transcriptomic approaches in the brain at cell type resolution: Analysis of neuron-glia interaction in Plp1 and Cnp1 null-mutant mice. Biol. Diss. Göttingen 2009

Wieser GL, Gerwig UC, Adamcio B, Barrette B, Nave K-A, Ehrenreich H, Goebbels S (2013): Neuroinflammation in white matter tracts of *Cnp1* mutant mice amplified by a minor brain injury: Neurodegeneration in *Cnp1* $^{--}$ Mice. Glia 61, 869–880

Wisniewski H-G, Maier R, Lotz M, Lee S, Klampfer L, Lee TH, Vilcek J (1993): TSG-6: a TNF-, IL-1-, and LPS-inducible secreted glycoprotein associated with arthritis. J Immunol 151, 6593–6601

Wisniewski H-G, Naime D, Hua J-C, Vilcek J, Cronstein BN (1996): TSG-6, a glycoprotein associated with arthritis, and its ligand hyaluronan exert opposite effects in a murine model of inflammation. Pflugers Arch 431, R225–R226

Wisniewski H-G, Vilček J (1997): TSG-6: An IL-I /TNF-Inducible Protein with Anti-Inflammatory Activity. Cytokine Growth Factor Rev 8, 143–156

Wisniewski H-G, Colón E, Liublinska V, Karia RJ, Stabler TV, Attur M, Abramson SB, Band PA, Kraus VB (2014): TSG-6 activity as a novel biomarker of progression in knee osteoarthritis. Osteoarthritis Cartilage 22, 235–241

Wlodarczyk A, Holtman IR, Krueger M, Yogev N, Bruttger J, Khorooshi R, Benmamar-Badel A, Boer-Bergsma JJ, Martin NA, Karram K, et al. (2017): A novel microglial subset plays a key role in myelinogenesis in developing brain. EMBO J 36, 3292–3308

Xiang W, Chao Z-Y, Feng D-Y (2015): Role of Toll-like receptor/MYD88 signaling in neurodegenerative diseases. Rev Neurosci 26, 407–414

Xiao Y, Lai L, Chen H, Shi J, Zeng F, Li J, Feng H, Mao J, Zhang F, Wu N, et al. (2018): Interleukin-33 deficiency exacerbated experimental autoimmune encephalomyelitis with an influence on immune cells and glia cells. Mol Immunol 101, 550–563

Xu C, Fu F, Li X, Zhang S (2017): Mesenchymal stem cells maintain the microenvironment of central nervous system by regulating the polarization of macrophages/microglia after traumatic brain injury. Int J Neurosci 127, 1124–1135

Xu C, Diao Y-F, Wang J, Liang J, Xu H-H, Zhao M-L, Zheng B, Luan Z, Wang J-J, Yang X-P, et al. (2020): Intravenously Infusing the Secretome of Adipose-Derived Mesenchymal Stem Cells Ameliorates Neuroinflammation and Neurological Functioning After Traumatic Brain Injury. Stem Cells Dev 29, 222–234

Xu D, Jiang H-R, Kewin P, Li Y, Mu R, Fraser AR, Pitman N, Kurowska-Stolarska M, McKenzie ANJ, McInnes IB, et al. (2008): IL-33 exacerbates antigen-induced arthritis by activating mast cells. Proc Natl Acad Sci USA 105, 10913–10918

Xue F, Du H (2021): TREM2 Mediates Microglial Anti-Inflammatory Activations in Alzheimer's Disease: Lessons Learned from Transcriptomics. Cells 10, 321

Yamamoto M, Sato S, Hemmi H, Hoshino K, Kaisho T, Sanjo H, Takeuchi O, Sugiyama M, Okabe M, Takeda K, er al. (2003): Role of Adaptor TRIF in the MyD88-Independent Toll-Like Receptor Signaling Pathway. Science 301, 640–643

Yang H, Wu L, Deng H, Chen Y, Zhou H, Liu M, Wang S, Zheng L, Zhu L, Lv X (2020): Anti-inflammatory protein TSG-6 secreted by bone marrow mesenchymal stem cells attenuates neuropathic pain by inhibiting the TLR2/MyD88/NF-κB signaling pathway in spinal microglia. J Neuroinflammation 17, 154

Yang Y, Liu H, Zhang H, Ye Q, Wang J, Yang B, Mao L, Zhu W, Leak RK, Xiao B, et al. (2017): ST2/IL-33-Dependent Microglial Response Limits Acute Ischemic Brain Injury. J Neurosci 37, 4692–4704

Yasuoka S, Kawanokuchi J, Parajuli B, Jin S, Doi Y, Noda M, Sonobe Y, Takeuchi H, Mizuno T, Suzumura A (2011): Production and functions of IL-33 in the central nervous system. Brain Res 1385, 8–17

Yergert KM, Doll CA, O'Rouke R, Hines JH, Appel B (2021): Identification of 3' UTR motifs required for mRNA localization to myelin sheaths in vivo. PLoS Biol 19, e3001053

Yin X, Peterson J, Gravel M, Braun PE, Trapp BD (1997): CNP overexpression induces aberrant oligodendrocyte membranes and inhibits MBP accumulation and myelin compaction. J Neurosci Res 50, 238–247

Yu J-T, Song J-H, Wang N-D, Wu Z-C, Zhang Q, Zhang N, Zhang W, Xuan S-Y, Tan L (2012): Implication of IL-33 gene polymorphism in Chinese patients with Alzheimer's disease. Neurobiol Aging 33, 1014.e11-1014.e14

Yu Q, Zhang S, Wang H, Zhang Y, Feng T, Chen B, He Y, Zeng Z, Chen M (2016): TNFAIP6 is a potential biomarker of disease activity in inflammatory bowel disease. Biomark Med 10, 473–483

Zalc B, Goujet D, Colman D (2008): The origin of the myelination program in vertebrates. Curr Biol 18, R5112–R512

Zamanian JL, Xu L, Foo LC, Nouri N, Zhou L, Giffard RG, Barres BA (2012): Genomic Analysis of Reactive Astrogliosis. J Neurosci 32, 6391–6410

Zarpelon AC, Rodrigues FC, Lopes AH, Souza GR, Carvalho TT, Pinto LG, Xu D, Ferreira SH, Alves-Filho JC, McInnes IB, et al. (2016): Spinal cord oligodendrocyte-derived alarmin IL-33 mediates neuropathic pain. FASEB J 30, 54–65

Zeis T, Schaeren-Wiemers N (2008): Lame Ducks or Fierce Creatures? - The Role of Oligodendrocytes in Multiple Sclerosis. J Mol Neurosci 35, 91–100

Zeis T, Enz L, Schaeren-Wiemers N (2016): The immunomodulatory oligodendrocyte. Brain Res 1641, 139–148

Zhang Y, Chen K, Sloan SA, Bennett ML, Scholze AR, O'Keeffe S, Phatnani HP, Guarnieri P, Caneda C, Ruderisch N, et al. (2014): An RNA-Sequencing Transcriptome and Splicing Database of Glia, Neurons, and Vascular Cells of the Cerebral Cortex. J Neurosci 34, 11929–11947

Zhang Z, Ma Z, Zou W, Guo H, Liu M, Ma Y, Zhang L (2019): The Appropriate Marker for Astrocytes: Comparing the Distribution and Expression of Three Astrocytic Markers in Different Mouse Cerebral Regions. Biomed Res Int 2019, 9605265

Zhong Y, Hu Z, Wu J, Dai F, Lee F, Xu Y (2020): STAU1 selectively regulates the expression of inflammatory and immune response genes and alternative splicing of the nerve growth factor receptor signaling pathway. Oncol Rep 44, 1863–1874

# Acknowledgements

I owe gratitude to Prof. Dr. Klaus-Armin Nave for giving me the opportunity to work in his lab for my medical thesis. I address special thanks to Prof. Dr. Christine Stadelmann-Nessler for supervising my thesis, for the lab-rotation in 2016 and contact to Prof. Dr. Julia Edgar and Prof. Dr. Christopher Linington in Glasgow.

My special acknowledgement is due to Dr. Sandra Goebbels for the in-depth discussions and useful critiques, her patience, her enthusiastic encouragement and her confidence during the last years.

I address special thanks to Ulli Bode for her assistance and advice on so many aspects of the practical work in the laboratory. I want to thank Ramona Jung for teaching me myelin purifications and Silvia Thüne for her support with RNA isolation. Further thanks are due to Annette Fahrenholz for her great help with immunohistochemistry. I also express gratitude to Dr. Kathrin Kusch, Yeonsu Kim and Sophie Siems for supporting me with the Western blots and to Chalid Hasan for the collaboration regarding the immunohistochemistry of CNP1 null mutant mice. Thanks to Erik Späte for discussions and advice on my statistics and material and methods writing. Thanks to the department of medical statistics for advice.

I express gratitude to Prof. Dr. Hauke Werner, Dr. Vijay Tiwari and Dr. Sudhir Thakurela for providing the RNA-Sequencing data of myelin of CNP1 null mutant and wildtype mice. Furthermore, I thank Dr. Ting Sun for helping me analyzing the RNA-Seq. data.

Many thanks to the other members of the Department of Neurogenetics for their support and advice.